THE JOURNAL
OF
CHEMICAL PHYSICS

VOLUME 8 AUGUST, 1940 NUMBER 8

Mercury Photosensitized Reactions of Propane*

E. W. R. STEACIE† AND D. J. DEWAR†
Physical Chemistry Laboratory, McGill University, Montreal, Canada

(Received June 13, 1940)

An investigation has been made of the mercury photosensitized reactions of propane, alone and in the presence of hydrogen at temperatures from 25 to 323°C. The products of the reaction are predominantly hydrogen, hexanes (mainly 2,3-di-Me-butane and 2-Me-pentane), and a small amount of higher paraffins. The postulated mechanism is:

$$\begin{gathered}Hg(^3P_1)+C_3H_8\rightarrow Hg(^1S_0)+C_3H_7+H\\ Hg(^3P_1)+H_2\rightarrow Hg(^1S_0)+2H\\ H+C_2H_8\rightarrow C_3H_7+H_2\\ 2C_3H_7\rightarrow C_6H_{14}\\ 2H\rightarrow H_2\\ C_3H_7+C_3H_8\rightarrow C_6H_{14}+H.\end{gathered}$$

The quantum yield of hydrogen is approximately 0.15 at 25°C and rises somewhat with increasing temperature.

INTRODUCTION

MUCH valuable information concerning the kinetics of elementary processes has been been obtained from the investigation of photosensitized reactions. In the case of the mercury photosensitized decomposition of ethane[1–3] there seems to be no doubt that the primary process involves a C–H bond split,

$$C_2H_6+Hg(^3P_1)=C_2H_5+H+Hg(^1S_0). \quad (1)$$

It also seems to be well established that the main secondary reactions are[2–4]

$$H+C_2H_6=C_2H_5+H_2, \quad (2)$$

$$H+C_2H_5=2CH_3, \quad (3)$$

$$CH_3+C_2H_5=C_3H_8, \quad (4)$$

$$2C_2H_5=C_4H_{10}, \quad (5)$$

$$2H=H_2, \quad (6)$$

$$H_2+Hg(^3P_1)=2H+Hg(^1S_0). \quad (7)$$

In view of the interest attaching to the reactions of the aliphatic free radicals, it seemed desirable to investigate the reactions of propane as well.

An investigation of the reaction of hydrogen atoms, produced by the Wood-Bonhoeffer method, with propane has already been reported.[5]

* A preliminary account of some of this work was given in a paper presented at the Symposium on Photochemistry of the New York Academy of Science, May 3, 1940.

† Present address, National Research Laboratories, Ottawa, Canada.

[1] E. W. R. Steacie and N. W. F. Phillips, J. Chem. Phys. **6**, 179 (1938).

[2] E. W. R. Steacie and N. W. F. Phillips, Can. J. Research **B16**, 303 (1938).

[3] E. W. R. Steacie, W. A. Alexander, and N. W. F. Phillips, Can. J. Research **B16**, 314 (1938).

[4] H. S. Taylor, J. Phys. Chem. **42**, 763 (1938).

[5] E. W. R. Steacie and N. A. D. Parlee, Trans. Faraday Soc. **35**, 854 (1939); Can. J. Research **B17**, 371 (1939).

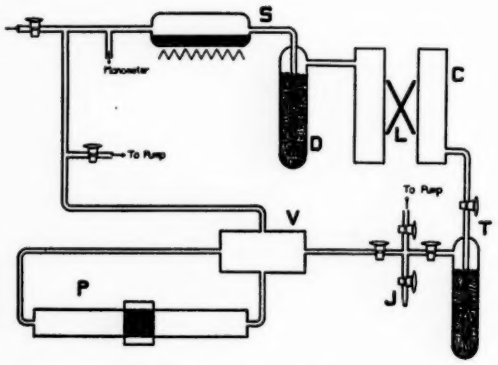

FIG. 1. Apparatus.

It was found that the products of the reaction were solely methane at low temperatures, and methane, ethylene, and ethane at higher temperatures. It was concluded that the results furnished very strong confirmation of the importance of reaction (3) in free radical processes. The main steps in the postulated mechanism were:

Primary reaction

$$H+C_3H_8=C_3H_7+H_2. \quad (8)$$

Secondary reactions at low temperatures

$$H+C_3H_7=CH_3+C_2H_5, \quad (9)$$

$$H+C_2H_5=2CH_3, \quad (3)$$

$$CH_3+H=CH_4. \quad (10)$$

Additional secondary reactions at high temperatures

$$C_3H_7=C_2H_4+CH_3, \quad (11)$$

$$2CH_3=C_2H_6, \quad (12)$$

$$H+C_2H_4=C_2H_5, \quad (13)$$

$$H+C_2H_5=C_2H_6, \quad (14)$$

$$H_2+C_2H_5=C_2H_6+H. \quad (15)$$

As far as we are aware, no previous work has been reported on the mercury photosensitized reactions of propane.

EXPERIMENTAL

A few preliminary experiments were first carried out in a "single pass" flow system of a type described elsewhere.[6] Such a system reduces complications due to secondary reactions to a minimum, but is very tedious in operation. The major part of the work was therefore carried out in a circulating system as described below. The two types of system yielded substantially the same results.

The apparatus employed is shown diagrammatically in Fig. 1. The mercury saturator *S* supplied the necessary mercury vapor to saturate the reactant gas. It was heated electrically to about 60°C. A desaturating trap *D*, filled with iron pellets, and maintained at 25°C, removed excess mercury vapor and maintained the mercury pressure at that corresponding to its vapor pressure at 25°C. The circulating pump *P* has been previously described.[1] It was connected to a series of mercury valves *V*, so arranged that the gas in the line always flowed in the one direction in spite of the reciprocating motion of the pump.

The condensable reaction products were collected in the trap *T* which was filled with iron pellets and maintained at −80°C.

The fused quartz reaction vessel *C* was annular in form, 10 cm long, 8 cm in diameter, with a 4-cm diameter hole through the middle. Its volume was 320 cc. The reaction vessel was illuminated by a Hanovia Sc2537 high voltage mercury lamp. The lamp was in the form of a double-U and was run at 100 milliamperes from a 5000-volt sign transformer.

As the Hanovia lamp was unsuitable for high temperature investigations, the runs at higher temperatures were made with a combined lamp reaction vessel of the type previously described.[7]

The reaction vessel was provided with a thermocouple well, and temperatures were measured with a Chromel-Alumel thermocouple. For high temperature runs the reaction vessel was enclosed in an electrically heated furnace, with the exception of the electrodes which projected from the furnace and were water or air-cooled.

The main proportion of the apparatus used for low temperature runs had a volume of 1680 cc. The high temperature apparatus had a volume of 2220 cc. The usual pumping system, gas reservoirs, Toepler pump, gas-holders, etc., were used.

[6] E. W. R. Steacie and R. L. Cunningham, J. Chem. Phys. in press.

[7] E. W. R. Steacie and N. W. F. Phillips, Can. J. Research **B16**, 219 (1938).

The intensity of the radiation emitted by the lamps was determined by measuring the rate of hydrolysis of monochloracetic acid.[8] The acid used was 0.5 *N*, and the procedure followed that of Steacie and Phillips.[1] Recent work[9] has indicated lower values of the quantum yield than those originally given by Rudberg. However, there are some indications from work in this laboratory that the quantum yield may be higher for high light intensities. In any case the absolute value of the quantum yield is not of great importance for the present purpose, and Rudberg's values have been used for the present to facilitate comparison with the ethane decomposition.

All runs were carried out at the vapor pressure of propane at −80°C (about 14 cm). Excess propane was admitted to the system, the trap was cooled to −80°C and part of the propane condensed in it. This acted as a reservoir to keep the partial pressure of propane constant during the experiment.

At this pressure the quenching by propane is sufficient to ensure practically 100 percent absorption of the resonance radiation.

Analyses

At the end of a run the gaseous products were pumped by a Toepler pump into a portable mercury gas-holder. The gas was then analyzed in a low temperature fractional distillation apparatus of the Podbielniak type. The hydrogen and methane were taken off together in the distillation and this fraction was analyzed by combustion as previously described.[2] Occasional tests on fractions for unsaturated hydrocarbons were made in a Burrell gas analysis apparatus.

The condensate in the trap, which consisted of higher boiling hydrocarbons, was weighed after each run and saved for future analysis. The liquid products from several runs were combined and separated by distillation in a semi-micro-fractionating apparatus.[10] Cuts from the micro-distillation apparatus were analyzed by combustion and tested for unsaturates by bromine absorption. Determinations were also made of their melting points and refractive indices.

[8] E. Rudberg, Zeits. f. Physik **24**, 247 (1924).
[9] W. G. Leighton, R. N. Smith, and P. A. Leighton, J. Am. Chem. Soc. **61**, 2299 (1939); **60**, 2566 (1938).
[10] E. W. R. Steacie, D. J. Dewar, and R. Potvin, forthcoming paper.

Materials

Propane was obtained in cylinders from the Ohio Chemical and Manufacturing Co. It was stated to be 99.8 percent pure and no appreciable impurities were detected in Podbielniak analyses. The gas was therefore used without further purification.

Hydrogen was obtained from commercial cylinders. It was purified by passage over platinized asbestos at 600°C and through a liquid-air trap.

Results

Some 20 preliminary runs were made in the "single-pass" system. These indicated a quantum efficiency of hydrogen production of approximately 0.18. The gaseous products consisted of hydrogen and a trace of methane. The liquid products are reported in Table IV.

The results of experiments with the circulating system are given in Tables I–IV. The initial and final pressures given in columns 3 and 4 of Table I are those with the trap at room temperature. The actual partial pressure of propane during a run was the vapor pressure of propane at −80°C, *viz.* approximately 14 cm.

The liquid condensate is expressed in column 9 as "C_6H_{14}" since the main fraction of the distillate had this composition. The condensate also contained some hydrocarbons of higher boiling point and traces of lower boiling hydrocarbons, so that this method of reporting the results is slightly in error.

TABLE I. *The mercury photosensitized decomposition of propane.*

Volume of system = 1680 cc. Propane vapor pressure = 14 cm.
Volume of reaction cell = 320 cc. Trap temperature = −80°C.
Arc current = 0.100 amp. Reaction temperature = 24–27°C
Resonance radiation absorbed = 4.0×10^{-6} Einstein/sec.
Circulation rate = 1900 cc/min.

Run No.	Time, min.	Pressure		Decomposition Rate, Moles per sec. $\times10^6$	Quantum Yield (of H_2+CH_4)	Products, Mole Percent		
		Initial, mm	Final, mm			H_2	CH_4	"C_6H_{14}"
1	180	364	301	0.73	0.18	54.3	0.6	45.1
2	180	367	319	0.70	0.17	52.2	1.4	46.4
3	180	365	325.5	0.68	0.17	—	—	—
4	180	365	323	0.72	0.18	51.7	0.6	47.7
5	180	405	370	0.71	0.18	53.2		46.8
6	150	414.5	—	0.78	0.19	51.9	0.9	47.2
7	180	397	—	0.74	0.18	55.3	1.9	42.8
8	150	165.5	142.5	0.64	0.16	43.5	(11.5?)	45.0
9	180	162	142.5	0.53	0.13	55.1	0.4	44.5
10	180	161.5	139	0.56	0.14	—	—	—
11	180	261	220	0.68	0.17	57.4	2.4	40.2
12	180	261	211.5	0.70	0.17	—	—	—

TABLE II. *The mercury photosensitized decomposition of propane at higher temperatures.*

Volume of system = 2215 cc. Circulation rate = 1900 cc/min.
Volume of reaction cell = 870 cc. Trap temperature = −80°C.
Arc current = 0.090 amp. Propane vapor pressure = 14 cm.
Resonance radiation absorbed = 9.5×10^{-6} Einstein/sec.

Run No.	Time, min.	Temperature, °C	Initial Pressure, mm	Decomposition Rate, Moles per sec. $\times10^6$	Quantum Yield (of H_2+CH_4)	Products, Mole Percent		
						H_2	CH_4	"C_6H_{14}"
13	180	76	280	1.62	0.17	57.9	0.0	42.1
14	90	103	370	1.78	0.19	53.8		46.2
15	60	107	350	1.56	0.16	53.9	0.0	46.1
16	75	105	380	1.36	0.14	—	—	—
17	75	107	360	1.26	0.13	49.0	0.2	50.8
18	75	107	360	1.51	0.16	52.6	1.9	45.5
19	75	175	250	2.28	0.24	51 9	3.5	44.6
20	75	175	360	2.37	0.25	57.1	2.3	40.6
21	75	175	360	3.34	0.35	—	—	—
22	37½	175	350	3 72	0.39	55 3	0.0	44.7
23	75	175	300	3.33	0.35	55.6		44.4
24	60	176	350	3.35	0.35	61.4	1.8	36.8
25	60	173	320	3.10	0.33	54.8		45.2
26	60	255	160	0.0	—	Blank run lamp off		
27	60	248	250	2.28	(0.24)*	54.5	1.7	43.8
28	66	249	360	2.42	(0.26)*	55.0	0.3	44.7
29	60	249	320	2.56	(0.27)*	51.3	1.7	47.0
30	60	250	300	2.68	(0.28)*	53.7		46.3
31	61	323	320	1.39	(0.15)*	51.4		48.6

* In these runs at higher temperatures, difficulty was encountered in keeping the electrodes sufficiently cool (owing to the fact that the electrodes were too close to the reaction vessel). Under these circumstances the mercury vapor pressure was too high, and λ2537 was partially reversed and therefore less intense than before. As a result these quantum yields have no real significance. At 175°C, however, the intensity was as stated, and the rise in quantum yield on going from room temperature to 175°C is definitely established.

The results of experiments in the presence of added hydrogen are given in Table III. In this table the quantity of hydrogen in the products is that formed during the reaction, i.e. the amount of hydrogen added initially has been subtracted from the amount found by analysis.

The results of analyses, etc., of the liquid products are given in Table IV. In these tests the products from several runs were combined in each case so as to provide a sample of 4 to 10 cc. In the table the high boiling products are expressed in volume percent of the total condensate.

It will be seen that, except for a trace of unsaturates, the main fraction of the liquid products consists of hexanes. Furthermore, within the accuracy with which distillations on very small amounts of liquid can be carried out, there is no appreciable change in the products with changing temperature, or in the presence or absence of added hydrogen.

In Table V the physical properties of the isomeric hexanes are summarized. The boiling point of the product definitely rules out the possibility of *n*-hexane, or of 2,2-di-Me-butane. The melting point data on Table IV are uncertain on account of the ease of supercooling and the tendency to the formation of glasses. However, the data are sufficiently reliable to rule out *n*-hexane and 2,2-di-Me-butane also.

Of the remaining three compounds, 3-Me-pentane may also be ruled out. In the first place it is intrinsically unlikely, since neither it nor 2,2-di-Me-butane can be formed directly by any possible combination of *n*-propyl or isopropyl radicals. Furthermore, its boiling point is rather high, its melting point low, and its refractive index high. Hence all the data combine to make its presence unlikely.

We are therefore left with the possibility of 2-Me-pentane and 2,3-di-Me-butane. 2-Me-pentane could be formed by the combination of a *n*-propyl and an isopropyl radical, while 2,3-di-Me-butane would result from the combination of 2 isopropyl radicals. As far as the data of Table IV are concerned, the distillation data are not reliable enough to enable any decision to be made between the two isomers. The refractive indices slightly favor 2,3-di-Me-butane, while the melting points somewhat favor 2-Me-pentane.

It may be observed that if, as appears probable, the hexanes result from the combination of two propyl radicals, then ignoring steric factors we may calculate the relative amounts of 2,3-di-Me-butane, 2-Me-pentane, and *n*-hexane which would result from any given relative amount of *n*-propyl and isopropyl radicals. Thus if we had equal amounts of the two radicals we would expect equal quantities of the three isomers. Now

TABLE III. *The mercury photosensitized decomposition of propane in the presence of added hydrogen.*

Volume of system = 1680 cc. Reaction temperature = 24–27°C.
Volume of reaction cell = 320 cc. Trap temperature = −80°C.
Arc current = 0.100 amp. Propane vapor pressure = 14 cm.
Resonance radiation absorbed = 4.0×10^{-6} Einstein/sec.
Circulation rate = 1900 cc/min.

Run No.	Time, min.	Pressures			Decomposition Rate, Moles per sec. $\times10^6$	Quantum Yield (of H_2+CH_4)	Products, Mole Percent		
		Initial Pressure		Final Total Pressure					
		of C_3H_8	of H_2				H_2	CH_4	"C_6H_{14}"
32	180	265.5	10	242.7	0.64	0.16	51.2	1.5	47.3
33	180	257.5	50	267	0.64	0.16	54.7		45.3
34	180	268.5	49.5	277	0.67	0.17	52.2	0.0	47.8
35	180	278	50	284	0.67	0.17	52.1	0.1	47.8
36	180	274	53	282	0.70	0.17	—	—	—

n-hexane is not detected. If we had say 5 *iso*- to 1 *n*-propyl radical, we would expect

25 2,3-di-Me-butane
5 2-Me-pentane
1 *n*-hexane.

It is certain that this amount of *n*-hexane would have escaped detection. It may be concluded therefore that on the basis of chance recombination of radicals, the absence of *n*-hexane indicates that the condensable products are probably preponderantly 2,3-di-Me-butane rather than 2-Me-pentane. This argument is, of course, weakened by steric considerations. However it receives support from the generally accepted idea that secondary hydrogen atoms are more weakly bound than primary.

The physical properties, combustion data, etc., indicate that the high boiling fraction of the products is probably predominantly nonanes. These are presumably formed by secondary reactions of propyl radicals with hexane or with hexyl radicals.

It may be remarked that since the "single-pass" runs and those in the circulating system yield the same products, it may be concluded that the products formed are those actually produced in the reaction, and that secondary reactions have little effect on the results.

TABLE V. *Physical constants of the hexanes.**

SUBSTANCE	CARBON SKELETON	M.P., °C	B.P., °C	n_D^{20}
n-hexane	C–C–C–C–C–C	−94	68.8	1.37506
2-Me-pentane		−153.7	60.2	1.37149
2,3-di-Me-butane	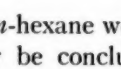	−128.8	58.0	1.37499
3-Me-pentane	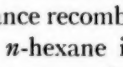	(−118)	63.2	1.3765
2,2-di-Me-butane	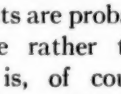	−98.2	49.7	1.36887

* From Egloff, *Physical Constants of Hydrocarbons* (New York, 1939), Vol. 1.

DISCUSSION

The fact that the products are almost exclusively hydrogen and hexanes, indicates that, as with ethane, the primary step is a C–H bond split,

$$C_3H_8+Hg(^3P_1)\rightarrow C_3H_7+H+Hg(^1S_0)$$
$$\text{or } \rightarrow C_3H_7+HgH. \qquad (16)$$

Furthermore the following secondary reactions are obviously reasonable,

$$2C_3H_7\rightarrow C_6H_{14}, \qquad (17)$$

$$2H\rightarrow H_2, \qquad (18)$$

$$H+C_3H_8\rightarrow C_3H_7+H_2. \qquad (19)$$

TABLE IV. *Liquid products of the reaction.*

	MAIN FRACTION					HIGH BOILING FRACTION		
RUNS	M.P. °C	B.P. °C	n_D^{20}	COMPOSITION (BY COMBUSTION)	REMARKS	AMOUNT (AS VOLUME PERCENT OF TOTAL LIQUID PRODUCTS)	B.P. °C	REMARKS
Preliminary single-pass runs	—	57.5±1	1.3736	$C_{5.9\pm0.1}$ $H_{13.7\pm0.5}$	Unsaturates, <5%	ca. 10%	142–149	$C_{8.9\pm0.5}$ $H_{20.7\pm1.0}$
1–7	—	58.0–58.5	—	$C_{6.0\pm0.1}$	—	present	—	—
8–12 } 32–36 }	−154	58.8–59.4	1.3735	—	—	present	—	—
13–18	−169	(a) 59.2–59.7 (b) 60.2–61.0	1.3736 1.3733	—	Trace of lower boiling fraction also present	10	—	—
19–25	(a) −167 (b) −169	58.6–59.9 61.0–61.2	1.3736 1.3734	—	Trace of lower boiling fraction also present	10–15	—	$n_D^{20}=1.3997$ to 1.4003
26–30	−167	58.8–59.4	1.3725	—	—	15	—	—

Since the products are unchanged when hydrogen is added initially, we obviously have in this case the same secondary reactions as above, together with the primary step

$$H_2+Hg(^3P_1)\rightarrow 2H+Hg(^1S_0)$$
$$\text{or } \rightarrow HgH+H. \qquad (20)$$

At first sight these results appear to conflict with those of Steacie and Parlee on the reaction of hydrogen atoms with propane. They suggested reaction (19) as the primary step in their investigation. They accounted for the formation of large amounts of methane (which are not found here) by reaction (9).

$$H+C_3H_7\rightarrow C_2H_5+CH_3. \qquad (9)$$

At higher temperatures these results also suggested strongly that the propyl radical was decomposing by

$$C_3H_7\rightarrow C_2H_4+CH_3, \qquad (11)$$

while here the products do not change appreciably with rising temperature.

However, in the case of mercury photosensitization the concentration of hydrogen atoms is very low, and that of propane relatively high, thus making (9) unimportant compared with (19). Furthermore, recombination reactions of radicals will be favored by the higher pressure, thus diminishing the chance of (11). There is also the possibility that hexane may occur here by

$$C_3H_7+C_3H_8\rightarrow C_6H_{14}+H, \qquad (21)$$

on account of the relatively high concentration of propane. The results of the investigation of the reaction of hydrogen atoms with propane are thus not in any way incompatible with the present work.

The assumption that reaction (21) plays an important part appears to be unavoidable. It seems to be very unlikely that propyl radicals could disappear fast enough by recombination alone at high temperatures to avoid some decomposition of the propyl radical by (11). If this occurred, methane and ethane would ultimately be formed. Since they are not present in appreciable quantities, propyl radicals must disappear by some reaction such as (21).

It may be added that the absence of *n*-hexane as an important product favors considerable hexane formation by (21). We may expect that the relatively weaker binding of secondary hydrogen atoms will lead to a preponderance of isopropyl radicals in reactions (16), (19), and (21). If this is the case, then (21) will lead almost exclusively to 2,3-di-Me-butane and 2-Me-pentane. The occurrence of reaction (21) would also impart chain characteristics to the reaction, and would explain the increase in quantum yield at higher temperatures.

We may therefore conclude that the main reactions of importance in the mechanism are

$$Hg(^3P_1)+C_3H_8\rightarrow Hg(^1S_0)+C_3H_7+H$$
$$Hg(^3P_1)+H_2\rightarrow Hg(^1S_0)+2H$$
$$H+C_3H_8\rightarrow C_3H_7+H_2$$
$$2C_3H_7\rightarrow C_6H_{14}$$
$$2H\rightarrow H_2$$
$$C_3H_7+C_3H_8\rightarrow C_6H_{14}+H.$$

In a forthcoming paper the present results will be compared with the results of an investigation of the cadmium photosensitized reaction.

The award of a Studentship to one of us (D. J. D.) by the National Research Council of Canada is hereby gratefully acknowledged.

The Infra-Red Absorptions of Organic Hydroxyl Compounds in the Solid State in the 3μ Region

MANSEL M. DAVIES
The Department of Physical Chemistry, Cambridge, England

(Received May 30, 1940)

The absorptions in the range 2.6μ to 3.5μ, covering the OH and CH fundamentals, have been measured for a variety of solid organic hydroxyl compounds in the form of thin films. For simple alcoholic and carboxylic structures the results, as expected, show complete association in the condensed state. In a number of other cases a sharp band with a narrow doublet structure ($\Delta\nu \sim 40$ cm^{-1}) is found near 2.9μ, and this is ascribed to relatively "free" OH groups in the solid resulting either from steric protection, as in triphenylmethyl carbinol, or weak intramolecular binding as in ethyl mandelate. Two very general features are the shift of the absorptions to longer wave-lengths in the condensed phases, and the doublet nature of the absorption of the "free" hydroxyl groups in the solid as well as in other phases. Both these factors are discussed in the light of the new and previous data.

THE examination of infra-red spectra has been extensively used in recent years to detect the inter- and intra-molecular interactions, more particularly of hydroxylic compounds. If only in view of the possible extensions of this method to such structural problems as occur in the carbohydrates, the proteins, and related synthetic polymers it was obviously of interest to examine first the absorptions of simple hydroxylic compounds in the solid state. A considerable proportion of the various hydroxylic derivatives studied had already been examined in dilute solution, usually in carbon tetrachloride. Comparison of the results for the two states leads to conclusions as to the degree of interaction of the hydroxyl groups in the solid and the extent to which "hydrogen bond" formation occurs in these cases. The results for the compounds studied are reported individually and are followed by a discussion of the more general features observed.

EXPERIMENTAL

As in previous work[1] the Hilger D. 83 spectrometer has been used with the quartz prism. Having realuminized the mirrors it was possible to work with slit widths of 0.020μ from 2.7μ to 3.5μ: generally $\delta\lambda$ was 0.025μ.

The usual form in which the solids have been examined is as a film pressed between two very thin glass slips. Care was taken to prove that the latter had no appreciable absorption in the region concerned and repeated measurement showed that two such glass slips together gave 80±2 percent transmission from 2.7μ to 3.5μ, the 20 percent loss of energy arising from four reflections at air-glass interfaces: the absorption curves have been corrected for this loss. A small quantity (some 10 or 20 mg) of the substance to be examined is gently heated to melting on one such glass slip (2.5 by 4 cm) and the second, previously warmed, pressed on it. This gives a reasonably uniform film whose mean thickness has been estimated from the area occupied and the loss in weight on cleaning the slips. Such films invariably scatter a certain proportion of the incident radiation, which accounts for the apparent background absorption in most of the curves: this scattering is minimized by inserting the film as nearly as possible at the focus in the absorption path, and in any case is considerably less than for similar films deposited from solutions. Liquids have been examined in the same way, the two glass slips holding together with no apparent loss during the course of a run. Cells of the usual type fitted with fluorite windows have been used for solutions.

The substances examined, unless of sufficient initial purity, were first carefully recrystallized or fractionally distilled.

RESULTS

In solution the simplest type of absorption corresponding to the valence O−H vibration is

[1] Davies and Sutherland, J. Chem. Phys. **6**, 755 (1938).

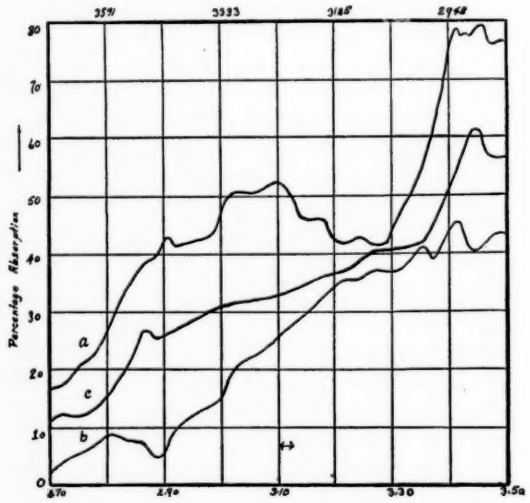

FIG. 1. Absorption of thin films of solids. (a) Cetyl alcohol, (b) lauric acid, (c) 1-Pentadecanol 15-acid. Wavelength scale (in μ) below, frequency scale (in cm^{-1}) above. For curve (b) add twenty percent to percentage absorption scale on left.

given by the primary alcohols. This is found to consist of two components: A very sharp well-defined band, showing no structure, is centered at 2.75μ and certainly arises from the free or monomeric molecules, while the intensity of a broad band extending from at least 2.8μ to 3.15μ, with a maximum near 3.0μ, increases with the number of associated molecules in solution.[2] Cetyl alcohol, $C_{16}H_{33}OH$, typical of the straight chain compounds, in a film estimated to be 10^4 molecules thick gave the absorption curve shown in Fig. 1. The absorption which spreads from 2.8μ to beyond 3.2μ corresponds almost exactly to the associational band in solution, with the difference that the maxima in the absorption are now given as 3.02μ and 3.10μ, whereas in carbon tetrachloride they are at 2.87μ and 2.99μ. The CH absorption, within the limits of its definition in this case, appears to be in its usual position between 3.4μ and 3.5μ. This result is entirely what would have been expected from the known x-ray crystal structure for such alcohols, where the hydroxyl groups come together and form a layer lattice with spacing twice the molecular length.[3] Obviously the association of the hydroxyl

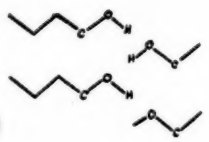

groups has now proceeded to completion, as may be represented by (a). The shift of the peak absorption by about 0.1μ to longer wave-lengths is found to be a frequent characteristic of OH bands on passing from solution, or vapor, to the solid state.

In further agreement with expectations, lauric acid, $C_{11}H_{23}\cdot COOH$, a simple, long chain, carboxylic acid, shows a rather featureless absorption starting below 2.9μ and extending beyond 3.5μ, the CH bands being only just discernible as peaks around 3.45μ (Fig. 1b). The greater extent of the association band for the acids has already been found in solution. The molecules of such acids, of course, crystallize in the same head-to-head fashion as the alcohols.[4]

The typical appearance of the normal alcoholic and carboxylic hydroxyl absorptions in carbon tetrachloride solution at 2.76μ and 2.83μ is shown by the curve for 15-pentadecanol 1-acid, $HOOC\cdot(CH_2)_{14}\cdot CH_2OH$, in Fig. 2. In the solid it shows the most featureless absorption, starting at 2.8μ and continuing into the CH bands at

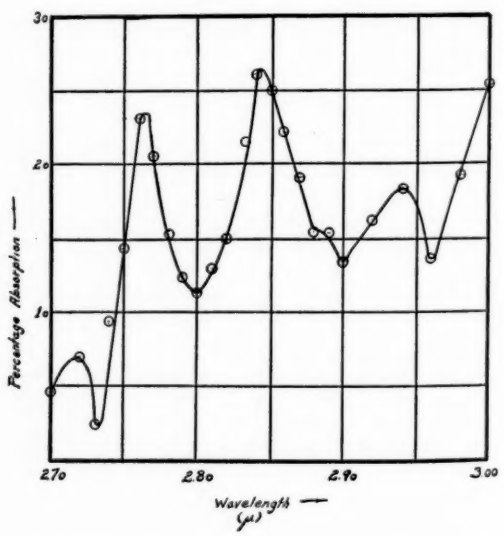

FIG. 2. 0.0189 molar 15-pentadecanol, 1-acid in 3.05-mm cell. Temperature 58°.

[2] Fox and Martin, Proc. Roy. Soc. **A162**, 419 (1937).
[3] Malkin, J. Am. Chem. Soc. **52**, 3739 (1930).
[4] Brill and Meyer, Zeits. f. Krist. **67**, 570 (1928).

3.4μ (Fig. 1, curve *c*). This conforms to a likely supposition that the crystal structure consists of alternate double layers of COOH and OH groups: —*B B*——*A A*——*B B*—. Association in pairs of the carboxyl heads is known to be pronounced even in dilute solutions.[5] In the solid both groups will be completely associated and their corresponding absorptions smeared into the unrelieved structure found.

Some of the most interesting results for the solid state are provided by triphenylmethyl carbinol, $(C_6H_5)_3 \cdot COH$, Fig. 3. This compound gives in the range 2.6μ to 3.5μ two relatively sharp absorptions whose identification as arising from the OH and CH vibrations follows immediately on comparison with the absorption of, say naphthalene, in the solid state: the hydrocarbon shows only the band at 3.3μ. For triphenylmethyl carbinol the CH band appears to have much the same structure as in solution, being correspondingly sharp but apparently shifted 0.02μ to longer wave-length. The OH absorption is broader than is usual in solution and now has a doublet structure, with peaks at $2.86_5\mu$ and $2.90_0\mu$ of equal intensity. The displacement from the center of the sharp peak in solution (at 2.769μ in carbon tetrachloride) is considerable: $\Delta\nu = 137$ cm^{-1}; the frequency difference of the components of the doublet is 42 cm^{-1}. These features will be discussed later, but it may be suggested here that the shift from 2.77μ to 2.88μ may be related to some directional field in the solid (electrostatic) as the macro-physical characteristics of the hydrocarbon medium (i.e., provided by the C_6H_5 groups) would appear to resemble those of the solvents CCl_4 and $CHCl_3$. The relative sharpness of the band, besides its position, is entirely against ascribing it to associated molecules, and the absence of any appreciable absorption characteristic of the latter shows that even in the solid state the steric influence of the bulky $(C_6H_5)_3C$ group prevents the hydroxyls of different molecules getting sufficiently close for their molecular fields to interact considerably.[2] This conclusion is readily appreciated from a molecular model for this compound.

Another interesting feature in Fig. 3 is the obviously greater intensity of the OH band compared with the CH, despite the great predominance of the latter groups. Relative to the CH, the OH absorption seems to increase in intensity about four times on passing from solution to solid. This recalls the increase in intensity of the HCl fundamental absorption between the gas phase and solution.[6] The intensity variation may prove to be general for strong dipole groups on condensation.*

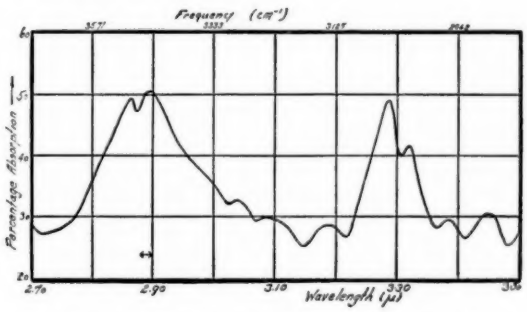

FIG. 3. Absorption of thin film of solid triphenyl methyl carbinol. $d = 0.012$ mm.

Two α-hydroxyacids have been examined both in carbon tetrachloride solutions and in the solid state. These compounds, mandelic acid ($C_6H_5 \cdot CHOH \cdot COOH$) and α-hydroxymyristic acid ($C_{12}H_{25} \cdot CHOH \cdot COOH$) show entirely similar results (Fig. 4a and b). In solution the normal alcoholic OH absorption is missing, being represented at most by a shoulder at 2.78μ on the main peak which is perfectly sharp on the long-wave-length side, and is centered at 2.83μ. This result is not so unexpected as at first appears. Thus, in the α-hydroxyketone, benzoin ($C_6H_5 \cdot CHOH \cdot CO \cdot C_6H_5$) the main OH absorption appears at 2.88μ although here the "normal" band at 2.78μ is clearly resolved from the latter.[7] Apparently the intramolecular interaction is not so intense in the α-hydroxyacids. From the form of the curve it would appear that there are only two

[5] Davies, Trans. Faraday Soc. **34**, 410 (1938), and J. Chem. Phys. **6**, 770 (1938).

[6] West and Edwards, J. Chem. Phys. **5**, 14 (1937).

* An attempt was made to examine the triphenylmethyl carbinol absorptions under the high dispersion of a grating instrument. With the present arrangement of the instrument, the higher orders overlapping the 3.0μ first-order spectrum are eliminated by the filter-shutter method (Sutherland, Lee, and Conn, to appear shortly), but this proved unsatisfactory for the present purpose owing to the scattering of the short-wave radiation by the film. Accordingly, for the present we shall have to be content with the above results.

[7] Davies, Trans. Faraday Soc. **36**, 333 (1940).

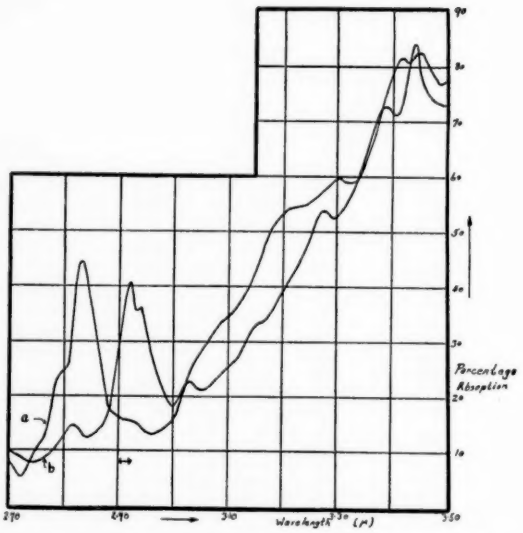

FIG. 4. Absorption of α-hydroxymyristic acid. (a) 0.0230 molar solution in carbon tetrachloride with 3.05-mm cell. Temperature 64°. (b) Thin film of solid $d=0.012$ mm.

components in the absorption: the sharpness and symmetry of the 2.83μ peak suggests that in the molecular orientation (c) both hydroxyl absorptions coincide, while a structure (b) provides the "free," 2.78μ, alcoholic band.

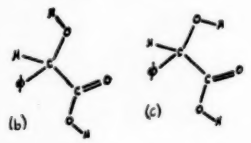

A comparison of the OH absorptions of the α-hydroxyacids with say acetic acid under the same conditions[1] shows that the intensity of the sharp band is distinctly greater in the former. This results from the presence of two OH groups in the acid molecule, and the fact that the intramolecular interaction in the α-hydroxyacids probably reduces the tendency of the carboxyl groups to associate. Unfortunately, owing to their sparing solubility, the latter point could not be checked by molecular weight determinations in carbon tetrachloride

In the solid both acids show a sharp band arising from the α-hydroxyl group. In α-hydroxymyristic acid it is centered at 2.92μ with a shoulder at $2.93_5\mu$, whilst in mandelic acid where it is not so sharp, it appears as a doublet peak at $2.90_5\mu$, $2.93_0\mu$ ($\Delta\nu=30$ cm^{-1}). In all cases an association band appears on the long wave side. If, as the results for solution suggest, the molecules are largely in the configuration (c), it is quite likely that the alcoholic OH group is little disturbed on association of the carboxyl heads and, its freedom of rotation both around the C−O bond and the C−C chain being removed, there is small likelihood of these OH groups in different molecules interacting with one another. The sharpness of the OH band in the solid then follows from the intramolecular "fixation" of the hydroxyl group configuration.

It would be expected that in comparison with the acids, the α-hydroxyesters would give even clearer results owing to the removal of the free OH group of the carboxylic structure. This has been found to be the case, and a careful study of ethyl mandelate has been made. In dilute carbon tetrachloride solution, 0.0232 molar or 0.28 percent by weight, the ester shows a single sharp band at $2.83_5\mu$, followed by no association band (Fig. 5a). The apparent symmetry of the absorption in the most dilute solution suggests that in the isolated molecules all the OH groups are in one configuration (*c*, of the acid). The small peak at 2.92μ (3425 cm^{-1}) often appears in this neighborhood with hydroxylic derivatives. While it is difficult to find conclusive evidence for its origin, it may possibly be due to an overtone or combination frequency involving the C−O bond.

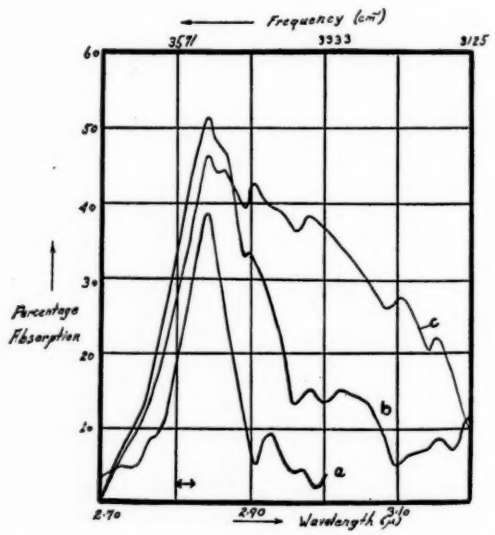

FIG. 5. Ethyl mandelate in carbon tetrachloride solution. (a) 0.0232 molar (i.e., 0.28 percent by weight in 3.05-mm cell. (b) 2.62 percent by weight in 0.35-mm cell. (c) 47 percent by weight between two glass strips.

Owing to the low melting point of ethyl mandelate (34°C), when the thin film of solid was placed in the focus of the beam it liquefied. Accordingly, by placing the film at some distance from the focus it has been possible in this case to measure the absorption of the same layer both as liquid and solid (Fig. 6a and b). To complete the sequence, solutions of 2.62 and 47 percent by weight in carbon tetrachloride have also been examined (Fig. 5b and c). It is first clear that ethyl mandelate in the solid gives an absorption somewhat similar to triphenylmethyl carbinol although broader than the latter: an important feature is the absence of an association band, in contrast with mandelic acid for which this component (arising from the COOH group) is very obvious. The free hydroxyl group in ethyl mandelate is again protected by its intramolecular interaction, the peak at 2.92μ corresponding to the doublet in triphenylmethyl carbinol. The peak at 3.00μ is more difficult of interpretation. It is clearly present in the liquid and probably appears at 2.98μ in the concentrated solution. A maximum near 3.00μ is found in the curves for a considerable number of the other compounds studied and it may again be due to a common overtone or combination frequency.

The clearest result of comparing the series of curves for ethyl mandelate is the gradual nature of the transition from the dissolved to the solid

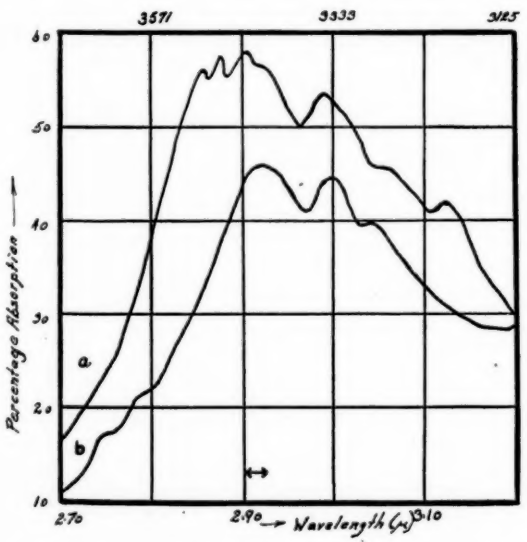

FIG. 6. Absorption of thin film of ethyl mandelate. (a) As liquid, (b) as solid, $d=0.016$ mm.

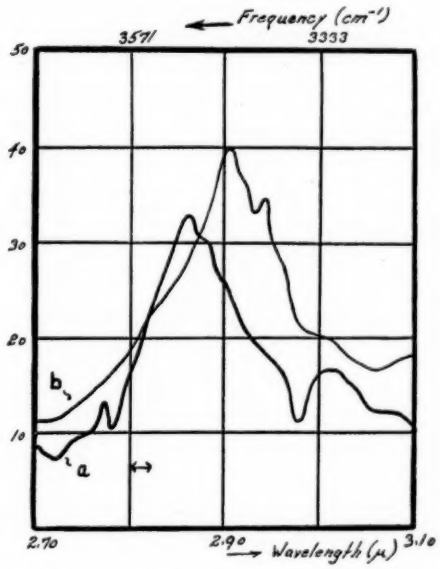

FIG. 7. Absorption of β-hydroxyester. (a) 0.0168 molar solution in carbon tetrachloride with 3.05-mm cell. (b) Thin film of solid. $d=0.019$ mm.

state. In the concentrated solution the sharp peak characteristic of the free molecules in dilute solution is still prominent, although shifted slightly to 2.84μ: the latter effect is probably more apparent than real, being a result of the overlapping with the strong absorption on the long wave side of the band. At the same time the absorptions at 2.9μ and 3.0μ found in the solid are already present. All these features are also shown in the liquid, with a change in emphasis shown by the increased intensity of the long wave components. This continuous change on increasing condensation of the molecules is in agreement with a growing mass of evidence on the nature of solutions and the liquid state.[8] The mean degree of aggregation (association) as indicated by the appearance of the spectrum characteristic of the solid, increases gradually through the solutions to the solid, in which phase there are no longer any "free" molecules.

A β-hydroxyester with the structure $\beta\cdot\beta\cdot\beta\cdot$-phenyl-diphenyl-hydroxyethyl propionate,

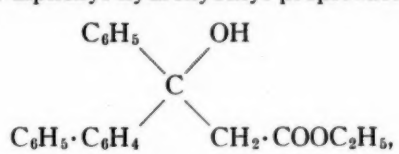

[8] Trans. Faraday Soc. **33**, 1–279 (1937).

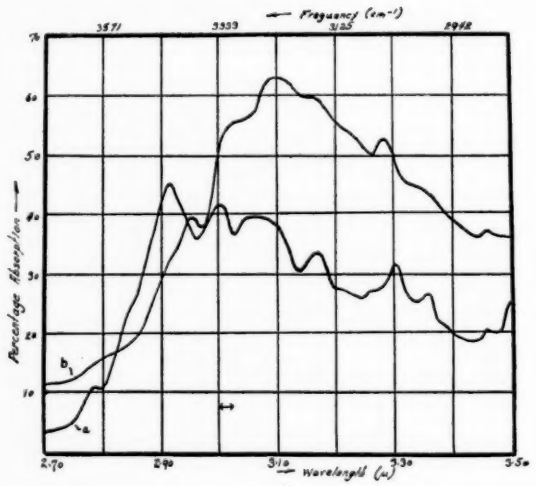

FIG. 8. Absorption of thin films of solids. (a) catechol, (b) resorcinol. $d=0.074$ mm.

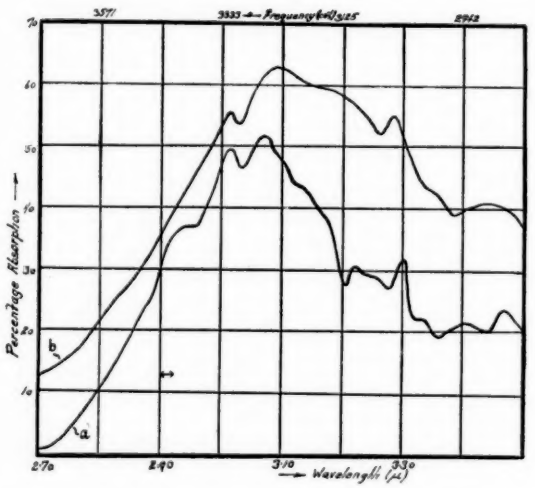

FIG. 9. Absorption of solid films. (a) hydroquinone, $d=0.024$ mm. (b) Quinhydrone, $d=0.016$ mm.

has also been examined in solution and as a solid (Fig. 7a and b). In solution the OH absorption is shifted to 2.86μ, where it is broader than most such bands in carbon tetrachloride. That the interaction between the OH and C=O is greater in this case than for the α-hydroxyester may be explained on the basis of observations with accurate molecular models for these structures. In mandelic ester it is always possible easily to get the OH rotating past the O of the C=O group of the carboxyl structure, but this is not always possible for the β-hydroxyester, where the interaction can accordingly become more pronounced, i.e., the OH and C=O groups can get closer to one another. The orientation in the γ- or higher hydroxyacids can also become entirely favorable to the OH and C=O interaction (but not more so than for the β-hydroxyacid) although the *a priori* probability of this configuration will rapidly decrease. In the solid the β-hydroxyester gives the sharpest OH band measured, centered at 2.90μ with perhaps a satellite at 2.94μ. The exceptional freedom of the OH vibration in this solid, as measured by the sharpness of the band, agrees with previous indications. An important point with the same significance is the small shift from dilute solution to the solid, only 0.04μ or 48 cm^{-1} compared with the mean displacements $\Delta\nu=137$ cm^{-1} for triphenylmethyl carbinol and $\Delta\nu=108$ cm^{-1} for the α-hydroxyacids and ester. Clearly the intramolecular binding and the steric protection of the hydroxyl group operate to stabilize the OH frequency on passing to the condensed phase and both these factors are large for the β-hydroxyester.

Three compounds of interest in the present study are the isomeric dihydroxybenzenes. Catechol, the orthocompound, gives in solution a clearly defined absorption with two peaks at $2.76_8\mu$ and $2.80_2\mu$.[9] The results for the solid show an absorption starting at 2.8μ and rising sharply to a main peak at $2.91\pm0.01\mu$, from which it continues, with decreasing intensity however, into the region of the CH bands which are just discernible at 3.3μ. By comparison with the previous results, the steepness of the curve up to and the peak at 2.91μ suggest a "free" hydroxyl group, the following broad band corresponding to associated groups. This is compatible with the *cis-trans* structure (d), apparently the only one existing in solution: that is, we deduce that the

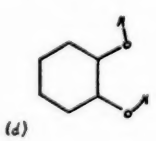

(d)

intramolecular interaction of some of the hydroxyls persists in the solid, the remainder being engaged in associative interaction.

[9] Davies, Trans. Faraday Soc. **34**, 1427 (1938).

Resorcinol, or meta-dihydroxybenzene, shows a notably different absorption from catechol (Fig. 8b). It has been found at 73° in carbon tetrachloride, to give a single sharp symmetrical peak at $2.77_5\mu$, indicating no interaction between the hydroxyls. In the solid the absorption starts about 2.85μ, has an insignificant peak at 2.95μ but increases in intensity up to a maximum at 3.10μ. The breadth and distribution of intensity in the band correspond to complete association of the hydroxyls. This agrees with the x-ray results of Robertson and Ubbelohde[10] whose crystal structure analysis points to "hydrogen bridges" throughout the solid. Compared with catechol, this is a consequence of the meta-position of the two groups preventing any degree of internal "protection" such as occurs for the *cis*-group in that case.

In hydroquinone, i.e. paradihydroxybenzene, the saturated solution in carbon tetrachloride shows the same single absorption peak at 2.77μ as in resorcinol. In the solid the absorption of these compounds is also similar, although the band appears a little narrower and at slightly shorter wave-length in hydroquinone (Fig. 9a). There is, however, no doubt that associative interaction of the hydroxyls is complete in the latter case also. Quinhydrone, $C_6H_4(OH)_2 \cdot C_6H_4O_2$, the molecular complex formed by hydroquinone and benzoquinone, has also been examined in the solid state (Fig. 9b). In carbon tetrachloride it was too sparingly soluble for the absorption to be measured. The broad, almost featureless absorption rising to a maximum at 3.10μ resembles that of hydroquinone, or better, resorcinol, and the "hydrogen bridges" must be in very much the same state in all these cases. With Badger's form of the relation of internuclear distance with force constant,[11] and a vibration frequency of 3225 cm^{-1} (i.e. corresponding to 3.10μ) for the associated OH groups, the calculated bond distance is 1.02A: this compares with a distance of 0.97A in the monomeric groups. This indicates that even for quinhydrone where the solid structure is found to consist of infinite chains of quinol-quinone molecules (e), the hydrogen bridges are far from symmetrical,

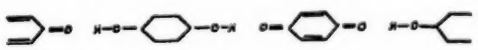

(e)

as the 0—0 distance between adjacent molecules can hardly be less than 2.4A. This conclusion supports the revised results for the x-ray crystal study of quinhydrone.[12]

Two long-chain isomeric compounds, the so-called *cis*- and *trans*-dihydroxybehenic acids[13] were found by Marsden and Rideal[14] to have very different properties as monomolecular films. As these differences appeared to be related to the different orientations of the hydroxyl groups, an

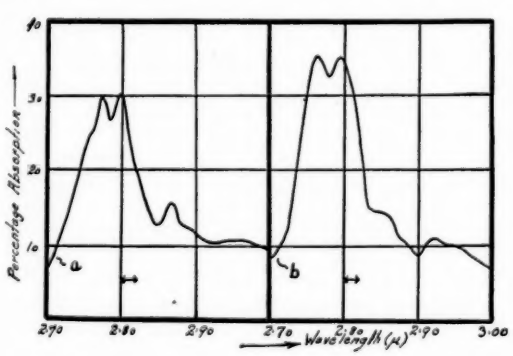

FIG. 10. Absorption of 9–10-dihydroxymethyl stearates in carbon tetrachloride. 3.05-mm cell. Temperature 51°. (a) 0.0173 molar, *cis*-compound. (b) 0.0219 molar *trans*-compound.

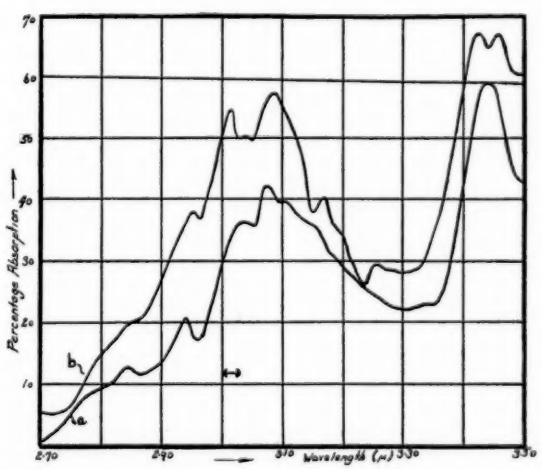

FIG. 11. Absorption of solid isomeric 9,10-dihydroxymethyl stearates. (a) *Trans*-compound, $d = 0.060$ mm. (b) *Cis*-compound.

[10] Robertson and Ubbelohde, Proc. Roy. Soc. **A167**, 122 (1938).

[11] Badger, J. Chem. Phys. **3**, 710 (1935).

[12] Palacios and Foz, Anal. Fis. Quim. **34**, 779 (1936).

[13] Hilditch, J. Chem. Soc. (London) 1828 (1926).

[14] Marsden and Rideal, J. Chem. Soc. (London) 1163 (1938).

infra-red study of their absorptions was of interest. In solution and in the solid state the isomers resembled one another markedly. The results, while clearly interpretable, are somewhat involved owing to the presence of an additional free OH group in the carboxylic structure. Accordingly, it seems preferable to give the comparable results for the isomeric 9.10·dihydroxymethyl stearates: $CH_3(CH_2)_7\cdot\cdot CHOH\cdot CHOH\cdot(CH_2)_7COOCH_3$. In carbon tetrachloride the *cis*-compound shows an absorption with two peaks at 2.77μ and 2.80μ (Fig. 10a). While the curves are not so clear as for the benzene derivative (in particular a peak near 2.86μ appears to be real) this presumably corresponds to a similar state of affairs to that in catechol. The fact that the *trans*-compound in solution also shows a doublet peak, perhaps best given as $2.76_5\mu$, $2.79_5\mu$, is confusing only so long as these compounds are considered to be really *cis*- and *trans*-isomers. Actually they are diastereoisomers and may be represented:

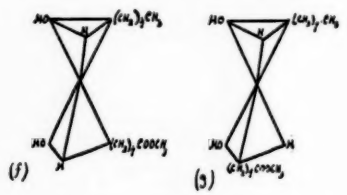

The point that emerges is that, insofar as the OH absorptions for both compounds are similar, the two hydroxyl groups occupy the same relative positions in both cases. By analogy with catechol where, according to Pauling,[15] the structure (d) is necessarily confined to one plane, in this case the free rotation about the 9.10 C−C bond may bring these groups opposite one another in the two esters, as shown in (f) and (g). The monomolecular films may well show differences of stability arising from the different ease of packing of the two structures (f) and (g).

The general similarity in the absorptions of the solids is again not unexpected on the above formulation: Fig. 11a and b. The curves are, however, different from that of solid catechol, the *trans*-ester showing a considerable resemblance to hydroquinone in the region 2.9μ to 3.2μ: in the *cis*-compound the band is somewhat narrower and the peaks at 3.01μ and 3.09μ better defined than usual. The differences in the melting points and solubilities of these isomers suggest different stabilities of their packing in the solid and the minor differences in their infra-red absorptions can be related to the same change in molecular orientation. The fact that for both isomers in the solid the absorption is far more typical of complete "hydrogen bonding" than in the case of catechol may be due to the possibility of rotation about the C−C bond between the two carbon atoms carrying the hydroxyl groups. The intramolecular interaction will by no means entirely eliminate this possibility and if the intermolecular attraction becomes sufficient (as it reasonably might in the solid) the two OH groups could swing away from one another and take part individually in hydrogen bonding with other molecules.

Discussion

There are two principal features in the foregoing results which need further discussion. The first is the general shift of the absorptions to longer wave-length in the condensed phases: the other is the doublet nature of the absorption of the "free" hydroxyl groups as observed in the solid for triphenylmethyl carbinol, ethyl mandelate, etc.

The former of these effects has long been recognized as of very general occurrence. For simple molecules, more particularly the hydrogen halides, it has been carefully studied by Hettner, West and co-workers, and Sutherland, Lee and Wu.[16] Thus, for HCl, the fundamental absorption centered at 2886 cm^{-1} in the gas at room temperatures, has its center shifted in carbon tetrachloride solutions to 2833 cm^{-1}, in the liquid (at 173°K) to 2785 cm^{-1}, and in the solid (at 100°K) it is at 2768 cm^{-1}. The largest change we have observed from solution to solid is $\Delta\nu = 137$ cm^{-1} for triphenylmethyl carbinol, and the smallest, for the β-hydroxyester, of $\Delta\nu = 48$ cm^{-1}. It must be emphasized that these figures refer to the sharp absorptions in the solid state and not to the change between monomeric and

[15] Pauling, J. Am. Chem. Soc. **58**, 94 (1936).

[16] Hettner, Zeits. f. Physik **89**, 234 (1934); West and Salant, Phys. Rev. **37**, 108 (1931); West and Edwards, J. Chem. Phys. **5**, 14 (1937); West, J. Chem. Phys. **7**, 795 (1939); Sutherland, Lee and Wu, Nature **142**, 669 (1938).

associated structures, for which $\Delta\nu$ can be observed in the gas, solution, liquid, or solid phases to be of the order of 350 cm^{-1}, depending on the type of association. Actually, of course, the association band itself shifts (e.g., for cetyl alcohol or hydroquinone) by about 140 cm^{-1} to lower frequencies on passing from solution to the solid.

Of the three general sources of interaction between saturated molecules, that is, the dipole-dipole, dipole-induced dipole, and dispersion effects, calculation for molecules as close together and maintaining a fixed orientation as are those in the solid state, shows that the first of these items largely predominates for polar molecules.[7] Accordingly, the purely dipole forces, which tend to assume a directed character in the solid phase, would seem to be mainly responsible for the perturbation in the OH bond vibration: that is, the molecular dipole field in the solid is sufficient to stretch the hydroxyl dipole the small amount necessary for the observed lowering of its frequency. On the basis of the Badger-Clark rule, the change in bond length involved for triphenylmethyl carbinol is 0.012A, in a bond of 0.98A, i.e. a matter of 1.2 percent. Similarly, for HCl in passing from the gas to solid, the bond length increases 1.4 percent. (If this change were effected on isolated molecules in the gas it can be estimated, on the assumption of Hooke's law applying to the extension, that it would necessitate an energy of 0.0047 ev.) That electrostatic forces are largely responsible for these changes is borne out by the following comparisons:

	RO−H	HCl	HBr	C−H
$\Delta\nu_{gas\ solid}$ cm^{-1}	180	118	93	19
μ in Debyes,	1.7	1.03	0.78	0.3.

This conclusion is in agreement with that of West and Edwards, whose paper should be consulted for a discussion of the other possibilities and a calculation of the dipole distortion made by Kirkwood. It also provides an explanation of the fact that the greater the intramolecular binding of the hydrogen, the smaller the frequency change on passing from solution to the solid. As a measure of the former we may take the displacement of the main OH frequency from its expected position in solution ($\delta\nu$): $\Delta\nu$ is the subsequent change on passing to the solid:

	Triphenylmethyl carbinol	Catechol	Ethyl mandelate	β-hydroxy-ester
$\delta\nu$	0	70	92	132
$\Delta\nu$	137	115	108	48

Clearly, the more firmly the hydrogen of the OH group is held internally by dipole interaction, the smaller will be its external field, with a corresponding decrease in intermolecular perturbation in the solid.

The doublet nature of the relatively sharp bands of a number of simple vibrators in the condensed state is also of fairly general occurrence. That the effect is not always confined to this phase is most clearly shown by hydroxylic compounds. Naherniac[17] in an examination of the second overtone of the valence OH vibration in a number of alcohols in the vapor and liquid states reports a doublet peak for twelve out of fifteen alcohols examined in the gas phase. Badger and Bauer[18] had earlier found the same doublet structure for three primary alcohols in the vapor. The frequency separation in these cases is usually about 50 cm^{-1}. For triphenylmethyl carbinol, mandelic acid and a β-hydroxy-ester, we have found doublet separations of 42, 30, and 46 cm^{-1} in the solid. Two possible interpretations of this splitting may be considered. (i) The peaks may arise from the occurrence of the hydroxyl groups in two states owing to varying degrees of interaction with adjacent groups, either within the same molecule or in neighboring molecules. (ii) The doublet may correspond to a combination of the OH valence vibration with a low frequency vibration, or libration, of the hydrogen in this group, probably in a direction roughly perpendicular to the OH and C−O bonds. These two factors almost certainly operate separately in various hydroxylic structures. The former is equivalent to Pauling's interpretation of the infra-red results for orthochlorphenol, etc.[15] and is the explanation favored by Badger and Zumwalt[19] for the slitting of the OH frequency in simple alcohols. Methyl alcohol is undoubtedly a special case in this

[17] Naherniac, Ann. d. Physik **7**, 528 (1937).
[18] Badger and Bauer, J. Chem. Phys. **4**, 711 (1936).
[19] Badger and Zumwalt, J. Chem. Phys. **7**, 87 (1939).

respect; thus the two components reported by Naherniac with $\Delta\nu$ only 30 cm^{-1} refer to prominent features in the fine structure of the band, resolved, owing to the smallness of the moments of inertia of this molecule, by Badger and Bauer.[20] Borden and Barker[21] have shown that the hydroxyl group is not free to rotate, at least in the ground state in methyl alcohol, and it seems likely that the restricting potential barrier, due to dipole and other interactions between the OH and adjacent CH groups, will increase for the higher homologues.

The second possibility has been used in accounting for the great breadth of the association band in alcohols and carboxylic acids,[1] and one important confirmation of its operation seems worth mentioning. It is to be expected that in the carboxylic dimer combination of the valence OH vibration will be most pronounced with "deformation" vibrations involving the OH groups. The frequencies of the latter will be notably decreased by substitution of deuterium, which should lead to a narrowing of the association band.* Wall and Claussen[22] have recently published results for the association band in both deutero- and normal acetic, propionic, and benzoic acids. They conclude that in the hydrogen acids the association band lies between 3.2μ and 4.0μ ($\Delta\nu$=625 cm^{-1}), in the deutero-acids between 4.3μ and 4.9μ ($\Delta\nu$=289 cm^{-1}). The difference is most pronounced and in the expected direction.

As the doublet structure both in the vapor and in the solid corresponds to quite narrow bands and the second factor results in a very broad absorption, it seems that the first interpretation will be the more satisfactory in the present circumstances. Some additional evidence in favor of this view may be mentioned. Naherniac[17] fails to comment on the fact that while the alcohols show this doublet structure, of six carboxylic acids examined in the vapor phase only one, and that formic acid, shows it for the COOH structure. In this grouping, however, the hydrogen is tied so firmly in the orientation

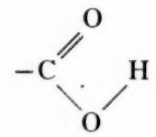

(with an estimated energy of 7400 cal. per g mole relative to the *trans*-structure),

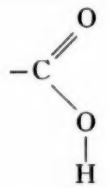

that the restoring force for the OH valence vibration must be uniquely determined. The anomaly of the first member of the series again results from the extended structure of the band due to the low moments of inertia of the molecule, as is proved by a comparison of the high dispersion work on formic and acetic acid vapors.[23] Closely similar to this point is the observation that for the two molecules where the intramolecular field is sufficient to tie the OH groups all in one orientation in solution and which give a "free" hydroxylic absorption in the solid, i.e., ethyl mandelate and the β-hydroxyester, the sharp absorption in the solid was not clearly resolved into a doublet.

While remembering that we are here dealing with the free hydroxyl in contrast to the associated group, it is not immediately obvious why the doublet structure is not generally observed for the alcohols in solution or in the liquid phase. In carbon tetrachloride, where the majority of the reliable measurements have been made, the monomeric band is usually a single peak of half-width about 60 cm^{-1} shifted by a similar amount from its position in the vapor phase. Presumably owing to the constantly varying interaction with adjacent molecules in this phase, the potential field to which the OH group is subject takes on a continuous series of values over a range determining the position of the band. That such an interaction with solvent molecules occurs is highly probable from the ob-

[20] Badger and Bauer, J. Chem. Phys. **4**, 469 (1936).
[21] Borden and Barker, J. Chem. Phys. **6**, 553 (1938).
* This point was raised in a discussion with Dr. Sutherland.
[22] Wall and Claussen, J. Am. Chem. Soc. **61**, 2812 (1939).
[23] Badger and Bauer, J. Chem. Phys. **5**, 605 and 852 (1937).

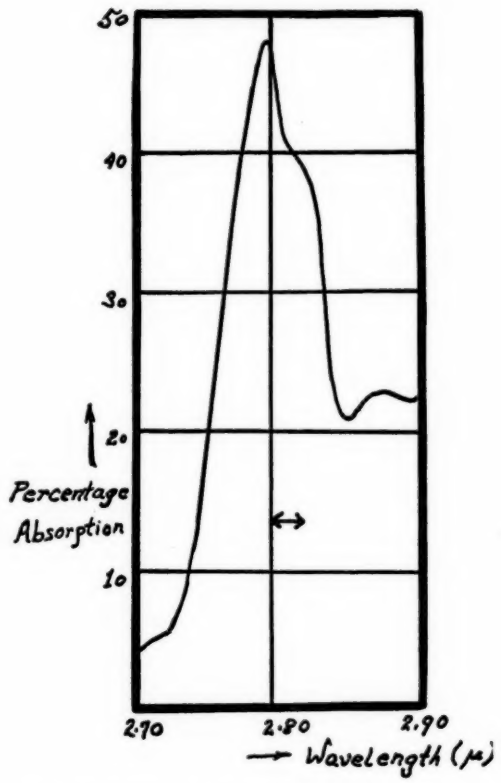

FIG. 12. 0.153 molar benzyl alcohol in benzene. 0.35-mm cell.

servation of the apparent doublet nature of the alcoholic OH absorption in benzene solutions. This is shown by the corrected absorption curve for a dilute solution of benzyl alcohol in benzene, Fig. 12. The center of the absorption maximum is now at 2.80μ (cf. 2.764μ in CCl_4, 2.770μ in $CHCl_3$) and the peak is no longer symmetrical: while sharp on its short wave side, a distinct shoulder is shown at $2.81_5\mu$, not resolvable as a separate peak with the quartz prism. In this solvent, owing to the ready polarizability of the double bonds of the benzene ring, the dipole-induced dipole interaction, added to the always-present dispersion effect, may become quite considerable. The result is that the distribution of the solute molecules between at least two energy states (corresponding to different degrees of interaction with the solvent) becomes detectable. The splitting of the OH frequency in this way has also been reported by Naherniac.[17] It is likewise very apparent for HCl solutions[6] where its magnitude varies with the dielectric constant of the medium.

Obviously the interaction of the OH with adjacent groups will be favored by the fixed orientations and close packing in the solid: thus the fixed orientation of the dipoles with respect to one another means that their interaction approaches the maximum possible ($U=-2\mu_1\mu_2/R^3$) where the dependence is upon R^{-3} rather than R^{-6} as occurs for random orientation at large distances. Taking $\mu_{OH}=1.6D$ and $\mu_{CH}=0.3D$, at a separation of 3.5A, which is a reasonable estimate for groups in neighboring molecules in the solid, these dipoles give $U=-325$ cal. per g mole. The frequency separation of $\Delta\nu\sim40$ cm^{-1} for the doublet in the solid may be roughly estimated on the empirical proportionality of energy difference and frequency separation[7] to correspond to an energy of 660 cal. per g mole. Certainly other contributions to the interaction energy should be added to the simple dipole effect: especially in structures with phenyl groups the dipole-induced dipole interaction may be considerable. (This should lead to a larger doublet separation in phenolic vapors than in aliphatic alcohols. For resorcinol, where the groups can hardly interact being in the meta-position, Naherniac gives $\Delta\nu=104$ cm^{-1}, but reports only one peak for phenol.) The occurrence of a doublet peak for the alcohols is then throughout referred to the same cause, the only difference being that in the vapor the interaction is intramolecular whereas when it occurs in solution and the solid it is more likely intermolecular.

The author wishes to thank Professor E. K. Rideal, Professor T. P. Hilditch, and Dr. P. Maitland for specimens of some of the compounds studied, and he gratefully acknowledges the helpful discussion of this paper with Dr. G. B. B. M. Sutherland. The work was carried out during the tenure of a Senior Award of the D.S.I.R. and was aided by a grant from the Chemical Society.

Packed Fractionating Columns and the Concentration of Isotopes*

KARL COHEN
Department of Chemistry, Columbia University, New York, New York
(Received May 9, 1940)

The behavior of isothermal packed fractionating columns is deduced from their differential equation. The relation between rates of production and over-all fractionation is studied, as is the rate of approach to equilibrium. The results are illustrated by problems of isotope separation.

THE theory of plate columns has been extensively treated. The behavior of packed columns is generally related to that of plate columns by determining the "height equivalent to a theoretical plate."[1,2]

For certain problems arising in the use of packed columns equivalent to hundreds of plates, the graphical and algebraic methods developed for small plate columns are inconvenient. Other problems, of importance for long columns only, such as time phenomena, have not yet been treated.

The present paper discusses these problems, starting from the consideration of a differential element of the column. The two steps in the theory of plate or packed columns, i.e., the determining of the relation between liquid velocities and surface and the number of theoretical plates, and then the finding of the properties of a column of n theoretical plates and given reflux ratio, are not separated. The solution compares favorably in simplicity with the second part of the usual procedure taken by itself.

We restrict ourselves to isothermal columns with constant liquid and gaseous hold-ups. Even for isotope concentration columns, these conditions are not strictly true, since the gaseous hold-up and to a smaller degree the liquid hold-up are affected by the pressure-drop across the columns. In the fractional distillation of two closely-related liquids, the hold-ups will depend on the equations of heat transfer. The idealizations of constant hold-ups and temperature could, of course, be obtained in practice: in the former case by compressors, in the latter case, by appropriate heating or cooling. The reality of these conditions in a particular case is, however, inessential. We consider here only the kernel of the problem. But the modifications necessary for any actual process will, we believe, be fairly obvious.

THE DIFFERENTIAL EQUATION

Refer to Fig. 1. Consider a two-component two-phase* system. One component will be described as "heavy," the other, "light." We will take N to be the mole fraction of heavy material in the liquid, $[N]$ the corresponding concentration (moles/liter); $1-N$ the mole fraction of light material in the liquid, $[M]$ its concentration; H the hold-up per unit length (moles/cm) of combined heavy and light material in the liquid; L the flow (moles/sec.) of combined material in the liquid: and let lower-case symbols denote the corresponding quantities in the gaseous phase. Z is the length of the column. z is the distance along the column, measured from the "condenser."

If $H\delta N/\delta t$ be the rate of transfer of heavy material to the liquid across the liquid-gaseous interface, the conservation of matter gives us

$$H\partial N/\partial t = -L\partial N/\partial z + H\delta N/\delta t$$
$$h\partial n/\partial t = l\partial n/\partial z - H\delta N/\delta t.$$

We will take

$$H\delta N/\delta t = -k\{[N^+][m]-\alpha[M][n]\}. \quad (1.1)$$

We will justify the use of (1.1) later. At this point we only remark that it is of the same form as $\delta[N]/\delta t$ for a bimolecular reversible reaction. k is a constant depending on the permeability of

* Publication assisted by the Ernest Kempton Adams Fund for Physical Research of Columbia University.

[1] C. S. Robinson and E. R. Gilliland, *Elements of Fractional Distillation* (McGraw-Hill, New York, 1939) (contains bibliography).

[2] J. R. Huffman and H. C. Urey, J. Ind. Eng. Chem. **29**, 531 (1937).

* Throughout we take these two phases to be liquid and gas. Obviously the two phases could equally be two immiscible liquids (extraction), etc.

the interface, α is either the chemical equilibrium constant of a reaction such as

$$HC^{13}N(g)+C^{12}N^{-}(aq.) \rightleftharpoons HC^{12}N(g)+C^{13}N^{-}(aq.) \quad (1.2)$$

(for the case of the concentration of isotopes), or, should we be fractionating two closely related liquids such as isomeric heptanes, the ratio of the partial pressures. In either case, *at equilibrium*

$$\frac{N}{1-N}\Big/\frac{n}{1-n}=\frac{[N][m]}{[M][n]}=\alpha. \quad (1.3)$$

Substituting for $H\delta N/\delta t$ from (1.1), and introducing mole fractions, the differential equations governing the behavior of the column become

$$H\frac{\partial N}{\partial t}=-L\frac{\partial N}{\partial z}-kcC\{N(1-n)-\alpha n(1-N)\}, \quad (1.4)$$

$$h\frac{\partial n}{\partial t}=l\frac{\partial n}{\partial z}+kcC\{N(1-n)-\alpha n(1-N)\}, \quad (1.5)$$

where

$$\begin{aligned} c&=[m]+[n]=\text{a constant}\\ C&=[M]+[N]=\text{a constant.}\end{aligned} \quad (1.6)$$

Equations (1.4) and (1.5) are nonlinear, and, except for the stationary state, cannot easily be solved. Considering N as always small, and thus writing 1 for $1-N$, is not justified; the entire purpose of the use of columns is to obtain N's which are *not* small. Let us introduce $R=N/1-N$ and $r=n/1-n$. Then (1.4) and (1.5) transform into

$$H\frac{\partial R}{\partial t}=-L\frac{\partial R}{\partial z}-kcC\frac{1+R}{1+r}(R-\alpha r), \quad (1.7)$$

$$h\frac{\partial r}{\partial t}=l\frac{\partial r}{\partial z}+kcC\frac{1+r}{1+R}(R-\alpha r). \quad (1.8)$$

Since R/r varies only between 1 and α, we have, to terms of the order of $(1-\alpha)^2$

$$H\frac{\partial R}{\partial t}=-L\frac{\partial R}{\partial z}-kcC(R-\alpha r), \quad (1.9)$$

$$h\frac{\partial r}{\partial t}=l\frac{\partial r}{\partial z}+kcC(R-\alpha r). \quad (1.10)$$

In the steady state ($\partial R/\partial t=\partial r/\partial t=0$), (1.9) and (1.10) give

$$l\partial r/\partial z-L\partial R/\partial z=0$$

or

$$lr-LR=\text{constant}, \quad (1.11)$$

whereas the exact Eqs. (1.4) and (1.5) possess as their integral of conservation

$$ln-LN=\text{constant}. \quad (1.12)$$

This discrepancy is unimportant so far as the rate of approach to equilibrium is concerned. But since the question of conservation of matter is of the utmost importance in the separation of isotopes, in addition to solving the approximate Eqs. (1.9) and (1.10) for the steady state, which gives easily the *general sweep* of the relationship between over-all fractionation and production, we shall also solve the rigorous Eqs. (1.4) and (1.5) for the steady state. From this latter solution we can find in any *particular* case the exact relationship between fractionation and production.

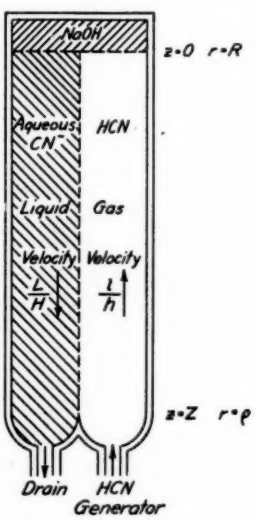

FIG. 1. Schematic diagram of fractionating column.

THE STEADY STATE: PRODUCTION AND FRACTIONATION (APPROXIMATE SOLUTION)

The set-up is essentially as shown in Fig.1. In the case of a fractional distillation, the NaOH solution which here absorbs the HCN gas and transforms it into NaCN solution is replaced by a total condenser. In the case of the concentration

TABLE I.

p_{HCN}	2σ	$e^{2\sigma}$
0.05 atmos.	3.11	22.4
.06	3.24	25.5
.07	3.32	27.7
.08	3.37	29.1
.09	3.39	29.7
.10	3.40	30.0
.11	3.39	29.7
.12	3.38	29.4
.13	3.36	28.8
.14	3.33	27.9
.15	3.29	26.8
.16	3.25	25.8

of $N^{15}H_3$, the roles of the liquid and gas are interchanged, and the NaOH solution serves to strip the ammonia from the liquid. In all cases the boundary conditions are

$$\text{At } z=Z: r=\rho=\text{normal abundance ratio} \tag{2.1}$$

$$\text{At } z=0: r=R. \tag{2.2}$$

If P be the production in moles/sec. of mixed gases,

$$l=P+L. \tag{2.3}$$

Introducing $p=P/l=$fraction of flow drawn off, we find

$$L/l=1-p. \tag{2.4}$$

We are now to solve (1.9) and (1.10) with $\partial R/\partial t=\partial r/\partial t=0$, subject to the boundary conditions (2.1) and (2.2). The solution is easily found to be

$$R=\rho\frac{e^{-\mu z}+\alpha\theta}{(1-p)e^{-\mu Z}+\theta}, \tag{2.5}$$

$$r=\rho\frac{(1-p)e^{-\mu z}+\theta}{(1-p)e^{-\mu Z}+\theta}, \tag{2.6}$$

where $\theta=p/(1-\alpha)$ and

$$\mu=(kcC/L)(1-\alpha)(1+\alpha\theta).$$

When there is no production, (2.5) and (2.6) reduce to

$$R=r=\rho e^{2\sigma(1-z/Z)}, \tag{2.7}$$

introducing the quantity σ, which will be useful to us later.

$$\sigma=\frac{kcC}{2L}(1-\alpha)Z. \tag{2.8}$$

The over-all fractionation is given by

$$\frac{r(0)}{r(Z)}=e^{2\sigma}\sim\left(\frac{1}{\alpha}\right)^{kcCZ/L}, \tag{2.9}$$

the approximation being valid when α is near 1.

For the system defined by (1.2) and (1.3), $\alpha<1$ and the column therefore accumulates heavy carbon at the production end. Since $R=r$, (2.7) is an exact solution of the rigorous Eqs. (1.7) and (1.8) or (1.4) and (1.5) for no production. The expression (2.9) for the over-all fractionation agrees with the well-known formula for plate columns, with $kcCZ/L$ the number of theoretical plates. We conclude that (1.4) and (1.5) are of the correct form, and therefore that $H\delta N/\delta t$ is correctly given by (1.1). $H\delta N/\delta t$ is generally given as[3] $H\delta N/\delta t=k'(N-N^*)$ (for a liquid-film-controlling transfer) or $H\delta N/\delta t=k''(n-n^*)$ (for a gaseous-film-controlling transfer), where N^* and n^* are the concentrations in equilibrium with the opposing phase. These expressions depend on the distance from equilibrium in the same way (to terms in $(1-\alpha)^2$) as does (1.1). (1.1) is preferable since k (but neither k' nor k'') is independent of concentration.

Let us see whether (2.8) cannot be verified. The reaction represented schematically by (1.2) is composed of two parallel reactions.

$$\begin{cases} HC^{13}N(g)+C^{12}N^-(aq.) \\ \qquad\rightleftharpoons HC^{12}N(g)+C^{13}N^-(aq.) \\ HC^{13}N(g)+HC^{12}N(aq.) \\ \qquad\rightleftharpoons HC^{12}N(g)+HC^{13}N(aq.), \end{cases} \tag{2.10}$$

whose equilibrium coefficients we will take, in

TABLE II.

REACTION	C_1	f	$(\rho_g)_{opt}$ FROM (2.12)	EXPERIMENTAL
$NH_4NO_3-NH_3$	9.6	56.7	0.063 atmos.	0.075[a, b]
$NaCN-HCN$	4.7	10.4	.11	.10[c]; .13*[d]
$NaHSO_3-SO_2$	3.4	1.23	.26	.30*[e]
$NaHCO_3-CO_2$	2.6	.034	1.65	—

* At the foot of the columns.
[a] H. C. Urey, J. R. Huffman, H. G. Thode and M. Fox, J. Chem. Phys. **5**, 11 (1937).
[b] H. G. Thode and H. C. Urey, J. Chem. Phys. **7**, 1 (1939).
[c] I. Roberts, H. G. Thode and H. C. Urey, J. Chem. Phys. **7**, 137 (1939).
[d] C. A. Hutchison, D. W. Stewart and H. C. Urey, reference 6.
[e] Results to be published.

[3] For example, reference 1, p. 127.

round numbers, as 0.98 and 1.005, respectively. Supposing that the rate of transfer is controlled by a relatively slow diffusion across a gaseous interface, k will be proportional to the self-diffusion constant of HCN, and we may consider the reaction in solution to be sufficiently defined by

$$1-\alpha=\frac{0.02C_{CN^-}-0.005C_{HCN(aq.)}}{C_{CN^-}+C_{HCN(aq.)}}.$$

The C's represent concentrations.

Diffusion constants vary inversely as the pressure. Taking account of the presence of water vapor in the simplest possible way,

$$k\sim 1/(p_{HCN}+p_{H_2O}).$$

Remembering that $c=p_{HCN}/22.4$ where p_{HCN} is measured in atmospheres, using the same value for $C_{HCN(aq.)}$ as for pure water (namely $C_{HCN(aq.)}=10\,p_{HCN}$), and taking $C_{CN^-}=4.7$ according to our usual practice,

$$\sigma=\text{const.}\times\frac{4.7Z}{44.8L}\times\frac{p_{HCN}}{p_{HCN}+0.03}\times\frac{0.02\times4.7-0.005\times10p_{HCN}}{4.7+10p_{HCN}} \qquad (2.11)$$

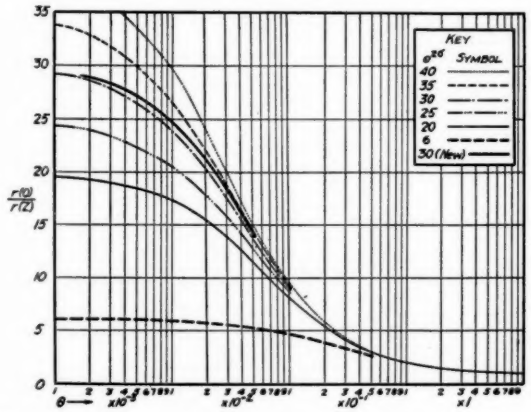

FIG. 2. Fractionation *vs.* production. $e^{2\sigma}$ is fractionation at no production.

TABLE III.

θ	$r(0)/r(Z)$ (2.13) (APPROXIMATE)	$r(0)/r(Z)$ (3.7) (EXACT)
0.000	702	702
.001	413	578
.002	293	467
.003	227	376

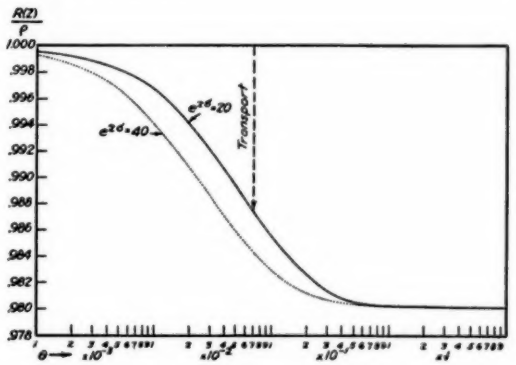

FIG. 3. Ratio of abundance ratios in liquid and in gas at foot of column, *vs.* production. Transports are proportional to deviation of curves from unity.

has a maximum at $p_{HCN}=0.1$ atmosphere. Although σ has a flat maximum, the fractionation $e^{2\sigma}$ varies very considerably with the pressure. Table I shows the relationship between fractionation and pressure according to (2.11) for a column whose fractionation factor is 30 at 0.1 atmosphere partial pressure of HCN. The pressure in the system is therefore quite critical.

In general, for any system similar to (2.10), if C_1 represents the concentration of the ions in solution, α_{H_2O} the equilibrium constant of the exchange reaction between the gas and its water solution, α_{ion} the exchange equilibrium constant between the gas and the ions, m_g the molarity of the gas in solution under partial pressure p_g, $w=-(1-\alpha)_{H_2O}/(1-\alpha)_{ion}$ and $f=m_g/p_g$, then the pressure at which fractionation will be a maximum is given very nearly by

$$p_g=0.17\,C_1/(fC_1(1+w))^{\frac{1}{2}}. \qquad (2.12)$$

It will be observed that p_g depends only slightly on w (which is of course less than 1). Taking $w=\frac{1}{4}$, taking for f its limiting value at zero pressure and zero concentration of salt[4] and for C_1 the concentrations used in experiments in these laboratories, we obtain Table II. In the last column are given the experimental optimum pressures, determined by trial-and-error. For those reactions which have been successfully used in the production of isotopes, the agreement is all that could be desired.

Returning now to the general formulae (2.5)

[4] All values from Lewis and Randall's *Thermodynamics* (1923).

and (2.6), $p \neq 0$

$$\frac{r(0)}{r(Z)} = \frac{(1-p)+\theta}{(1-p)(e^{-2\sigma})^{1+\alpha\theta}+\theta} \tag{2.13}$$

and

$$\frac{R(Z)}{r(Z)} = \frac{(e^{-2\sigma})^{1+\alpha\theta}+\alpha\theta}{(1-p)(e^{-2\sigma})^{1+\alpha\theta}+\theta}. \tag{2.14}$$

$r(0)/r(Z)$ is practically a function of $e^{2\sigma}$ and θ alone. Only for those values of θ near 1 does the value of α begin to count. For concreteness, we take $\alpha = 0.98$ and we obtain for various values of $e^{2\sigma}$ the curves shown in Fig. 2.

We see from these curves that even a very small production (if $\theta = 10^{-2}$ the fraction of flow drawn off is 0.02 percent), reduces the fractionation very markedly. The obverse of this phenomenon is that the transport, the amount of *heavy* material saved from the drain, is practically zero for small θ (large fractionation) and is only at its maximum for large θ (fractionation nearly 1). The transport is proportional to

$$1 - R(Z)/r(Z)$$

and is readily followed from Fig. 3, which gives $R(Z)/r(Z)$ against θ from Eq. (2.14).

From (2.13)

$$e^{-2\sigma} = \left\{ \frac{1+\theta/(1-p)}{r(0)/r(Z)} - \frac{\theta}{1-p} \right\}^{1/(1+\alpha\theta)}. \tag{2.15}$$

This gives the necessary value of σ to obtain a fractionation $r(0)/r(Z)$ and a production p.

The Steady State: Production and Fractionation (Exact Solution)

We return to (1.4) and (1.5), $\partial N/\partial t = \partial n/\partial t = 0$. The integral of conservation is

$$-(1-p)N + n = pn_0, \tag{3.1}$$

where n_0 is the value of n at $z = 0$. Solving for N, and inserting in (1.5) we find

$$\frac{dn}{dz} = -\frac{kcC}{l(1-p)}\{-pn_0 + n[(1-\alpha)(1+pn_0)+\alpha p]+n^2(\alpha-1)\} \tag{3.2}$$

or

$$-\frac{kcC}{l(1-p)}dz = \frac{dn}{a+bn+cn^2} \tag{3.3}$$

with obvious definitions for a, b and c. The integral of (3.3) is

$$-\frac{kcC}{l(1-p)}z + \text{constant} = \frac{-2}{(-D)^{\frac{1}{2}}}\tanh^{-1}\frac{2cn+b}{(-D)^{\frac{1}{2}}}, \tag{3.4}$$

where $D = 4ac - b^2$. Only values of $\theta < .05$ are of interest. With this restriction, to terms of the order of $(1-\alpha)^2$

$$b = 1-\alpha+p$$
$$c = -(1-\alpha)$$
$$(-D)^{\frac{1}{2}} = (1-\alpha)\{1+\theta-2n_0\theta\}$$

and (3.4) becomes

$$1+\theta-2n = (1+\theta-2n_0\theta)\tanh\left\{\frac{(1-\alpha)(1+\theta-2n_0\theta)kcCz}{2l} + \text{const.}\right\}. \tag{3.5}$$

When $z = Z$, $n = \xi$ = mole fraction of heavy isotope in ordinary matter. This determines the constant. Therefore

$$1+\theta-2n = (1+\theta-2n_0\theta)\tanh\left\{\frac{(1-\alpha)(1+\theta-2n_0\theta)kcC(z-Z)}{2l} + \tanh^{-1}\frac{1+\theta-2\xi}{1+\theta-2n_0\theta}\right\}. \tag{3.6}$$

The n_0 in (3.6), introduced by (3.1), is as yet unknown. However, taking $z = 0$, (3.6) becomes an

implicit equation for n_0:

$$1+\theta-2n_0=(1+\theta-2n_0\theta)\tanh\left\{-\sigma(1+\theta-2n_0\theta)+\tanh^{-1}\frac{1+\theta-2\xi}{1+\theta-2n_0\theta}\right\}. \tag{3.7}$$

(3.7) contains all the information we wish to know, and its solutions for various values of θ give the relationship between fractionation and production. For $\theta=0$ we find

$$\frac{n_0/1-n_0}{\xi/1-\xi}=e^{2\sigma},$$

which is precisely (2.9). The other values must be found by computation. The roots have been found for $e^{2\sigma}=30$, $\xi=.01$; $r(0)/r(Z)$ calculated from them, and the results plotted as the heavy solid line on Fig. 2. Taking $e^{2\sigma}=702$, $\xi=0.0038$ gives a more striking difference between $r(0)/r(Z)$ calculated from (2.13) and $r(0)/r(Z)$ calculated from (3.7) (Table III). And in fact it can be shown that (2.13) becomes a worse approximation as $\rho e^{2\sigma}$ increases: it ceases to be useful about $\rho e^{2\sigma}=0.5$.

The Rate of Approach to Equilibrium

We take the production zero. (2.4) becomes $L/l=1$. To the boundary conditions (2.1) and (2.2) we add

$$\text{At } t=0: \quad R=r=\rho. \tag{4.1}$$

(1.10) may be written as

$$R=\alpha r+\frac{h}{kcC}\left\{\frac{\partial r}{\partial t}-\frac{l}{h}\frac{\partial r}{\partial z}\right\} \tag{4.2}$$

and introducing in (1.9) we obtain

$$\frac{\partial^2 r}{\partial t^2}-(v-V)\frac{\partial^2 r}{\partial t\partial z}-Vv\frac{\partial^2 r}{\partial z^2}=-A\frac{\partial r}{\partial t}+BV\frac{\partial r}{\partial z}. \tag{4.3}$$

v, V, A and B are defined by

$$\begin{cases} A=\dfrac{kcC}{hH}(h+H\alpha) & V=L/H, \\ B=\dfrac{kcC}{h}(1-\alpha) & v=l/h. \end{cases} \tag{4.4}$$

Eliminating R from the boundary conditions, these become

$$\begin{aligned} &\text{At } z=0: \quad \partial r/\partial t-v\partial r/\partial z=Br, \\ &\text{At } z=Z: \quad r=\rho. \end{aligned} \tag{4.5}$$

$$\text{At } t=0: \quad r=\rho, \quad \partial r/\partial z=0, \quad \partial r/\partial t=B\rho. \tag{4.6}$$

Introducing*

$$G(z,p)=\int_0^\infty e^{-pt}r(z,t)dt, \tag{4.7}$$

(4.3) becomes[5]

$$G-\frac{\rho(p+D)}{p^2+Ap}=\frac{(v-V)p+BV}{p^2+Ap}\frac{dG}{dz}+\frac{Vv}{p^2+Ap}\frac{d^2G}{dz^2}, \tag{4.8}$$

* This parametric p will not be confused with the p defined in (2.4).

[5] A problem perfectly analogous to this one, the time dependent equation of the Clusius column, has been treated by J. Bardeen, Phys. Rev. **57**, 35 (1940). The various steps of the operational method, which are sketched in here, are there exposed in more detail.

calling

$$A+B=D=(kcC/hH)(h+H).$$

The boundary conditions transform into

$$\begin{aligned} -vdG/dz&=(B-p)G+\rho \quad \text{at } z=0\\ Gp&=\rho \quad\qquad\qquad \text{at } z=Z. \end{aligned} \tag{4.9}$$

The solution of (4.8) satisfying the boundary conditions (4.9) is

$$pG=\frac{\rho(p+D)-\rho(BD/v)e^{-E_0 z}\gamma^{-1}\sinh\gamma z}{p+A}+\frac{e^{-E_0 z}f(p)g(p,z)}{(p+A)g(p,Z)}, \tag{4.10}$$

where

$$E_0=\frac{(v-V)p+BV}{2Vv}, \tag{4.11}$$

$$E_1=\frac{(v+V)p-BV}{2Vv}, \tag{4.12}$$

$$f(p)=-\rho Be^{E_0 Z}+\rho(BD/v)\gamma^{-1}\sinh\gamma Z, \tag{4.13}$$

$$g(p,z)=E_1\gamma^{-1}\sinh\gamma z+\cosh\gamma z, \tag{4.14}$$

$$\gamma=+\left[\left\{\frac{(v-V)p+BV}{2Vv}\right\}^2+\frac{p^2+Ap}{Vv}\right]^{\frac{1}{2}}. \tag{4.15}$$

And therefore, by the Heaviside expansion theorem

$$r=\rho e^{2\sigma(1-z/Z)}+\sum_j \frac{f(p_j)g(p_j,z)}{(p_j+A)p_j g'(p_j,Z)}e^{p_j t-E_0(p_j)z}, \tag{4.16}$$

where the p_j are the roots of

$$g(p,Z)=0. \tag{4.17}$$

For any column, $v\gg V$ and $A\gg B$. Introducing the quantities $\psi=1/(1-\alpha)$ and $\epsilon=BV/v=2\sigma L/HZ$, and neglecting terms of the order of B/A or V/v

$$E_0=(\sigma/Z)(p/\epsilon+1), \tag{4.18}$$

$$E_1=(\sigma/Z)(p/\epsilon-1), \tag{4.19}$$

$$\gamma=\frac{\sigma}{Z}\left(\frac{p^2}{\epsilon^2}+4\psi\frac{p}{\epsilon}+1\right)^{\frac{1}{2}} \tag{4.20}$$

and (4.17) becomes, discarding a root at $\gamma=0$

$$\tanh\sigma\left(\frac{p^2}{\epsilon^2}+4\psi\frac{p}{\epsilon}+1\right)^{\frac{1}{2}}=\frac{(p^2/\epsilon^2+4\psi p/\epsilon+1)^{\frac{1}{2}}}{1-p/\epsilon}. \tag{4.21}$$

(4.21) has no positive roots. The smallest (and most significant) roots of (4.21) may best be obtained by successive approximations. One solves first the equation

$$\tanh\sigma\left(\frac{p^{0^2}}{\epsilon^2}+4\psi\frac{p^0}{\epsilon}+1\right)^{\frac{1}{2}}=\left(\frac{p^{0^2}}{\epsilon^2}+4\psi\frac{p^0}{\epsilon}+1\right)^{\frac{1}{2}}, \tag{4.22}$$

then the equation

$$\tanh \sigma\left(\frac{p^{12}}{\epsilon^2}+4\psi\frac{p^1}{\epsilon}+1\right)^{\frac{1}{2}}=\frac{(p^{12}/\epsilon^2+4\psi p^1/\epsilon+1)^{\frac{1}{2}}}{1-p^0/\epsilon},$$

etc. The convergence is excellent: p^0-p^1 is in the third significant figure for $\psi=80$. The first approximation gives $p\psi/\epsilon$ as a function of σ alone.

For all ordinary purposes, only the smallest negative root is necessary, and the first approximation to this will be ample. Figure 4 gives a plot of $p_1\psi/\epsilon$ against σ from (4.22).

No simple curve can be constructed to read off the coefficient $f(p_1)/(p_1+A)p_1g'(p_1, Z)$ since this depends on ψ as well as σ. The coefficients of the immediately ensuing terms can, however, be adequately approximated to by $\rho/\sigma\psi p_j$.

Figure 4 gives us immediately the most important information about the approach to equilibrium. From (4.16), setting $z=0$

$$r(0)=\rho e^{2\sigma}-C_1e^{-|p_1|t}-C_2e^{-|p_2|t}-\cdots, \tag{4.23}$$

where the C_1, $C_2\cdots$ are positive constants, and

$$\rho(e^{2\sigma}-1)>C_1\gg C_2>C_3\cdots$$
$$|p_1|\ll|p_2|<|p_3|\cdots.$$

$r(0)$ is given by a fixed term $\rho e^{2\sigma}$ and a series of transient terms, of which $-C_1e^{-|p_1|t}$ is the largest and the slowest to vanish. The time of coming to equilibrium is therefore determined by p_1.

Let us define the quantity $\tau=-1/p_1$, the "period" of the column: it is the time required for the principal transient term to diminish to $1/e$th of its initial value. $p_1=-\epsilon F(\sigma)/\psi$ where $F(\sigma)$ is the ordinate in Fig. 4. Therefore

$$\tau=\frac{\psi}{\epsilon F(\sigma)}=\frac{H}{(1-\alpha)^2\nu LF(\sigma)} \tag{4.24}$$

with $\nu=kcC/L=$number of plates/unit length (2.9). Huffman and Urey[2] found, by other considerations, the same dependence on H, α, ν, and L.

For concreteness, we choose the figures

$$\psi=\frac{1}{1-\alpha}=50,\quad \frac{L}{H}=V=0.238\frac{\text{cm}}{\text{sec.}},\quad \frac{2\sigma}{Z}=1.25\times10^{-3}/\text{cm},\quad \epsilon=\frac{2\sigma V}{Z}=25.9\,\text{deg.}^{-1}=1.08\,\text{hour}^{-1}. \tag{4.25}$$

Holding ψ and ϵ (thus V and the number of plates per unit length) constant, we can vary σ by varying the length of the column (2.8) (Table IV). For all practical purposes equilibrium will have been reached at 3τ.

To find the precise form of an $r-t$ curve, and as an example of a detailed solution, we have computed the first five terms of (4.16), with the roots correct to the third significant figure for $\psi=1/0.0126=79.4$; $\epsilon=25.9$ day^{-1}; $\sigma=0.90$, $e^{2\sigma}=6.05$. The result is

$$\frac{r(0)}{\rho}=6.05-4.61e^{-0.0982t}-0.18e^{-2.11t}-0.05e^{-6.06t}-0.03e^{-12.0t}-\cdots. \tag{4.26}$$

Substituting (4.16) into (4.2), and evaluating, we find likewise

$$\frac{R(Z)}{\rho}=1-0.0139e^{-0.0982t}+0.0025e^{-2.113t}-0.0014e^{-6.06t}+\cdots. \tag{4.27}$$

In both of these t is measured in days. It will be seen that after the first day, only the first two terms contribute to $r(0)$ or $R(Z)$. (4.26) is plotted on Fig. 5, (4.27) on Fig. 6. The transport, which is proportional to $1-R(Z)/\rho$, is also represented on Fig. 6.

It should be noticed that with the aid of the relations between production and fractionation it is possible to determine the time necessary to attain a given rate of production. For purposes of illustration, suppose we want to find how long we must wait before the sixfold column considered in Fig. 5 will produce at maximum fractionation with reflux ratio $p=1\times10^{-3}$. In this case $\theta=1\times10^{-3}/1.26\times10^{-2}=7.9\times10^{-2}$, and from Fig. 2 we find $r(0)/r(Z)=5$. This is the maximum possible fractionation with the given reflux ratio. And, reading off the value from Fig. 5, we see that it requires 14 days to attain this fractionation.

Interpretation of Experiments

In laboratory procedure a single long column (say 30×) is never used since (Table IV) its approach to equilibrium is too slow. Thus the best experimental material is on compound columns of two or three units. Although there is no conceptual difficulty in treating such compound columns as above, the amount of computation would be discouraging, while there is no reason to expect that we could gain much insight into the behavior of the columns. The following comparisons of properties of compound columns with the above results on simple columns are therefore made with due reserve.

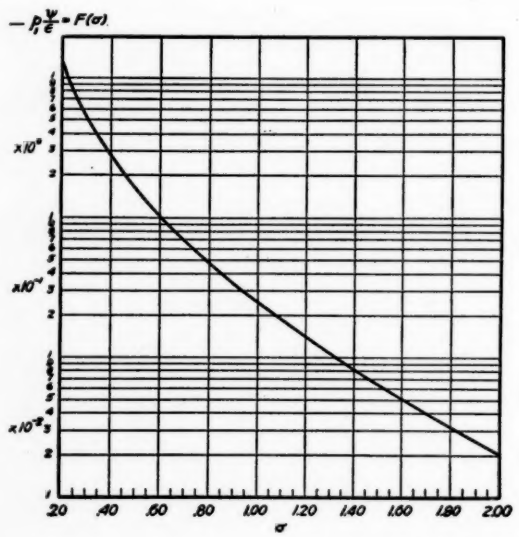

Fig. 4. $-p_1\psi/\epsilon=F(\sigma)$ *vs.* σ. p_1 is the smallest negative root of (4.21).

The approach to equilibrium is found[6] (Fig. 7) to be adequately described by a straight-line relationship between $r(0)/\rho$ and t right up to the maximum value. Figure 5 indicates that equilibrium is approached very slowly after an initial steep rise. The discrepancy is undoubtedly caused by experimental fluctuations in L, which are of the order of 5 percent, and errors in determination of $r(0)/\rho$. Clearly, experimental equilibrium will be reached when fluctuations in $r(0)/\rho$ from these causes is about double the theoretical daily increase in $r(0)/\rho$. This point would be reached, on Fig. 5, after about 15 days. The column would then be at only 5/6 of its true equilibrium. Up to this point, the curve is sufficiently steep to give an experimental straight line. Taking 33 as the experimental equilibrium, the true equilibrium is near $33\times(6/5)=40$.

It was found[6] that drawing off 0.046 mole of HCN per day resulted in a product for which $r(0)/\rho=28$. Taking $1-\alpha=0.026$, we find $\theta=1.9\times10^{-2}$. From the exact curve on Fig. 2, we see that for $\theta=0.019$, $r(0)/\rho$ is reduced from 30 to 21.3. If this ratio were maintained, it would indicate that for $\theta=0$ the HCN units would come to equilibrium at $r(0)/\rho=39$. This is in good agreement with the estimate of true equilibrium made in the preceding paragraph.

It has been the practice, in these laboratories, to take the transport as invariable, proportional to $1-\alpha$. Knowing the distribution in the columns, and having determined experimentally the time necessary to arrive at this distribution, the transport per day and thus $1-\alpha$ was calculated. It is clear from Fig. 6 that the transport is always less than $1-\alpha$, and the average efficiency of the column there considered for the first 15 days is 63 percent. The values of $1-\alpha$ calculated from the transport must represent an effective

Table IV.

σ	$\epsilon^{2\sigma}$ = Fractionation	$F(\sigma)$	τ = Period
0.20	1.5	13.1	3.5 hours
.35	2.0	3.75	12 hours
.70	4.0	.68	2.8 days
.80	5.0	.47	4.1 days
.90	6.0	.34	5.7 days
1.70	30.0	.041	47 days

[6] C. A. Hutchison, D. W. Stewart and H. C. Urey, J. Chem. Phys. **8**, 532 (1940).

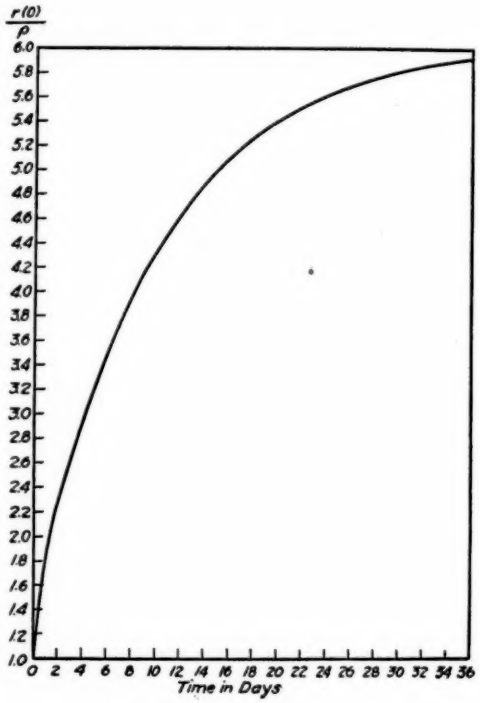

FIG. 5. Approach to equilibrium of a typical column: fractionation *vs.* time.

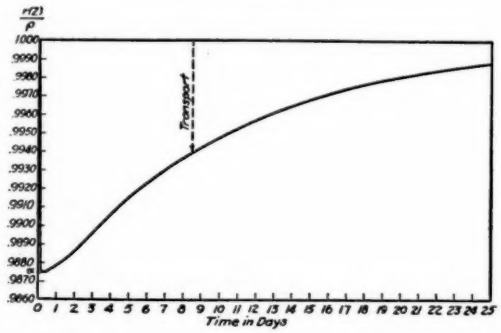

FIG. 6. Ratio of abundance ratios in liquid and in gas at foot of typical column, *vs.* time. Transports are proportional to deviation of curves from unity.

$1-\alpha$, and we should expect them to be less than the theoretical values calculated from band spectra. In the system CN′−HCN(g) the computed value of $1-\alpha$ is 0.026, and the experimental value from the transport is 0.0126: an efficiency of 50 percent.

Presuming the theory, whose postulates certainly seem eminently reasonable, to be sufficiently confirmed, we obtain interesting light on the operation of the columns. Because of the slowness of approach to equilibrium, and also

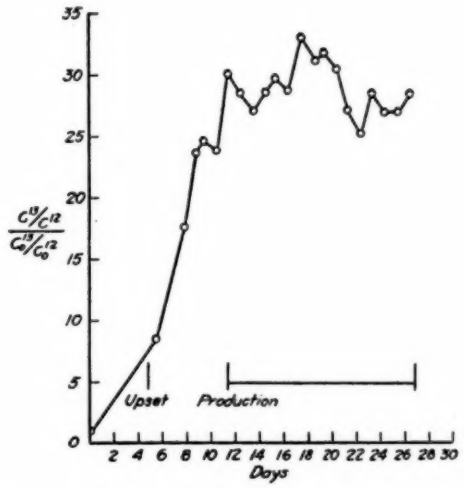

FIG. 7. Fractionation *vs.* time, experimental. Two units working on the system CN^-(aq.)−HCN(g). Hutchison, Stewart and Urey, reference 6.

because of the tremendous loss of efficiency with production, it is not profitable either to wait for equilibrium or to produce near maximum fractionation (for this would mean producing very little). It is preferable to start drawing off as soon as the $r-t$ curve begins to flatten out. One thus reduces the nonproductive time of waiting for equilibrium, and, since the column is at low fractionation efficiency, obtains a respectable yield. Finally, the most economical way of producing a given concentration of isotope is to build a column whose equilibrium fractionation is at least 30 percent larger.

One can obtain from Eqs. (4.24), and (2.8) the best conditions for the run. It can be at once seen that there is every advantage to increasing the concentration of the solution. $(1-\alpha)$ varies inversely as the absolute temperature T, k varies as $T^{1.5}$. There is a slight advantage in fractionation, if it is not counterindicated by other considerations, such as polymerization, to increasing the temperature. However, the period which varies as $(1-\alpha)^2 k$, will be also increased.

ACKNOWLEDGMENT

The author is pleased to acknowledge his indebtedness to Professor Harold C. Urey, who suggested the problem, and to Dr. David W. Stewart for illuminating discussions.

Some Hydrogen Bridge Models for Globular Proteins*

MAURICE L. HUGGINS
Eastman Kodak Company, Rochester, New York

(Received May 8, 1940)

Two hypothetical types of structure, derived by folding from basic patterns containing extended zigzag polypeptide chains, joined together by hydrogen bridges, are described and critically discussed. The (idealized, undistorted) 288-residue open-ended octahedron model has suitable horizontal dimensions but is somewhat too large vertically to fit satisfactorily into the unit cell of air-dried insulin.

WRINCH[1] has proposed that, except for differences in the *R* groups, globular proteins in general have structures derivable from the same type of "fabric," folded, in such a way as to maintain stable bond angles and distances, to give closed polyhedra. Starting with a given type of fabric, she has shown that the possible sizes (i.e., numbers of amino acid residues) of closed polyhedra of a given class (e.g., truncated tetrahedra) are strictly limited. For the "basic cyclol fabric," for example, she deduces structures for molecules containing $72\ n^2$ residues, n being an integer. This ingenious postulate thus accounts for the definiteness of molecular weight for a given globular protein and for the apparent "quantumicity" of molecular weights (or of numbers of amino acid residues) in globular proteins as a class.

The "basic cyclol pattern" and molecular models deduced from it have met with a large number of objections,[2] some of which seem to the writer to be insurmountable. The idea of folding to form a closed system of definite size is, however, also applicable to other types of pattern. Other types of pattern have, in fact, been suggested[3,4] but models of globular proteins derived from these have not been discussed in print.

One of these proposed patterns[3] consists of polypeptide rings held together by means of hydrogen bridges ("hydrogen bonds"). From chemical evidence and by analogy with other known, comparable structures, hydrogen bridging would seem to be much more probable than cyclol condensation as a means of joining together polypeptide chains or rings.

If globular proteins were composed of small rings, containing only a few amino acid residues, however, one would expect to find such small rings among the decomposition products. So far as the writer is aware, they have never been found.

In fibrous proteins, the best available evidence indicates structures consisting of polypeptide chains (extended or coiled) held to each other in sheets or layers by means of hydrogen bridges. One is tempted to try structures of this sort as basic patterns, to see if, on folding, they might produce satisfactory models for globular protein molecules.

In this connection it may be pointed out that Astbury and co-workers,[5] after an x-ray study of several globular proteins, state, "The x-ray interpretation of protein denaturation suggests that it always involves the liberation or generation of peptide chains which aggregate on coagulation into parallel bundles like those found in the structure of β-keratin and similar fibers." With regard to excelsin, for instance, "At the moment it appears that the original crystal structure is symmetrical about a triad axis perpendicular to three dyad axes and that it degenerates into six sets of fibrous crystallites

* Communication No. 762 from the Kodak Research Laboratories. Presented before the Division of Colloid Chemistry at the Cincinnati Meeting of the American Chemical Society, April, 1940. The models discussed in this paper were also briefly described in a paper on "The structure of insulin," presented before the Division of Physical and Inorganic Chemistry at the Baltimore Meeting, April, 1939.

[1] D. M. Wrinch, Proc. Roy. Soc. **A161**, 505 (1937); Trans. Faraday Soc. **33**, 1368 (1937).

[2] See, for example, M. L. Huggins, J. Am. Chem. Soc. **61**, 755 (1939) and L. Pauling and C. Niemann, *ibid.* **61**, 1860 (1939).

[3] D. M. Wrinch and D. Jordan Lloyd, Nature **138**, 758 (1936).

[4] W. T. Astbury and D. M. Wrinch, Nature **139**, 798 (1937).

[5] W. T. Astbury, S. Dickinson and K. Bailey, Biochem. J. **29**, 2351 (1935).

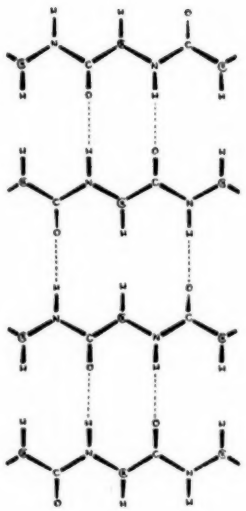

FIG. 1. Hypothetical protein pattern.

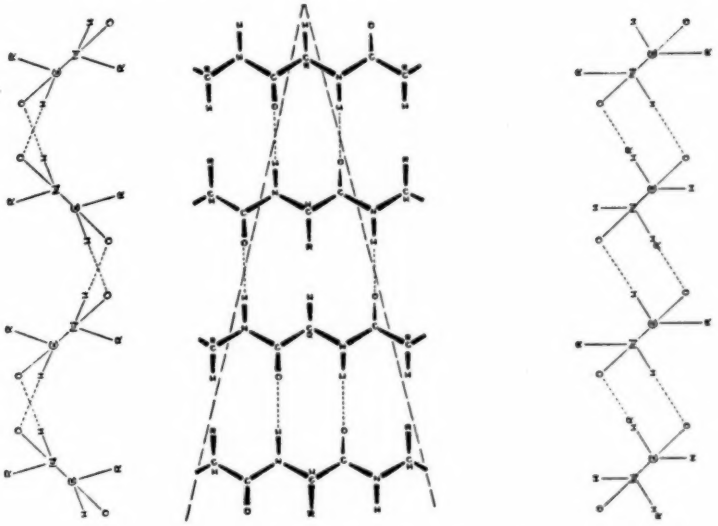

FIG. 2. Hypothetical protein pattern.

lying approximately parallel with the basal plane, with the side-chain spacing also roughly parallel and the backbone spacing roughly perpendicular to this plane."

In this paper will be considered only fabrics which are composed of zigzag polypeptide chains, fully extended or nearly so. Analogy with other known structures (silk, keratin, glycine, diketopiperazine, isatin) suggests that these chains are held together by means of NHO bridges. Tentatively postulating this, we arrive at the two patterns represented in Figs. 1 and 2. In the pattern of Fig. 1, the sequence $-CHR-NH-CO-$ runs in *opposite* directions in adjacent chains; in the pattern of Fig. 2, the sequence is *the same* in all the chains.

The first type (Fig. 1) can be folded, without breaking any bonds or doing violence to any of the accepted ideas regarding bond distances and angles, about lines at right angles to the chain axes. The angle between adjacent "planes" of the fabric at each fold is 120°, if the bond angles are the usual "tetrahedral" angles. By repeated folding, an open-ended hexagonal prism structure can be produced (Fig. 3), in which the polypeptide chains are now large rings. (Folding parallel to the chain axes, to give rodlike prism molecules of indefinite length, is also hypothetically possible. For the present, we shall neglect such models.) If we make the reasonable assumptions that all the faces of the basic framework are alike and that all corners are alike, the number of polypeptide rings must be an even number and the number of amino acid residues in each ring must be a multiple of 12. These requirements thus limit the total number of residues per prism molecule to 24 n, where n is an integer. There would be too much crowding in the interior of prisms composed of rings containing only 12 residues, unless the average interior R group is very small, hence one would expect a minimum ring size of at least 24 residues, corresponding to a molecule size of at least 48 residues. There is nothing apparent in the nature of this model to limit the size further, although one might expect a 2-ring structure to be less stable than one containing 4 or more rings. A molecule containing 288 residues, if built according to this scheme, would be expected to consist of 6 rings of 48 residues each, or 12 rings of 24 residues each.

From the bond distances and angles in diketopiperazine and glycine, one would predict an average distance per residue, along an extended zigzag chain, of about 3.6A. The chain-to-chain distance would be expected to be in the neighborhood of 4A, with this type of structure. The prism faces would, therefore, be expected to be about 29A wide and 20A high (between top and bottom chain axes), for one 288-residue model or 14.5A wide and 44A high for the other. Neither of

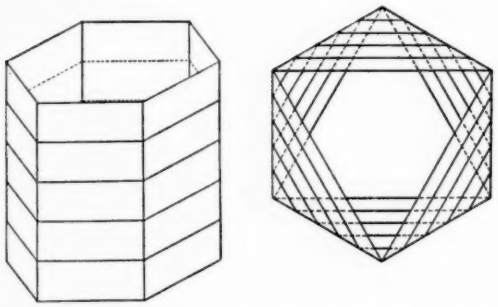

FIGS. 3 AND 4. Illustrating the distribution of polypeptide chain axes in hypothetical molecules derived by folding from structures such as those represented in Figs. 1 and 2.

these alternatives seems to be in accord with the x-ray data for insulin.[6]

The pattern of Fig. 2 folds without strain to give open-ended octahedra (Fig. 4). Making the requirement that all corners are alike, the number of residues per ring must be 12 n and the number of rings 6 n. The total number of residues per molecule is thus 72 n^2. Except for the 72-residue structure, in which there would seem to be too much crowding in the interior, the smallest possible molecule would have 288 residues in the framework. The top and bottom triangular rings would be about 29A on a side (the same as the octahedron edge in the Wrinch cyclol model). Assuming about 4A between chain axes, the molecule would have a vertical height (bottom-chain axis to top-chain axis) of, roughly, 43A. Minor alterations in the structure might decrease this figure somewhat, but it appears unlikely that it could be small enough to enable molecules of this sort to fit into the structure of (air-dried) insulin, for which the unit distance in the direction of the hexagonal axis is 31A.

A discussion of structures similar to the foregoing but containing kinked or folded chains—rather than extended zigzags—will be postponed. For the present, the writer merely wishes to point out that structures of this general nature, which are reasonable from many points of view, have many of the advantages of the cyclol models previously proposed, without some, at least, of their disadvantages.

[6] D. Crowfoot, Proc. Roy. Soc. London, **A164**, 580 (1938).

The Radial Distribution Method in Electron Diffraction

JOHN WALTER AND J. Y. BEACH
Frick Chemical Laboratory, Princeton University, Princeton, New Jersey

(Received April 8, 1940)

A new radial distribution function for use in interpreting the electron diffraction photographs of gas molecules has been obtained. Instead of replacing the inverted Fourier integral by a sum the integration is performed by assuming that the shapes of the maxima and minima are those of cosine functions. The amount of scattering matter $r^2D(r)$ is calculated rather than the density $D(r)$. Comparison between radial distribution functions calculated by this method and by other methods is made for a diatomic molecule, a nonlinear triatomic molecule (to test resolving power), a linear triatomic molecule and carbon tetrachloride.

IN the study of the structure of gas molecules by the electron diffraction method the radial distribution method is frequently used to assist in the interpretation of the photographs. The method consists of taking the theoretical intensity formula which gives intensity of scattering as a function of the distribution of scattering matter in the molecule and inverting it to obtain a formula giving the radial distribution of scattering matter in the molecule as a function of the scattering pattern. This method was first described by Pauling and Brockway.[1] The Pauling and Brockway formula has been modified by Degard[2] and Schomaker[3] to give more reliable results. The formulae differ because of the different approximations which are used in their derivations. We wish to discuss these approximations and to propose a new formula.

METHOD

The complete expression for the coherent scattering by gas molecules is given by the formula[4]

$$I(s)=K\sum_i\sum_j\frac{(Z_i-F_i)(Z_j-F_j)}{s^4}e^{-A_{ij}s^2}\frac{\sin sr_{ij}}{sr_{ij}}, \tag{1}$$

where $s=((4\pi/\lambda)\sin\theta/2)$ and

$$A_{ij}=\overline{\delta r_{ij}^2}/2.$$

This expression can be simplified in accordance with the usual visual method by omitting the s^4 in the denominator, the $Z-F$ and temperature factor, however, being retained. We have calculated the product $(Z_i-F_i)(Z_j-F_j)e^{-A_{ij}s^2}$ for several interatomic distances in several molecules and have found that when s is between 5 and 20 it remains reasonably constant and roughly proportional to Z_iZ_j. As this product, $(Z_i-F_i)(Z_j-F_j)e^{-A_{ij}s^2}$, is dependent only on r it can be replaced by $r^2D(r)$. $r^2D(r)$ is equal to the product whenever r is equal to r_{ij} and is equal to zero otherwise. As $D(r)$ is a density it must be multiplied by r^2 to be proportional to the amount of matter at the distance r. The double sum (1) can now be expressed as an integral

$$I(s)=K'\int_0^\infty r^2D(r)\frac{\sin sr}{sr}dr \quad \text{or} \quad sI(s)=K'\int_0^\infty rD(r)\sin srdr. \tag{2}$$

This is a Fourier integral and can be inverted to give

$$rD(r)=K''\int_0^\infty sI(s)\sin srds. \tag{3}$$

[1] L. Pauling and L. O. Brockway, J. Am. Chem. Soc. **57**, 2684 (1935).
[2] C. Degard, Bull. Soc. Roy. Sci. Liège, 115 (1938).
[3] V. F. H. Schomaker, paper presented to the American Chemical Society, Baltimore, April, 1939.
[4] L. Pauling and L. O. Brockway, J. Chem. Phys. **2**, 867(1934).

$I(s)$ consists of a series of maxima and minima, the positions and intensities of which are measured on the photographs. The shape of a maximum or a minimum can be represented approximately by

$$I(s)=I(s_k)\cos\frac{(s_k-s)\pi}{2a_k},$$

where s_k is the measured position of the maximum or minimum, $I(s_k)$ is the intensity[5] of the maximum or minimum, and a_k is the distance, in s, from s_k to the zero of intensity (minima are given negative intensities). a_k is roughly the half-width of the maximum or minimum. The integral (3) can now be broken up into a sum of integrals, one for each maximum and minimum, giving

$$rD(r)=K''\sum_k I(s_k)\int_{s_k-a_k}^{s_k+a_k} s\cos\frac{(s_k-s)\pi}{2a_k}\sin rsds,$$

which is nearly equal to

$$rD(r)=K''\sum_k s_kI(s_k)\int_{s_k-a_k}^{s_k+a_k}\cos\frac{(s_k-s)\pi}{2a_k}\sin rsds, \tag{4}$$

since s is nearly equal to s_k in the range s_k-a_k to s_k+a_k. This integral can be evaluated in a fairly straightforward manner and is equal to

$$rD(r)=K''\sum_k s_kI(s_k)\frac{4\pi a_k}{\pi^2-4a_k^2r^2}\cos a_kr\sin s_kr$$

or

$$r^2D(r)=K'''r^2\sum_k\frac{\cos a_kr}{\pi^2-4a_k^2r^2}a_kI(s_k)s_k^2\frac{\sin s_kr}{s_kr}. \tag{5}$$

In applying this expression, the product $a_kI(s_k)$, which is proportional to the area of the maximum, should be estimated directly from the photographs. If the peaks are all of the same width, a_k is the same for all maxima and minima, and Eq. (5) becomes

$$r^2D(r)=K'''\frac{r^2a_k\cos a_kr}{\pi^2-4a_k^2r^2}\sum_k s_k^2I(s_k)\frac{\sin s_kr}{s_kr}. \tag{6}$$

The factor $\cos a_kr/(\pi^2-4a_k^2r^2)$ is relatively insensitive to a_k except at large values of r.

Applications and Discussion

If the radial distribution function is to represent the amount of scattering matter at a distance r, the density $D(r)$ must be multiplied by $4\pi r^2$ (the 4π has been dropped in Eq. (6)). The integral (3) has in previous derivations been set equal to a sum with one term for each maximum and minimum. Introducing a cosine function for the shape of a maximum and performing the integration leads to the factor

$$a_k\cos a_kr/(\pi^2-4a_k^2r^2)$$

in Eq. (6). In place of this factor Degard[2] used e^{-ar^2} where a is equal to our a_k. This factor, however, decreases much too rapidly with increasing r. When $a=1$ it decreases by a factor of 500 when r changes from 1 to 3A°, whereas the factor $a_k\cos a_kr/(\pi^2-4a_kr)$ decreases by about 40 percent. e^{-ar^2} is nearly proportional to

$$a_k\cos a_kr/(\pi^2-4a_k^2r^2)$$

if a is about one-tenth of a_k.

The factor s_k^2 in Eq. (6) was originally omitted by Pauling and Brockway. Including it increases the resolving power considerably, makes the peaks sharper and improves their positions slightly. Degard[2] and Schomaker[3,6] included s_k^2.

[5] In this treatment $I(s)$ is assumed to be represented by Eq. (2). In this equation the intensities of the maxima and minima decreases approximately as $1/s$. Therefore the visually estimated intensities should on the average decrease as $1/s$.

[6] Schomaker's function, as it has been used in published electron diffraction work, is:

$$D(r)=\Sigma_kI_k^0s_ke^{-a's_k^2}\sin s_kr/s_kr,$$

where I_k^0 is essentially I_ks_k and $e^{-a's_k^2}=0.1$ for the largest ring.

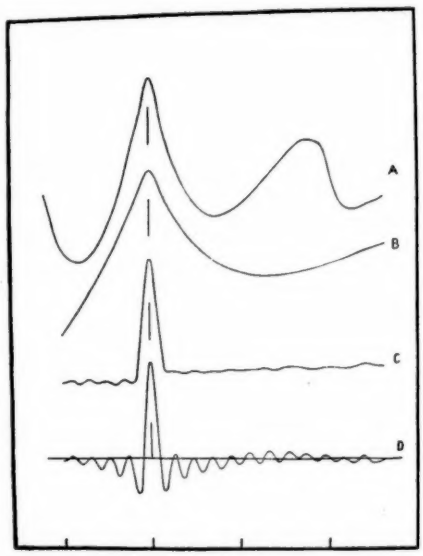

FIG. 1. Radial distribution function for a diatomic molecule ($r=2.00$A). Curve A, ordinary radial distribution function, $D(r)$, using nine maxima. Curve B, ordinary radial distribution function, $D(r)$, using nine maxima and minima. Curve C, modified radial distribution function, $D(r)$, using nine maxima and minima. Curve D, radial distribution function, $r^2D(r)$, present research, using nine maxima and eight minima.

Degard introduced a factor $e^{-as^2k^2}$ into Eq. (6). This was to take into account the $(Z_i-F_i)(Z_j-F_j)$ in Eq. (1). However, if the temperature factor is also included in Eq. (1), we have shown that nothing need be done about the $(Z_i-F_i)(Z_j-F_j)$.[7]

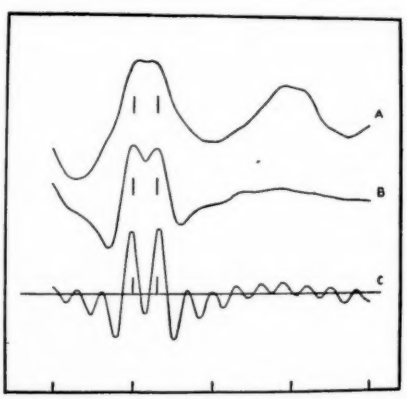

FIG. 2. Radial distribution function for a molecule having interatomic distances of 2.00A and 2.30A. In each case six maxima and five minima were used. Curve A, ordinary radial distribution function, $D(r)$ (maxima only). Curve B, modified radial distribution function, $D(r)$. Curve C, radial distribution function, $r^2D(r)$, present research.

[7] If it were desired to use the radial distribution method to estimate the amplitude of oscillation of an oscillating group the temperature factor should be included to $D(r)$, and some such function as Degard's e^{-as^2} introduced to take care of $(Z_i-F_i)(Z_j-F_j)$.

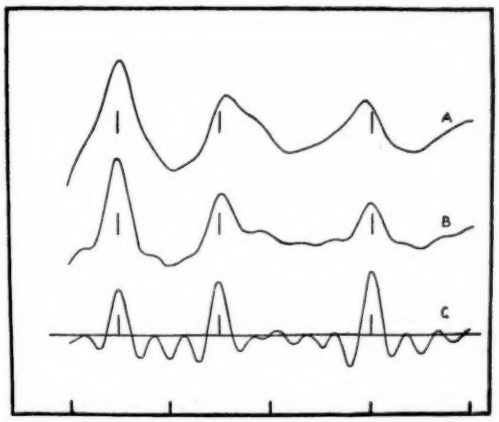

FIG. 3. Radial distribution function for a linear triatomic molecule having interatomic distances 1.50A, 2.50A and 4.00A, using 6 maxima and 6 minima. Curve A, ordinary radial distribution function, $D(r)$ (maxima only). Curve B, modified radial distribution function, $D(r)$. Curve C, radial distribution function, $r^2D(r)$, present research.

The radial distribution function (Eq. (5) or (6)) should possess peaks whose heights are proportional to the average value (with respect to s) of $n(Z_i-F_i)(Z_j-F_j)e^{-A_{ij}s^2}$ (n is the number of interatomic distances at $r=r_{ij}$). We shall now test the method and compare it with the other methods.

We have applied the various radial distribution methods to the theoretical intensity curve for a diatomic molecule ($r=2.00$A). Curve A in Fig. 1 is calculated by the original method of Pauling and Brockway, using maxima only. A bad harmonic appears at about 3.8A. If the minima are included in the same method, curve B is obtained. Curve C is calculated by the method of Schomaker. The peak is much sharper and the base line much flatter. Curve D, calculated by Eq. (6), is even sharper but the base line is not so flat, although it stays closer to the line of zero density (the horizontal line).

To test the resolving powers of the methods we have calculated the theoretical curve for a XY_2 molecule in which $r_{xy}=2.00$A and $r_{yy}=2.30$A. Using these maxima and minima we have calculated the radial distribution functions. In Fig. 2 curve A is calculated by the method of Pauling and Brockway (maxima only), curve B by the method of Schomaker, and curve C by Eq. (6).

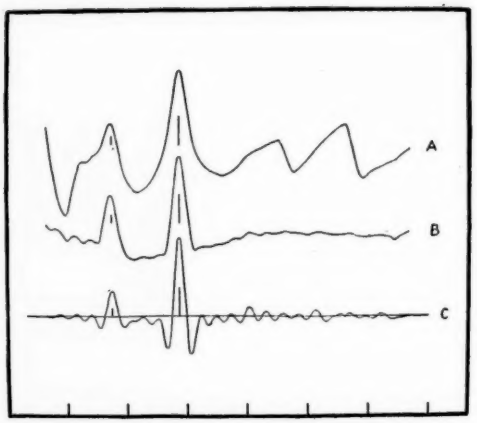

FIG. 4. Radial distribution function for CCl_4, using ten maxima and nine minima. Curve A, ordinary radial distribution function, $D(r)$, (maxima only). Curve B, modified radial distribution function, $D(r)$. Curve C, radial distribution function, $r^2D(r)$, present research.

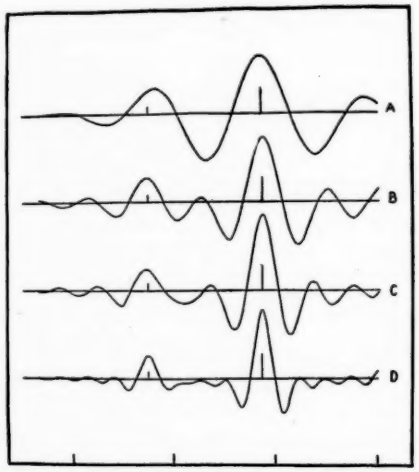

FIG. 5. Radial distribution functions, $r^2D(r)$, present research, for CCl_4. Curve A, three maxima and two minima. Curve B, five maxima and four minima. Curve C, seven maxima and six minima. Curve D, ten maxima and nine minima.

The resolution is seen to improve. In curve C the resolution is a little too good, the two peaks being at 1.98A and 2.32A instead of 2.00A and 2.30A. This is probably due to the fact that only six maxima and five minima were used in the calculation.

Figure 3 shows radial distribution functions calculated from the theoretical intensity curve for an unsymmetrical linear triatomic molecule having distances of equal importance at 1.50A, 2.50A and 4.00A. The peaks on curve A are at 1.52A, 2.57A and 3.93A; those on curve B are 1.50A, 2.52A and 2.98A; and those on curve C are at 1.51A, 2.49A and 4.00A.

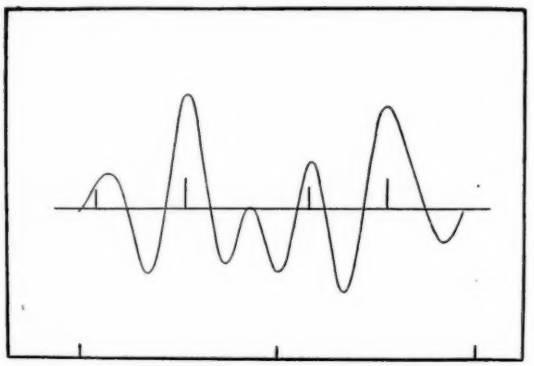

FIG. 6. Radial distribution function for isobutane, $r^2D(r)$, present research.

The theoretical scattering curve was calculated for carbon tetrachloride and radial distribution curves were calculated from it. These curves are shown in Fig. 4. Curve A is slightly different from the one calculated by Pauling and Brockway because their curve was calculated from actual data instead of from the theoretical curve. Curve B calculated by the method of Schomaker, is much smoother than the curve A. The peaks are at 1.75A and 2.87A (assumed values were 1.76A and 2.87A). The peaks on curve C are somewhat sharper and are located at 1.76A and 2.87A. The ratio of their heights above the zero line, 3.1, is nearly equal to the ratio of the average values of $(Z_i-F_i)(Z_j-F_j)e^{-A_{ij}s^2}$ for the two distances, this ratio being 3.2. In Fig. 5 we have reproduced the radial distribution curves for carbon tetrachloride using a smaller number of maxima to show roughly how many maxima are needed to obtain a certain accuracy.

In Fig. 6 is shown a radial distribution for isobutane. The fairly important C−H peak at 2.16A which was not present on previously published curves[8] is now present in the right proportion to the other peaks.

We wish to express our appreciation to Professor Linus Pauling for valuable criticism and advice regarding this paper.

[8] J. Y. Beach and John Walter, J. Chem. Phys., **8**, 303 (1940).

Conductivity in Insulators and Its Interpretation*

A. VON HIPPEL
Electrical Engineering Department, Massachusetts Institute of Technology, Cambridge, Massachusetts

(Received April 17, 1940)

The migration of charge carriers in insulators is discussed in this paper on the basis of a large amount of experimental material on hand. Beginning with deviations from Ohm's law, the trapping of charge carriers is considered and the formation of the "*F*" band in alkali-halide crystals. Then the laws of electronic conductivity in solid dielectrics are formulated.

THE old conception of insulators as "nonconductors" of electricity is dead. It became undermined by accumulating experimental evidence demonstrating that conductivity can be created in insulators if only the proper conditions are chosen. These conditions are manifold and changing from case to case; time and temperature, field strength and illumination, structure and previous history, even the surrounding atmosphere and the contacting electrodes prove to be of importance. The definition "insulator" has become vague; it can mean anything but a metal. Consequently theoretical physics defined insulators directly as "nonmetals" with the help of the zone structure of the electronic levels.[1] But this is not sufficient; detailed knowledge is needed about the elementary processes providing mobile charge carriers and about the laws regulating their motion. These laws of motion are discussed in the following pages.

Deviations from Ohm's Law

The concept of conductivity is normally based upon Ohm's law. It implies constant density of the charge carriers and assumes that they move in the field direction with an average velocity

$$v = bE \qquad \begin{matrix}(b = \text{mobility}) \\ (E = \text{field strength}).\end{matrix} \qquad (1)$$

This assumption of a friction factor $1/b$ independent of the driving force (1) has proved invalid lately in several cases.

M. Wien,[2] measuring the conductivity λ of electrolytes with high impulse voltages (10^5 volt/cm), found an *increase* of λ with field strength to a final value λ_∞, which corresponds to the equivalent conductivity for infinite dilution. This fact was explained[3] with Debye's concept of the ionic atmosphere: Each ion in solution surrounds itself preferentially with ions of the opposite sign, with a space-charge cloud characterized by a radius and a relaxation time. At the high voltages used, the mobility increases because the ions begin to move faster than their atmosphere can form.

Another deviation from Ohm's law was found by the author[4] while studying the laws of electric breakdown in ionic single crystals. In metals the number of free electrons about equals that of the atoms, local space-charge effects cannot develop, and Fermi statistics result. Consequently the electrons have a long free path between inelastic collisions because the coupling with the lattice ions is weak, the time of interaction is short, and the number of free final states into which the electrons can go is limited. In nonmetals such as the alkali-halides the situation is quite different. If surplus electrons exist, their concentration is low; they are slow, because Boltzmann statistics apply, and act as space charges distorting the surroundings. The electrostatic coupling between electron and structure is strong and far-reaching; the electrons are in a state of permanent interaction with the lattice. The probability of exciting lattice vibrations dominates the friction factor $1/b$ of Ohm's law. This probability may be roughly described by an excitation function coordinated to the spectrum of vibrations of the

* Invited paper presented before the Division of Industrial and Engineering Chemistry at the Spring Meeting of the American Chemical Society, Cincinnati, 1940.

[1] See, for instance, F. Seitz and R. P. Johnson, J. App. Phys. **8**, 84, 186 (1937).

[2] M. Wien, Ann. d. Physik **83**, 327 (1927); **85**, 795 (1928).

[3] G. Joos and M. Blumentritt, Physik. Zeits. **28**, 836 (1927); G. Joos, *ibid.* **29**, 755 (1928).

[4] A. von Hippel, Zeits. f. Physik **75**, 145 (1932); J. App. Phys. **8**, 815 (1937).

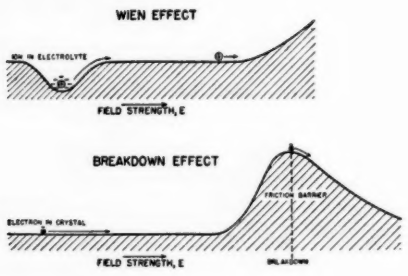

FIG. 1.

material. The interaction time between electron and surroundings decreases with increasing velocity of the electron; therefore the function passes over a maximum above a critical field strength, the friction decreases, and acceleration, impact ionization, and breakdown result.[5]

TRAPPING OF CHARGE CARRIERS

The two deviations from Ohm's law discussed are interrelated, as Fig. 1 illustrates. Debye's ionic atmosphere can be pictured as a potential minimum floating along with the ion under consideration. It represents a polarization of the medium, which is normally slight because the number and mobility of the charge carriers of opposite sign are about equal. In extreme cases, on the other hand, it can become very large, as the movement of protons in palladium indicates;[6] the swarm of electrons around the H^+ in the metal is so dense that the ion responds only with $\frac{1}{25}$ of its charge to an outside field. Wien's effect indicates that the potential cup flattens out in electrolytes when the ions reach velocities of meters per second.

This final state of ionic migration is, thanks to the small electron mass, more or less the initial state of electronic motion. The charge carriers move along, distorting temporarily the electron clouds of the molecules; the nuclei tending to swing into new equilibrium positions set up sound waves.[7] While the heavy ions stay practically at the lower end of this friction barrier of vibrations, the electrons in high fields may pass it (breakdown effect).

The space-charge potential around ions in electrolytes is the first indication of ionic binding; it comes to a full development in lattice structures like rocksalt, where each charge carrier is surrounded by six opposite ions and kept locally trapped in a potential cup several electron volts deep. Figure 1 suggests that also around electrons a polarization of the medium should take place if they are slow enough. In crystals with strong binding forces they do not even need to be very slow, because the ions respond quickly. Hence also electrons should be trapped if they are strongly coupled to locally bound particles.

Such a capture of a surplus electron in a NaCl lattice, for instance, may be described quite graphically: An electron traveling with the kinetic energy of $1/10$ e volt has a wave-length $\lambda = h/mv = 3.8\ 10^{-7}$ cm, and acts therefore like a space charge of one elementary charge spread over a volume λ^3 containing about 2500 lattice ions. The distortion produced is small but far-reaching, thanks to the slow decay of the Coulomb potential with distance. The ions respond with a top frequency higher than $5.7\ 10^{12}$ vibrations per second ("Reststrahl"-frequency); therefore the distant ions have time enough to be somewhat displaced by the electron speeding with a velocity of $1.9 \cdot 10^7$ cm/sec. through the structure. A small potential cup begins to form around the electron; it slows down by dissipating energy into lattice vibrations. But the Coulomb field springing up around the electron, thanks to the lattice distortion, increases the total kinetic energy of the electron because it must oscillate or rotate in this field with a kinetic energy equaling half the potential energy.[8] Therefore the wave-length shortens, space-charge density and interaction time increase, the potential cup deepens into a local trap, and the electron becomes localized around a positive ion of the lattice.

THE "F" BAND OF THE ALKALI-HALIDES

If this picture of electron capture is correct, an optical absorption band should appear, indicating by its location the position of the surplus electrons in the material and by its color the

[5] The quantitative theory is being developed in the last years by H. Fröhlich, R. J. Seeger, and E. Teller, W. Franz and F. Seitz, but has not yet reached a final form.

[6] J. Franck, Nach. Ges. der Wiss., Göttingen **44**, 293 (1933); B. Duhm, Zeits. f. Physik **95**, 801 (1935).

[7] A calculation of the longitudinal vibrations excited is given by E. Teller and his co-workers, Phys. Rev. **57**, 1084A (1940).

[8] N. Bohr, Phil. Mag. **26**, 24 (1913).

energy needed for their photoelectric liberation. Now Pohl and his co-workers[9] have found an absorption band in the alkali-halides, the "*F*" band, which can be created by photo-effect, heat treatment in alkali vapor, or electric current at high temperature. This band moves in the electric field like an electron cloud, as Stasiw[10] first found, and has been identified by the author with the trapping band he expected.[11] But there is a strong controversy at the moment about the correctness of this model; another possibility exists, which we shall consider next, because the discussion of it introduces concepts of importance.

Landau[12] first proposed a quantum-mechanical trapping mechanism for electrons, taking the standpoint that slow electrons cannot be trapped on account of their long wave-length, but that electrons might be captured if speeded up sufficiently by an activation energy. The author came, without knowing of this paper, to the opposite conclusion—that slow electrons will be trapped by the mechanism outlined above. By comparing both processes it can be seen that the Coulomb field of the distorted surroundings performs the service of the activation energy to shrink the wave-length of the electron. Gurney and Mott[13] took first our standpoint—that an electron can be trapped in the ideal lattice—but later they discarded this model[14] in favor of one given by de Boer.[15] De Boer assumes that an electron is captured at a lattice point where a negative ion is missing (Fig. 2). That such vacant lattice points exist can be concluded from the fact of ionic conduction. The ions in an ideal lattice, like rocksalt, fill out the crystal structure by very tight packing; their activation energy is much too high to explain the large conductivity observed. There must be defects in the structure, such as ions in interstitial positions or transferred

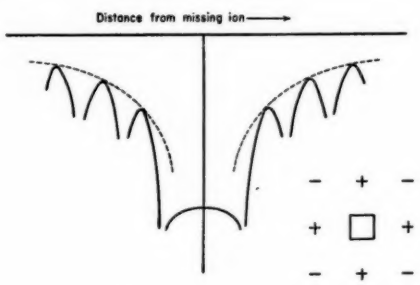

FIG. 2. Potential energy of an electron in the neighborhood of a missing negative ion according to de Boer and Mott. The dotted lines give the curve $-e^2/\kappa r$.

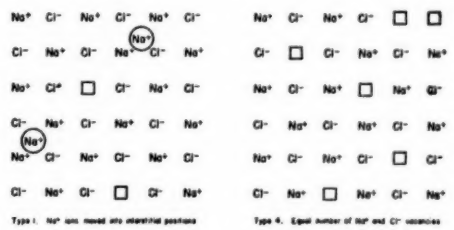

FIG. 3. Lattice disorder.

to the surface, leaving vacant places (Fig. 3) for ionic migration.[16] In NaCl, in thermal equilibrium at 1000°K, about 10^{-5} of the lattice points should be disordered to account for the ionic mobility measured. Frenkel, Wagner, Jost, and Schottky mainly have developed this theory, and Schottky and others[17] have calculated that in the alkali-halides the dominant kind of disorder is his "Type 4" of vacant places (see Fig. 3).

It is of importance to establish which of the two models given above represents the "*F*" band, because a deeper insight into the properties of ideal and defective crystal structures is involved. From the standpoint of our model, a decision might be reached by the following cycle process (Fig. 4): Given the ideal lattice of NaCl and a migrating surplus electron in its conduction band. Now (1) remove one Na^+ ion into vacuum by spending the lattice energy $U_0=183$ kcal. minus a polarization energy U_p, because the lattice around the hole becomes distorted and settles down into a new equilibrium position. U_p, ac-

[9] See, for instance, R. W. Pohl, Proc. Phys. Soc. **49**, 3 (1937).
[10] O. Stasiw, Nach. Ges. Wiss., Göttingen, No. 50 (1933).
[11] A. von Hippel, Ergebnisse d. exakt. Naturwiss. **14**, 113 (1935); Zeits. f. Physik **101**, 680 (1936).
[12] L. Landau, Physik. Zeits. Sowjetunion **3**, 664 (1933).
[13] R. W. Gurney and N. F. Mott, Proc. Phys. Soc. **49**, 32 (1937).
[14] That the reason given at the Bristol Conference (Proc. Phys. Soc. **49**, 36 (1937)) is invalid, has been pointed out already (A. von Hippel, J. App. Phys. **8**, 832 (1937)).
[15] J. H. de Boer, Rec. Trav. Chim. Pays-Bas **56**, 301 (1937).
[16] J. Frenkel, Zeits. f. Physik **35**, 652 (1926); C. Wagner and W. Schottky, Zeits. f. physik. Chemie **11**, 163 (1930); W. Jost, J. Chem. Phys. **1**, 466 (1933); W. Schottky, Zeits. f. physik. Chemie **29**, 335 (1935).
[17] W. Jost and G. Nehlep, Zeits. f. physik. Chemie **32**, 1 (1936); N. F. Mott and M. J. Littleton, Trans. Faraday Soc. **34**, 485 (1938).

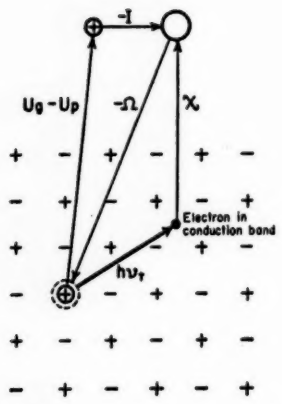

FIG. 4. Cycle for calculation of release energy. (F band.)

cording to Mott and Littleton,[17] amounts to about 77 kcal. (2) Remove the electron from the crystal by spending the energy of the work function $\chi = 11.5$ kcal.[18] (3) Combine electron and ion, gaining the ionization potential $J = 118$ kcal. (4) Place the sodium atom back into the hole; a small energy gain Ω in the order of 37 kcal. results.[18] (5) Remove the electron by light absorption back into the conduction band; the quantum $h\nu_t$ necessary should represent the energy of the "F" band. Result:

$$h\nu_t = -U_0 + U_p - \chi + I + \Omega = 37.5 \text{ kcal.} = 1.63 \text{ ev} \quad (2)$$

as compared with the experimental value 2.73 ev.[19] This difference can be in the limits of error, and the value calculated indicates that an electron will be trapped in the ideal lattice, but a decision between the two models can only be made by new experimental evidence. We are engaged in this study.

ELECTRONIC CONDUCTIVITY IN SOLIDS

Conductivity in solid insulators, as the preceding discussion shows, is normally not produced by a free flow of charge carriers through a resistant medium but by a progression of the charges in jerks. The carriers are trapped after an average displacement distance $\bar{w}$; they stick until the heat vibration of the structure supply with statistical probability the activation energy for their release.

[18] N. F. Mott, Trans. Faraday Soc. **34**, 500 (1938).
[19] E. Mollwo, Zeits. f. Physik **85**, 56 (1933).

For electrons in crystals this conduction process can be followed up step by step in direct experiments. The liberation of the charges can be produced photoelectrically by a narrow light beam; if the insulator is kept cool, no second release of the electrons after capture will take place. The current measured as function of distance between light beam and anode (Fig. 5) reflects directly the decay of the number of charge carriers with the distance of migration.[20] An expo-

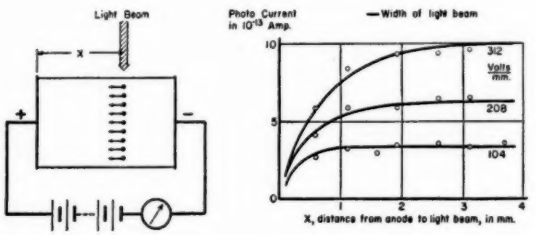

FIG. 5. Measurement of the displacement distance of electrons in AgCl at −186°C.

nential decay law has been found,

$$N = N_0 e^{-x/\bar{w}}; \quad (3)$$

the displacement distance $\bar{w}$ increases proportionally to the field strength applied and has a value $\bar{w}_0$ of $2.5 \cdot 10^{-5}$ cm in AgCl, and of about 10^{-7} cm in NaCl at a field of 1 volt/cm.[21] The large difference between the two crystals of identical lattice structure is to be expected from the picture of electronic migration given in the preceding paragraphs. While the alkali halides are strongly ionic crystals coupling the electron intensely to an extended volume of the material, the silver halides have a large portion of atomic binding, and a much weaker and more limited interaction results. Values for the free path of surplus electrons found by "Hall-effect" measurements give additional evidence. No effect could be found in NaCl[22] indicating that the free path was below 10^{-7} cm, while in diamond crystals a large free path of 10^{-6} cm has been observed.[23] It is quite possible that in atomic structures like diamond the coupling is so weak

[20] W. Flechsig, Physik. Zeits. **32**, 843 (1931); K. Hecht, Zeits. f. Physik **77**, 235 (1932).
[21] G. Glaser, Nach. Ges. der Wiss. Göttingen, **3**, No. 2 (1937).
[22] J. Evans, Phys. Rev. **54**, 47 (1940).
[23] H. Lenz, Ann. d. Physik **77**, 449 (1925); **82**, 775 (1927).

that electrons are not trapped in the free volume but only on boundaries or impurities; such materials should also have a comparatively low breakdown strength if they do not possess electronic excitation levels as a second barrier against impact ionization.

The velocity of the surplus electorns in alkali-halide crystals can be measured by observing the motion of the color centers forming the "F" band or by calculating the density of the centers and the electronic current transferred.[24] An exponential temperature dependence

$$v = v_0 \cdot e^{-U/kT} \tag{4}$$

has been found in this way which can be easily understood. The outside observer, integrating over the intermittent motion of the charge carriers records the average velocity

$$v = \bar{w}/(t_t + t_f), \tag{5}$$

where t_t marks the mean time of capture at one point, and t_f the mean time of free travel between two capture acts. The time t_t is ended statistically by the temperature motion of the crystal supplying the activation energy U for release of the electron

$$t_t = a \cdot e^{U/kT}. \tag{6}$$

t_f is normally $\ll t_t$; therefore the form (4) results

$$v = (\bar{w}/a) \cdot e^{-U/kT} \tag{7}$$

and the conductivity can be written

$$\lambda = N \cdot e \cdot (\bar{w}_0/a) \cdot e^{-U/kT}$$
(N = number of surplus electrons per cm^3). (8)

The factor a measures the degree of coupling between the trapped electron and its surroundings; $1/a$ can be interpreted as the frequency of oscillation produced by this binding. It should be appreciably lower than the "Reststrahl" frequency of the lattice points because the size of an alkali atom is large; therefore the electron will be shared in the trapped state by one central ion and a group of neighbors. With Smakula's values for NaCl:[24] $U = 0.94$ ev, $v_0 = 20$ cm/sec./volt/cm, $T = 973°$K; and Glaser's[21] $\bar{w}_0 = 1.10^{-8}$ cm[25]) for a concentration of color centers 10^{17}/cm^3 we find: $a = 5 \cdot 10^{-10}$ sec., $t_t = 4.9 \cdot 10^{-5}$ sec.; $\nu_t = 1/a = 2 \cdot 10^9$ sec.$^{-1}$ as expected $\ll \nu_r = 5.7 \cdot 10^{12}$ sec.$^{-1}$. With increasing temperature the lattice structure widens, the oscillation frequency goes down, and the maximum of the "F" band shifts towards the red, as observed.[26] The ratio between thermal activation energy U and optical absorption energy $h\nu_t$ is 1 : 2 in the limits of error; this it should be, according to the Franck-Condon principle, if the electron is trapped by lattice distortion.

Equation (8) takes care of the conductivity produced by surplus electrons, but this is only one side of the problem. If these movable charge carriers are created by transferring electrons from a lower filled zone into a conduction band, normally *two* possibilities for conduction are created in each case—one excess electron and one hole (Fig. 6). By treating the hole as positron of electronic mobility, the anomalous Hall effect has been explained,[27] and since that time the theoretical discussion has normally distinguished between the two modes of conduction only by the sign. But the processes may be very different, as the case of the alkali-halides demonstrates. If an electron is transferred from the halogen ion into the conducting state, it represents the excess electron moving along distances $\bar{w}$ between trapping, as discussed; the observer sees a sodium atom moving relatively fast towards the anode. The missing electron at the halogen ion represents the hole; it may also move and transfer the chlorine atom towards the cathode, but it can do so only in jerks $\bar{w}_h$ of atomic distances by electron exchange from neighbor to neighbor. Keeping this difference in mind, the hole conductivity can be represented by an equation like (8)

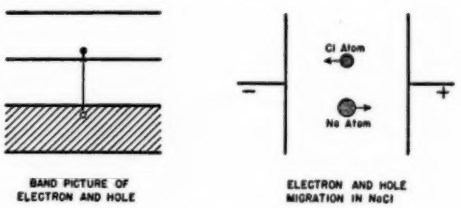

FIG. 6.

[24] A. Smakula, Nach. Ges. der Wiss. Göttingen, **1**, No. 4 (1934).

[25] It is hard to see how such small distances can be explained with the de Boer-Mott model of trapping.

[26] U and v_0 in (4) are therefore dependent on T.

[27] W. Heisenberg, Ann. d. Physik **10**, 888 (1931).

and semiconductors with excess- and defect-conductance can now be treated as individuals characterized by N, $\bar{w}$, a, and U.

Concluding Remarks

The discussion of conductivity in the preceding paragraphs has limited itself to the laws of motion. But charges have not only to be transported, they have to be generated; they have to enter the material and to leave it; they have to be balanced by counter-charges providing the necessary electroneutrality. Only this more general picture, which includes the space-charge effects and field distortion, can explain the peculiar reactions of insulators observed in rectifiers and barrier-layer photo-cells. The author will come back to these questions elsewhere.

AUGUST, 1940 JOURNAL OF CHEMICAL PHYSICS VOLUME 8

Gaseous Heat Capacities. II[1]

G. B. Kistiakowsky and W. W. Rice
Department of Chemistry, Harvard University, Cambridge, Massachusetts
(Received May 8, 1940)

The present paper describes a continuation of the work on the heat capacities of lower hydrocarbons by the Lummer-Pringsheim adiabatic expansion method. The apparatus and the procedure described in the first paper of this series, henceforth to be denoted as Part I, was used in the present research without important modifications.

SINCE an absolute calibration of the resistance thermometer forms the most important feature of the present work, Fig. 1 shows the resistance temperature coefficients of the Wollaston wire which was used in most of the measurements here described. To appreciate the reliability of these coefficients it may be pointed out that in a year's time the resistance of the wire at the ice point has changed by only 0.02 ohm out of a total of 280 ohms. Determinations of the thermal resistance coefficients which were made with every gas studied gave points which fell perfectly on the curve given in Fig. 1.

As discussed in Part I the temperature of the wire does not remain constant after expansion but changes linearly with time. This was tentatively explained as due to absorption of thermal radiation from the warmer walls of the expansion vessel by the gas and it was proposed to minimize the effect by using a vessel with surfaces of very low emissivity. With this idea in mind the present research was conducted with the same expansion vessel and thermometer wires as in Part I except that the inside of the expansion vessel was gold-plated and polished to a mirror-like surface. Unfortunately it was found that the constancy of the wire temperature after expansion was thereby only slightly improved.

The failure of the gold plating to improve the appearance of the experimental records and to reduce experimental errors is very disappointing. However, this failure does not eliminate radiation as the possible source of the temperature inconstancy because at the low temperatures of the experiments rather long wave-lengths may

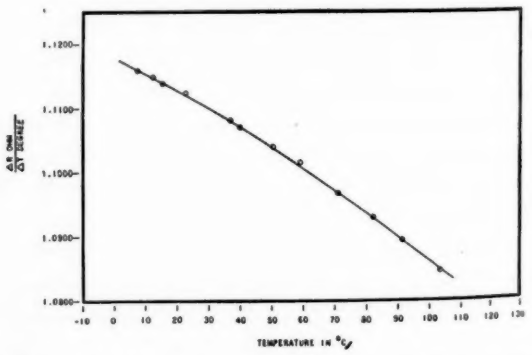

FIG. 1. The resistance-temperature coefficient of the Wollaston wire thermometer plotted against the temperature in °C.

[1] Part I, G. B. Kistiakowsky and W. W. Rice, J. Chem. Phys. **7**, 281 (1939).

be chiefly responsible for the heating of the gas and for these wave-lengths the ordinary unpolished brass surface is hardly a poorer reflector than polished gold plate. Dr. Bernard Lewis has called to our attention the possibility that the changing temperature after expansion may be the evidence that only incomplete energy exchange occurs between the translational and some internal degrees of freedom of the molecules. In that case extrapolation to zero time would give erroneous values of the heat capacities and hence the whole method would be in doubt. However, the perfect agreement of thus measured values with the theory in the case of carbon dioxide and that of ethane (cf. Part I) practically eliminates this possibility and we consider therefore the discussion of errors as given in Part I to apply to the present data also.

An additional error which was insignificant in experiments on ethane makes its presence felt in the present research. It is the correction of the experimental data to the ideal gas state[2] which is so uncertain with some of the gases here discussed that the resultant error is larger than all the other errors.

For some of the hydrocarbons, fortunately, accurate equation of state data have recently been obtained by Lamb and Roper[3] and they form, so to speak, landmarks by which others can be estimated. The general mathematical procedure for the correction to the ideal state was the same as described in Part I. The gas correction for the hydrocarbons allene, propylene and both butene-2 isomers reported here were obtained from Roper's measurements. For propane critical data are available and these were substituted into the Keyes equation of state[4] thus giving the second virial coefficient. The gas correction for propane was also calculated using the Beattie equation of state[5] and the correction was found to agree within 0.02 cal./mole degree with that obtained by the use of the critical data. For propane the critical data used were $T_c = 368.7°K$ and $P_c = 43$ atmos. For methyl acetylene only the critical temperature has been determined and is given as 394.8°K.[6] We have collected therefore, the known critical data for lower hydrocarbons which show that a simple relation exists between the critical temperature and pressure of these compounds (with the exception of acetylene) as seen in Fig. 2. From this graph the critical pressure of methyl acetylene is obtained as 40.5 atmos. if it is assumed that this compound obeys

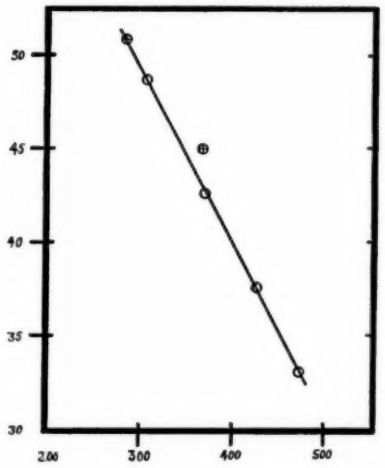

FIG. 2. A graph of the critical pressure *vs.* the critical temperature for the C_2, C_3 and C_4 hydrocarbons. Circles represent the saturated hydrocarbons; circles with crosses represent the unsaturated hydrocarbons.

TABLE I. *Correction to ideal state. All values in cal./mole degree.*

		$C_p^0 - C_p'$			$C_p - C_p'$	
T°K	COMPOUND	CALC. 1	CALC. 2	CALC. 3	CALC. 1	CALC. 2
270	Acetylene	.02	.07			
270	Ethylene	.07	.06	.06		
270	Ethane	.14	.12			
272	Propylene	.30	.30		.62	.50
272	Allene	.27		.33		
299	*Trans*-butene-2	.90		.78		
370	Ethylene	.05	.05	.05		
370	Ethane	.09	.08			
367	Propylene	.17	.18			
367	Allene	.15		.20		
370	*Trans*-butene-2	.55		.47		

Calc. 1 from the known equation of state data.
Calc. 2 from the known critical data and the Keyes equation of state.
Calc. 3 from the known critical temperature, graphically estimated critical pressure and the Keyes equation of state.

[2] The recalculations of the second virial coefficient of ethane by E. E. Roper (J. Chem. Phys. **8**, 290 (1940)) from the data of Eucken which was used in Part I, changes the heat capacity data there given by less than 0.01 cal./mole degree. The value of the gas constant (R) used in all these calculations was taken as 1.9864 cal./mole degree. The thermodynamic temperature of the ice point was taken as 273.16°K.

[3] A. B. Lamb and E. E. Roper, J. Phys. Chem. (to appear shortly).

[4] F. G. Keyes, J. Am. Chem. Soc. **60**, 1761 (1938).

[5] Beattie, Kay and Kaminsky, J. Am. Chem. Soc. **59**, 1589 (1939).

[6] F. R. Morehouse, Can. J. Research **5**, 306 (1931).

TABLE II. *Heat capacity of allene.*

No. of Runs	T_{Av} °K	Range of ΔP mm	P_{final} av. mm	$\frac{dR \text{ ohm}}{dT \text{ deg.}}$	Rad. Corr. Percent	C_p'	C_p	C_p^0 cal. / deg. mole^{-1}	C_p^0 calc.
6	272.16	40.230–29.048	759.65	1.2245	0.16*	12.93±.03	13.56	13.20	13.27
5	300.00	33.614–16.081	754.70	1.1110	.11	13.96±.02	14.42	14.18	14.16
6	334.00	33.731–18.100	752.20	1.1004	.12	15.06±.03	15.41	15.25	15.23
6	366.45	34.752–16.649	754.80	1.0887	.13	16.08±.02	16.34	16.22	16.23

* The wire used in these measurements was annealed less extensively.

TABLE III. *Heat capacity of methyl acetylene.*

No. of Runs	T_{Av} °K	Range of ΔP mm	P_{final} av. mm	$\frac{dR \text{ ohm}}{dT \text{ deg.}}$	Rad. Corr. Percent	C_p'	C_p^0 cal. / deg. mole^{-1}	C_p^0 calc.
5	272.28	37.094–28.454	768.10	1.1182	0.11	13.42±.01	13.76	13.77
5	299.59	37.080–28.274	772.10	1.1110	.12	14.29±.02	14.58	14.58
5	332.83	34.923–31.447	770.80	1.1010	.16	15.31±.01	15.56	15.55
6	369.21	35.555–24.721	768.30	1.0876	.20	16.31±.03	16.52	16.56

TABLE IV. *Heat capacity of cyclopropane.*

No. of Runs	T_{Av} °K	Range of ΔP mm	P_{final} av. mm	$\frac{dR \text{ ohm}}{dT \text{ deg.}}$	Rad. Corr. Percent	C_p'	C_p^0 cal. / deg. mole^{-1}	C_p^0 calc.
5	272.15	36.754–28.622	762.80	1.1182	0.13	11.83±.02	12.10	12.13
5	300.48	37.785–28.231	766.00	1.1108	.12	13.28±.02	13.50	13.47
5	333.70	37.710–26.456	767.10	1.1006	.14	14.91±.03	15.10	15.11
6	368.46	39.244–25.083	769.20	1.0878	.20	16.62±.03	16.77	16.82

the normal relation. These critical values for methyl acetylene were used in the Keyes equation to obtain the gas correction for this compound. For cyclopropane, finally, no critical data are available; since the boiling point of this substance is very close to that of allene, it was assumed that the second virial coefficients are identical.

Table I gives the results of calculations of the correction to the ideal state by the different methods here outlined, insofar as enough data were available to perform more than one calculation on the same substance. The data of the first column were obtained from reliable equation of state data and should be accurate to 0.02 to 0.04 cal./mole degree depending on the magnitude of the correction. For acetylene, measurements of Schaefer[7] were available: for ethylene, measurements of Roper and for ethane, measurements of Eucken.[8]

The agreement of the first column in Table I with the other two shows that the errors due to extrapolation to the ideal state are about 0.05 to 0.08 cal./mole degree for gases for which no accurate equations of state are available. For cyclopropane they may rise to as much as 0.1 cal./mole degree because of the complete lack of experimental data. These errors are estimated to apply only to the correction from C_p' to C_p^0. When the Keyes equation is employed to determine C_p (the heat capacity at a pressure of approximately one atmosphere) very much larger errors are committed. This is demonstrated in Table I for the case of propylene and it is found that the Keyes equation gives too low values for both dB/dT and d^2B/dT^2, so that the calculation of C_p results in too low values. This is especially true at temperatures near the boiling point of the compound. Fortunately, however, in the further correction to C_p^0 the first error is almost completely compensated.

In the following paragraphs we shall take up, one by one, the five hydrocarbons with which this paper is concerned.

[7] K. Schaefer, Zeits. f. physik. Chemie **B36**, 85 (1937).
[8] Eucken and Parts, Zeits. f. physik. Chemie **B20**, 184 (1933).

Allene (C_3H_4)

The sample of allene used in these heat capacity determinations was part of the material used in the measurements of the heat of hydrogenation by Kistiakowsky and co-workers.[9] It was contaminated by air and moisture and was therefore subjected to repeated bulb to bulb distillations in vacuum, pumping after each distillation, and was finally distilled into the expansion vessel and the storage flasks.

Table II presents the summary of the experiments on allene. None of the experiments have been disregarded because of too large deviations from the mean in forming the averages of this table. The same is true of other heat capacity tables given in this paper.

In this table and those following, T_{Av} represents the average of the temperature of the gas before and after expansion, ΔP gives the pressure change of the gas upon expansion, P_{final} represents the average barometric pressure for the series of runs, dR/dT is the temperature coefficient of resistance for the thermometer wire. The column labeled "Radiation Correction" is discussed in Part I. The next column gives C_p', the uncorrected heat capacity as given by Eq. (3b) in Part I and the mean deviation from the average. C_p gives the heat capacity of the gas at atmospheric pressure, see Eq. (3a) in Part I, and C_p^0 represents the heat capacity of the gas at infinitely low pressure. Finally the last column of the table gives the theoretical heat capacities calculated using the harmonic oscillator rigid rotator model with the frequency assignment which has been given by Linnett and Avery:[10] 2992(1), 1430(1), 1069(1), 820(1), 3000(1), 1968(1), 1389(1), 3062(2), 1031(2), 852(2), 353(2), all frequencies in cm^{-1} and the numbers in parenthesis indicating the statistical weights attached to each frequency.

The agreement between the experimental and theoretical values is excellent. Only at the lowest temperature is the difference slightly larger than the mean deviation of the individual experimental values from the average. The experiments at this temperature however were made much earlier than the rest of the experiments, using a wire which was not so thoroughly annealed. This same wire gave less satisfactory results also in the work on air (see Part I). The agreement between the experimental and the theoretical heat capacities may be regarded as an indication of the correctness of the above vibrational assignment. In fact, the agreement of experimental and theoretical values in Table I is somewhat better than we should expect allowing for the accidental and systematic experimental errors and the uncertainty of extrapolation to the ideal gas state. Together these errors may amount to as much as 0.4 percent. On the other hand the molecular model used in the theoretical calculations is probably too simple but the effect of this on the heat capacity we cannot estimate. It may be only suggested that all these errors cancel more or less accidently.

Methyl Acetylene (C_3H_4)

A sample of methyl acetylene was available from the work on its heat of hydrogenation[11] and it was used without purification except for an ordinary bulb to bulb distillation in vacuum.

Table III presents a summary of the experimental data for methyl acetylene. The theoretical heat capacities have been calculated using the harmonic oscillator, rigid rotator model and the vibrational frequencies proposed by Crawford[12] who suggests the following: 926(1), 1380(1), 2125(1), 2910(1), 3300(1), 333(2), 642(2), 1035(2), 1444(2), 2975(2). The frequencies were ob-

Table V. *Corrected values for the free energy, entropy and heat capacity of cyclopropane.*

$T°K$	$-(F-E_0^0)/T$	S	C_p^0
100	38.71	46.66	7.96
150	41.93	49.92	8.25
200	44.25	52.43	9.30
250	46.11	54.69	11.14
300	47.73	56.92	13.44
350	49.21	59.18	15.88
400	50.60	61.46	18.33
500	53.22	66.03	22.64
600	55.72	70.47	26.14
700	58.15	74.73	29.04
800	60.47	78.78	31.45
900	62.71	82.61	33.57
1000	64.90	86.24	35.37

[9] Kistiakowsky, Ruhoff, Smith and Vaughan, J. Am. Chem. Soc. **58**, 146 (1936).
[10] J. W. Linnett and W. H. Avery, J. Chem. Phys. **6**, 686 (1938).
[11] Conn, Kistiakowsky and Smith, J. Am. Chem. Soc. **61**, 1868 (1939).
[12] B. L. Crawford, J. Chem. Phys. **7**, 140 (1939).

TABLE VI. *Heat capacity of propylene.*

No. of Runs	T_{Av} °K	Range of ΔP mm	P_{final} av. mm	$\frac{dR \text{ ohm}}{dT \text{ deg.}}$	Rad. Corr. Percent	C_p'	C_p	C_p^0 cal. / deg. mole^{-1}
5	272.29	37.937–32.379	765.40	1.1182	0.11	14.06±.03	14.68	14.36
5	299.33	37.798–23.211	765.30	1.1110	.11	15.22±.03	15.68	15.47
6	333.86	36.182–22.441	769.75	1.1006	.11	16.54±.04	16.88	16.74
5	367.11	35.656–19.363	772.30	1.0884	.14	17.76±.02	18.03	17.93

TABLE VII. *Calculated heat capacity of propylene.*

T_{Av} °K	C_p^0 Exp.	C_{vib} Assignment used by K. L. R.	$C_{i.r.}$ Assignment used by K. L. R.	C_{vib} Assignment by P.	$C_{i.r.}$ Assignment by P.	C_{vib} Assignment by W. and W.	$C_{i.r.}$ Assignment by W. and W.	$C_{i.r.}$ $V=800$	$C_{i.r.}$ $V=2100$ cal./mole
272.29	14.36±.03	5.268	1.15	5.021	1.39	4.331	2.08	1.38	2.13
299.33	15.47±.03	6.399	1.12	6.115	1.40	5.337	2.19	1.30	2.11
333.86	16.74±.04	7.882	.91	7.566	1.21	6.679	2.11	1.26	1.98
367.11	17.93±.02	9.279	.70	8.924	1.06	7.995	1.99	1.24	1.89

tained by Crawford from the Raman spectrum of liquid methyl acetylene and hence it is not excluded that the true frequencies of the gaseous molecule are slightly higher than the above. However the resultant change in the theoretical heat capacity should be quite small and will not alter materially the excellent agreement of the experimental and theoretical values given in Table III. The present work therefore provides strong support for Crawford's analysis of the vibrational spectrum of methyl acetylene.

CYCLOPROPANE (C_3H_6)

The sample of cyclopropane was obtained through the courtesy of Dr. V. H. Wallingford of the Mallinckrodt Chemical Company to whom we wish to express our indebtedness. It was part of the material which was analyzed by Dr. F. D. Rossini of the National Bureau of Standards who found 0.25 mole percent of some impurity.[13] The sample was freed from air and moisture by bulb to bulb distillations in vacuum so that the remaining impurity should be composed of substances with heat capacities not greatly different from that of cyclopropane. The uncertainty in the experimental heat capacity values resulting from this effect is certainly less than 0.25 percent. Table IV gives the experimental heat capacities obtained for cyclopropane.

Linnett[14] has studied the Raman and infra-red spectrum of cyclopropane and was able to give a frequency assignment to all normal vibrations but one. Using the heat capacity data of the hot wire method, then available in this laboratory, he concluded that the unknown frequency is 1250 cm^{-1}. This value gave satisfactory theoretical heat capacities and was used to explain the observed 385 cm^{-1} frequency as a difference (1250–865).

Theoretical heat capacities calculated on Linnett's original assignment for cyclopropane deviate from the present experimental data by approximately 0.1 to 0.2 cal./mole degree, at the lowest and the highest temperatures, respectively. The theoretical heat capacities presented in Table IV have been calculated therefore with the following assignment: 3000(1), 1485(1), 1187(1), 1070(1), 3000(2), 1435(2), 1022(2), 860(2), 1000(1), 3050(1), 1041(1), 3080(2), 1125(2), 740(2), which differs from that of Linnett in that 1125 cm^{-1} is taken as the frequency of the unknown vibration. They are seen to be in excellent agreement with the experimental data. The new choice of the unknown frequency has the further advantage that the observed 385 cm^{-1} frequency can be represented now as a transition from the lowest vibrating state of the molecule, or (1125 −740=385). This transition is permitted by the selection rules as an inspection of Linnett's paper will readily show.

The values of the thermodynamic functions of cyclopropane as calculated by Linnett are

[13] Private communication from Dr. Wallingford.
[14] J. W. Linnett, J. Chem. Phys. **6**, 692 (1938).

changed only very slightly by the suggested modification of the fundamental frequencies, cf. Table V.

Propylene (C_3H_6)

The propylene used in the present measurements was part of the material obtained for the determination of its heat of bromination,[15] and was stated to be of 99.9 percent purity. It was contained in the original cylinder but like the other hydrocarbons discussed in this paper was subjected to repeated bulb to bulb distillations in vacuum, to remove traces of air and water before using. Table VI presents the summary of the experimental heat capacities obtained for propylene.

In a preliminary note Kistiakowsky, Lacher and Ransom[16] have discussed the heat capacity data of propylene at low temperatures obtained by the hot wire method. They concluded that the experimental data was in agreement with the suggestion of Pitzer[17] that the internal rotation of the methyl group in propylene is hindered by a potential barrier of 600 to 800 cal./mole, there being three positions of minimum potential energy.

As a means of comparison we have compiled Table VII which gives in the second column a summary of the new experimental data on the heat capacity of propylene. Column three records the vibrational contribution to the heat capacity at the various temperatures according to the assignment used by Kistiakowsky, Lacher and Ransom. Column four gives the residues obtained on deducting the vibrational heat capacity plus $4R$ from the experimental values for the heat capacity. This should be the heat capacity due to internal rotation, but since the values decrease considerably below the classical value of $(\frac{1}{2})R$ for free rotation at the higher temperatures it is evident that the vibrational assignment is erroneous. The next two columns contain the vibrational heat capacity and the contribution due to internal rotation calculated from an approximate vibrational assignment given by Pitzer,[17] and the following two columns similar calculations using the recently developed vibrational assignment of Wilson and Wells,[18] based on an assignment which is still only provisional, although based upon an experimental study of the infra-red and Raman spectra of propylene and a normal coordinate treatment of the molecule. This assignment is given as: 432(1), 580(1), 921(1), 940(1), 1000(1), 1022(1), 1100(1), 1111(1), 1297(1), 1399(1), 1445(1), 1468(2), 1647(1), 3000(6), cm^{-1}. The last two columns of the Table VII contain internal rotation contributions calculated from Pitzer's tables[19] for the potential barrier of 800 cal./mole and Crawford's method[20] for the higher barrier of 2100 cal./mole.

On the basis of Table VII alone a final decision between Pitzer's assignment and a low potential barrier or the Wilson-Wells assignment and a high barrier would be difficult, although the differences between experimental and calculated data can be better smoothed out by a small change in the height of the barrier in the latter case. The better agreement between the Wilson-Wells calculation and experiment is more pronounced at lower temperatures, where the hot wire method has been used. Finally, the third law entropy data on propylene, obtained recently by Powell and Giauque,[21] favors strongly the higher barrier.

These authors themselves draw the conclusion that the third law is inapplicable to propylene because their experimental entropy is lower by about 1 E. U. than that calculated using the low potential barrier and either the Pitzer or the K., L., and R. vibrational assignment. However, with the Wilson-Wells assignment and the 2100 cal./

Table VIII. *Theoretical and experimental entropy of propylene.*

	225.35°K	298.1°K
$S_{(t.+r.)}$	57.00	59.23
$S_{(vib)}$	.89	2.00
$S_{(i.\ r.)}$ ($V=2100$ cal./mole)	1.98	2.58
$S_{(total\ calc.)}$	59.87	63.81
$S_{(Third\ Law)}$	59.93	63.86*

* $S_{298.1}-S_{225.3}$ obtained by graphical integration of the experimental heat capacity curve.

[15] Conn, Kistiakowsky and Smith, J. Am. Chem. Soc. **60**, 2766 (1938).
[16] Kistiakowsky, Lacher and Ransom, J. Chem. Phys. **6**, 900 (1938).
[17] K. S. Pitzer, J. Chem. Phys. **5**, 473 (1937).
[18] Crawford, Kistiakowsky, Rice, Wells and Wilson, J. Am. Chem. Soc. **61**, 2980 (1939).
[19] K. S. Pitzer, J. Chem. Phys. **5**, 469 (1937).
[20] B. L. Crawford, J. Chem. Phys. **8**, 273 (1940).
[21] T. M. Powell and W. F. Giauque, J. Am. Chem. Soc. **61**, 2366 (1939).

TABLE IX. *Heat capacity of propane.*

No. of Runs	T_{Av} °K	Range of ΔP mm	P_{final} av. mm	$\frac{dR}{dT}$ ohm deg.	Rad. Corr. Percent	C_p'	C_p	C_p^0 cal. deg. mole^{-1}
6	272.38	37.954–30.245	765.36	1.1182	0.10	15.84±.01	16.39	16.19
7	300.37	41.380–30.669	761.80	1.1108	.11	17.28±.02	17.73	17.58
7	334.05	41.878–32.450	753.85	1.1004	.15	18.98±.02	19.35	19.25
6	368.55	40.367–31.583	763.05	1.0878	.17	20.67±.01	20.97	20.90

mole potential barrier, the experimental entropy is perfectly reproduced, as shown in Table VIII where the experimental entropy increase from 225.35°K to 298.1°K was calculated from a graphical integration of the now available experimental heat capacity data (including hot wire data at the lower temperatures). The correction for the hindrance of internal rotation was made with Crawford's treatment.[18] It becomes therefore unnecessary to suppose that in crystals of propylene end-over-end randomness exists, a randomness which is difficult to understand in view of very different properties of the CH_2 and CH_3 terminal groups. Pitzer[22] has recently criticized our selection of the higher potential barrier for propylene because he is unable to obtain agreement between calculated equilibrium constants in the propane, propylene and hydrogen reaction and those measured by Frey and Huppke.[23] However he is using an unquestionably wrong vibrational assignment for propane (see the following section) and if the assignment here proposed and tested on the heat capacity data for propane is taken, the statistical equilibrium constant is found to be 0.0014 at 673°K while the experimental value is 0.0022. The discrepancy between these figures is not as serious as Pitzer leads one to believe. Even the determination of the ethane, ethylene equilibrium by Frey and Huppke gave too high equilibrium constants[24] and the authors themselves point out that less satisfactory results were obtained for higher hydrocarbons.

PROPANE (C_3H_8)

The sample of propane was obtained by the hydrogenation of 99.9 percent propylene of the same material described above and according to the method of Kistiakowsky and co-workers.[25] In order to secure as pure a sample of propane as possible the first portion of the hydrogenation was entirely discarded, a sample was then collected and tested for olefins. The test showed about 0.002 mole percent of unsaturated compounds present. In obtaining the sample extreme care was taken to allow no moisture to contaminate it. The sample of propane was transferred to the vacuum system and subjected to repeated bulb to bulb distillations. The middle portion of the sample only was used. Table IX presents the summary of the experimental data on propane.

Sage, Webster and Lacey[26] have measured the heat capacity of propane over a similar temperature range as given in Table IX. Table X gives a comparison of the heat capacities determined by Sage, Webster and Lacey and our measurements interpolated to their temperatures by graphical means and calculated to 1 atmos. pressure of real gas. The molecular weight of propane was taken as 44.06 in computing Sage, Webster and Lacey's data to our scale. We are at a loss to explain the large discrepancy between the two sets of measurements which is many times greater than our experimental errors including the gas correction.

Kemp and Egan[27] have measured the third

TABLE X. *Heat capacity of propane.*

T°K	C_p (S. W. and L.)	C_p (K. and R.)
294.31	17.83	17.41
311.00	18.29	18.25
327.60	18.77	19.04
344.30	19.27	19.81
361.00	19.78	20.61

[22] Petroleum Symposium, Am. Chem. Soc. Meeting in Cincinnati, 1940.
[23] F. E. Frey and W. F. Huppke, Ind. Eng. Chem. **25**, 54 (1933).
[24] Smith and Vaughan, J. Chem. Phys. **3**, 341 (1935).
[25] Kistiakowsky, Romeyn, Ruhoff, Smith and Vaughan, J. Am. Chem. Soc. **57**, 65 (1935); *ibid.* **57**, 876 (1935).
[26] Sage, Webster and Lacey, Ind. Eng. Chem. **29**, 1309 (1937).
[27] Kemp and Egan, J. Am. Chem. Soc. **60**, 1521 (1938).

law entropy of propane obtaining for the ideal gas at one atmosphere pressure and 231.04°K the value of 60.45±0.10 E. U. Their statistical calculations for the entropy showed that the experimental value for the entropy and the statistical calculations could be brought into agreement with the assumption of a potential barrier of 3300 cal./mole restricting rotation of the methyl groups; this confirmed the conclusions drawn by Pitzer.[17] Kistiakowsky, Lacher and Ransom[16] found from low temperature heat capacity measurements that a barrier of 3200 to 3600 cal./mole gave the best fit for the heat capacity data, but that the vibrational assignment used by Kemp and Egan and that given by Pitzer both gave systematic trends of the barrier with temperature, indicating that the vibrational assignments were in error. As Table XI shows, neither of these vibrational assignments is consistent with the present heat capacity data. In the third and fourth columns of this table have been given vibrational heat capacities and those due to internal rotation on the basis of Pitzer's assignment, while columns five and six reproduce similar calculations taking the Kemp and Egan choice of frequencies. Variable internal rotation restricting potentials reaching 10,000 cal./mole are necessary to reconcile these data with experiment,[28] as will be seen on inspecting the last column in which are given heat capacity contributions from the restricted rotation of two methyl groups with a potential barrier of 3300 cal./mole.

Kohlrausch and Koppl[29] have studied the Raman spectrum and Bartholome[30] has studied both the Raman and the infra-red spectrum of propane. With these observed frequencies and by a comparison with other molecules we have arrived at the following assignment for the vibrational frequencies for propane: 373(1), 870(1), 940(1), 3000(8), 1450(7), 735(1), 1150(1), 1278(1), 1050(2), 1250(2). Insofar as was possible, only the observed frequencies have been used. However the last two frequencies have been chosen to fit the internal rotational heat capacity curve calculated on the basis of a barrier of 3300 cal./mole, using Pitzer's tables. The results are shown in columns seven and eight of Table XI. It is seen that the agreement is quite good, but of course cannot be regarded as conclusive until the assignment has been checked by a normal coordinate treatment of the molecule.

TABLE XI. *Calculated heat capacity of propane.*

T_{Av} °K	C_p^0 EXP.	C_{vib} ASSIGNMENT BY P.	$C_{i.r.}$	C_{vib} ASSIGNMENT BY K. AND E.	$C_{i.r.}$	C_{vib} K. AND R.	$C_{i.r.}$	$C_{i.r.}$ calc $V=3300$ CAL./MOLE
272.38	16.19	4.819	3.42	4.938	3.32	4.300	3.94	4.04
300.37	17.58	6.122	3.52	6.254	3.38	5.457	4.18	4.16
334.05	19.25	7.810	3.50	7.945	3.36	6.955	4.36	4.26
368.55	20.90	9.539	3.40	9.674	3.28	8.571	4.38	4.32

TABLE XII. *Theoretical and experimental entropy of propane.*

	231.04°K	298.1°K
$S_{trans+rot}$ assuming free rotation (as given by Kemp and Egan)	62.80	65.33
S_{vib}	1.03	2.05
$S_{total\ calc}$	63.83	67.38
S_{exp}	60.45	64.62
$S_{calc}-S_{exp}$	3.38	2.76
Internal barrier from $S_{calc}-S_{exp}$ and Pitzer's tables	3200 cal./mole	3100 cal./mole

The theoretical entropy calculations given by Kemp and Egan[27] for propane were corrected at 231°K and 298°K using our frequency assignment. We have also integrated our heat capacity curve (using hot wire data at lower temperatures) in order to get the experimental entropy at 298.1°K. Table XII gives the summary of these calculations.

In concluding this article we should like to point out that surprisingly good agreement between experimental heat capacities and statistical calculations using the harmonic oscillator, rigid rotator model are obtained for molecules having no internal rotations (cf. data on allene, cyclopropane and methyl acetylene). The disagreements between similar calculations for molecules having internal rotation, assuming free rotation, and experimental data, are to be taken therefore as positive evidence for the existence of potential barriers restricting internal rotation. An exact calculation of such barriers, however, is

[28] The use of the experimental data of Sage, Webster and Lacey would make the situation still less satisfactory.
[29] Kohlrausch and Koppl, Zeits. f. physik. Chemie **B26**, 209 (1934).
[30] Bartholome, Zeits. f. physik. Chemie **B23**, 152 (1933).

impossible unless a complete vibrational analysis is available and the Third Law Entropy data are preferable for this purpose in case of more complex molecules since the vibrational contribution to the entropies is relatively small. But only by combining such entropy data with experimental heat capacities can one be assured of a reasonably accurate vibrational assignment and hence of a *reliable* as well as a precise value for the internal potential.

It is a pleasant duty to thank Professor E. B. Wilson, Jr., for his interest and many valuable contributions to this work. We would further like to express our appreciation to Mr. E. E. Roper of this laboratory for the use of his equation of state data before publication.

AUGUST, 1940 JOURNAL OF CHEMICAL PHYSICS VOLUME 8

Gaseous Heat Capacities. III[1,2]

G. B. KISTIAKOWSKY AND W. W. RICE
Department of Chemistry, Harvard University, Cambridge, Massachusetts

(Received May 8, 1940)

The present paper presents a continuation of measurements on the gaseous heat capacities by the adiabatic expansion method. The apparatus and the experimental procedure are exactly the same as described in the previous papers denoted herein as Part I and Part II. The compounds with which the present paper deals are dimethyl ether, ethylene oxide, dimethyl acetylene, *cis*-butane-2 and *trans*-butene-2. For the correction of the experimental data to the ideal gas state several procedures had to be used, as discussed in Part II.

FOR dimethyl ether critical data are available[3] and they were put into the Keyes equation of state[4] to obtain the second virial coefficient (B) and its derivatives. As pointed out in Part II, the resultant correction of the heat capacity data to atmospheric pressure (C_p) comes out too low, by as much as 10 to 25 percent, and therefore we do not list this heat capacity in the following tables. In the further correction to the ideal state (C_p^0) the error is fairly well compensated.

For ethylene oxide only the critical temperature[3] is known and the following somewhat dubious, procedure was resorted to. Maass and Boomer[5] have determined the gas density of ethylene oxide at several temperatures and pressures. Their data are not of sufficient accuracy to evaluate the second virial coefficient (B) as a series expansion in temperature but a satisfactory average value of ($V_a - RT/P$) could be obtained. This, together with the critical temperature, was substituted into the Keyes equation[2] and the correction to the ideal state thus calculated. The critical pressure calculated on this basis is found to be 49.1 atmos. as a weighted average.

For dimethly acetylene also only the critical temperature $T = 489°$K is known.[6] We have used the plot of critical temperatures *vs.* critical pressures given in Part II to estimate the latter as 31.3 atmos.[7]

Accurate equations of state were available for both butene-2 isomers[8] and were used directly. For these latter gases, therefore, the errors due to the correction are quite small, but in the other cases also, the final data should be accurate to better than 0.1 cal./mole degree, except perhaps in the neighborhood of the boiling points.

In the following sections the gases will be considered one by one.

[1] Part I, G. B. Kistiakowsky and W. W. Rice, J. Chem. Phys. **7**, 281 (1939).
[2] Part II, G. B. Kistiakowsky and W. W. Rice, J. Chem. Phys. **8**, 610 (1940), preceding article in this issue.
[3] Int. Crit. Tab., Vol. 3.
[4] F. G. Keyes, J. Am. Chem. Soc. **60**, 1761 (1938).
[5] Maass and Boomer, J. Am. Chem. Soc. **44**, 1726 (1922).
[6] Maass and Morehouse, Can. J. Research **11**, 640 (1934).
[7] Osborne, Garner and Yost (J. Chem. Phys. **8**, 131 (1940)), estimate this by a different procedure and find 41 atmos.
[8] A. B. Lamb and E. E. Roper, J. Phys. Chem. (to appear shortly) 1940.

Dimethyl Ether (C_2H_6O)

The sample of dimethyl ether used in these measurements was taken from a cylinder having a stated purity of 99.95 percent and obtained from the Ohio Chemical Company. It was subjected to repeated vacuum distillations to eliminate small traces of air and moisture which might be present.

The following Table I gives a summary of the experimental results obtained. As emphasized in Part II, none of the completed experiments have been disregarded in forming the averages of this table because of too large deviations from the mean. The same is true of other heat capacity tables given in this paper.

In Table I, T_{Av}°K is the average temperature of the gas before and after expansion for each series of runs. The column headed (range of ΔP), gives the maximum and minimum values of the pressure drop of the gas upon expansion. P_{final}Av. is the average barometric pressure for the series of runs. The temperature coefficient of resistance of the Wollaston wire thermometer is given in column five. Column six records the radiation correction (see Part I). Column seven shows the apparent heat capacity of the gas (C_p') calculated as in Part I, and finally the last column gives the heat capacity of the gas at zero pressure (C_p^0) which is to be used for comparison with the theoretical calculations.

Crawford and Joyce[9] have studied the infra-red spectrum of dimethyl ether and combining this with the available Raman data have given a tentative assignment of the vibrational frequencies: 2900(6), 1466(6), 1180(4), 1122(1), 940(1), 412(1); all but the lowest frequency 412 cm^{-1} were taken from the infra-red spectrum. The numbers in the parenthesis indicate the statistical weights attached to each frequency. Two degrees of freedom are allowed for the rotation of the methyl groups.

We have calculated the theoretical heat capacities on the above assignment, at the temperatures of the experimentally determined heat capacities, assuming the harmonic oscillator and classical rigid rotator as the molecular model. The results are shown in Table II.

In Table II, the third column gives the theoretical heat capacities calculated from Crawford's assignment exclusive of the internal rotation of the methyl groups, ($C_{\text{i.r.}}$). Column four gives the contribution to the heat capacity due to the internal rotation of the methyl groups, or $C^0{}_{p(\text{exp})} - (C^0{}_{p(\text{calc})} - C_{\text{i.r.}})$. The last column gives the contribution to the heat capacity for two methyl groups calculated from Pitzer's tables[10] for a barrier of 2500 cal./mole. The moments of inertia used were: $I_x^0 = 21.666$, $I_y^0 = 82.474$, $I_z^0 = 93.604$ and 5.18, the latter being for the methyl group. These moments are in units of $gcm^2 \times 10^{40}$ and were calculated on basis of the dimensions given by Pauling and Brockway.[11] I_z^0 is the moment of inertia about the axis through center of gravity and perpendicular to the carbon plane. I_y, the moment about axis bisecting the $C-O-C$ angle in carbon plane. I_x^0 = moment about axis through center of gravity and perpendicular to $Y+Z$ axis. The correlation with experimental data is seen to be excellent if a potential of 2500 cal./mole is taken to restrict the rotation of the methyl groups.

Table II. *Internal rotational heat capacity of dimethyl ether.*

T°K	C_p^0 (exp.)	$(C_p^0 - C_{\text{i.r.}})_{\text{calc}}$	$C_{\text{i.r.}}$	$C_{\text{i.r. calc}}$ (V = 2500 cal./mole)
272.20	14.82	10.79	4.03	4.20
300.76	15.75	11.59	4.16	4.24
333.25	16.81	12.63	4.18	4.20
370.42	17.96	13.89	4.07	4.12

Table I. *Heat capacity of dimethyl ether.* (C_2H_6O).

No. of Runs	T_{Av} °K	Range of ΔP mm	P_{final} Average mm	$\frac{dR}{dT}$ Ohm / Degree	Rad. Corr. Percent	C_p'	C_p^0 cal./mole deg.
5	272.20	37.609–33.882	757.10	1.1182	0.107	14.52±.02	14.82
6	300.76	38.385–33.611	759.73	1.1108	.113	15.49±.02	15.75
5	333.25	38.168–32.864	760.80	1.1008	.141	16.59±.02	16.81
5	370.42	37.163–30.563	746.60	1.0871	.174	17.77±.02	17.96

[9] B. L. Crawford, Jr., and L. Joyce, J. Chem. Phys. **7**, 307 (1939).

[10] K. S. Pitzer, J. Chem. Phys. **5**, 469 (1937).

[11] Pauling and Brockway, J. Am. Chem. Soc. **57**, 2684 (1935).

TABLE III. *Heat capacity of ethylene oxide* (C_2H_4O).

No. of Runs	T_{Av} °K	Range of ΔP mm	P_{final} Average mm	$\frac{dR}{dT}$ Ohm / Degree	Rad. Corr. Percent	C_p'	C_p^0 cal./mole deg.
5	307.18	36.712–30.090	762.05	1.1090	0.157	11.57±.01	11.80
4	337.04	37.778–31.342	763.70	1.0994	.183	12.57±.01	12.79
4	371.23	37.010–33.173	764.30	1.0868	.219	13.76±.03	13.96

The only significant deviation of calculated from experimental values is at the lowest temperature (272°K). Here, however, the correction to the ideal state is least certain and the discrepancy may be due to this cause. It has been shown[12] that the more complete calculation involving the consideration of the coupling of the angular momenta of the top and of the whole molecule may give results differing appreciably from the values given in Pitzer's tables for the heat capacity contribution due to restricted rotation; therefore the value of the restricting potential used in Table II should be regarded as provisional.

Ethylene Oxide (C_2H_4O)

The sample of ethylene oxide used in these measurements was a commercial sample obtained from the Matheson Chemical Company and had a stated purity of 99.9 percent. The sample was subjected to repeated vacuum distillations and pumping to remove traces of air and moisture. Only the middle portion of the sample was used for actual measurements. Since ethylene oxide boils at 10.7°C, the heat capacity was determined at only three temperatures. Table III gives the experimental results.

The infra-red and Raman spectra of ethylene oxide have been investigated by Linnett[13] who has given the following tentative vibrational assignment: 3000(2), 1494(1), 1122(1), 1270(1), 811(1), 1453(1), 1163(1), 868(1), 3062(2), 1172(1), 673(1), 807(1), ——(1), cm^{-1}, with the 811(1), 1172(1), and a frequency which may be correlated with the methylene rocking motion being uncertain.

We have calculated the theoretical heat capacities for ethylene oxide assuming, as suggested by Linnett, a value of 1350 cm^{-1} for the missing methylene rocking frequency. The following Table IV gives the results. It is seen that the agreement between the experimental and the theoretical values is not good. The discrepancy cannot be attributed to an error in the correction of the experimental heat capacities to the ideal state, as it is around 0.4 cal./mole degree, whereas the total gas correction as shown in Table III is only around 0.25 cal./mole degree and its uncertainty is at most about 0.1 cal./mole degree.

We have changed therefore the 811 cm^{-1} frequency to 1100 cm^{-1} because it is only a matter of conjecture as to whether there are two frequencies at 807 and 811 cm^{-1} or only one. The other two uncertain frequencies namely 1172 and 1350 cm^{-1} remain unchanged. Column four in Table IV gives the corrected calculations. The agreement with the experimental data is seen to be quite good but until heat capacity data over a larger temperature range are available, one cannot be sure that the new assignment is substantially correct.

Dimethyl Acetylene (C_4H_6)

The dimethyl acetylene used in these measurements was part of the same material which was prepared and used in the heats of hydrogenation by Kistiakowsky and co-workers.[14] The material was vacuum distilled before introducing it into the expansion chamber. Because of the high boiling point of dimethyl acetylene, the heat capacity was determined at only two temperatures. The experimental results are given in Table V.

TABLE IV. *Statistical heat capacity of ethylene oxide.*

T_{Av}°K	C_p^0 (exp.)	C_p^0 Linnett's Assignment	C_p^0 New Assignment
307.18	11.80	12.16	11.80
337.04	12.79	13.18	12.78
371.23	13.96	14.34	13.94

[12] B. L. Crawford, J. Chem. Phys. **8**, 273 (1940).
[13] J. W. Linnett, J. Chem. Phys. **6**, 692 (1938).
[14] J. B. Conn, G. B. Kistiakowsky and E. A. Smith, J. Am. Chem. Soc. **61**, 1868 (1939).

TABLE V. *Heat capacity of dimethyl acetylene* (C_4H_6).

No. of Runs	T_{Av} °K	Range of ΔP mm	P_{final} Average mm	$\frac{dR}{dT}$ Ohm / Degree	Rad. Corr. Percent	C_p'	C_p^0 cal./mole deg.
5	336.07	40.796–33.643	771.55	1.0998	0.162	19.41±.03	20.21
6	369.46	40.102–34.384	770.90	1.0874	.200	20.76±.04	21.43

Crawford[15] has studied the infra-red and Raman spectra of dimethyl acetylene and has given an assignment for the vibrational frequencies of this molecule: 725(1), 1380(1), 2270(1), 2916(1), 1126(1), 1380(1), 2976(1), 213(2), 1050(2), 1468(2), 2976(2), 371(2), 1029(2), 1448(2), 2966(2).

Crawford and Rice[16] using this assignment and the heat capacities given in Table V have calculated the contribution to the heat capacity due to the internal rotation of the methyl groups relative to each other and find the restricting potential to be at most 500 cal./mole. Table VI reproduces these calculations. The experimental results for ($C_{i.r.}$), the contribution from the internal rotation, are in good agreement with the value 0.99 cal./mole degree expected for a completely free rotator, or a restricting potential of zero; 500 cal./mole is undoubtedly the upper limit.

Recently Yost *et al.*[7] have published measurements on the third law entropy of dimethyl acetylene, from which they also conclude that the restricting potential in this molecule is very low, possibly zero. Their conclusion is less dependent on a correct vibrational assignment than the evidence given here and together the two studies offer indisputable proof of a practically complete absence of hindrance to the rotation of the methyl groups in this molecule. It seems to us that the theory of restricting potentials offered some time ago by Gorin, Walter and Eyring[17] will find it rather difficult to account simultaneously for the existence of a rather high potential in dimethyl ether and the absence of same in dimethyl acetylene.

TABLE VI. *Internal rotational heat capacity of dimethyl acetylene.*

T_{Av}°K	C_p^0 (exp.)	$(C_p^0 - C_{i.r.})_{calc}$	$C_{i.r.}$	$C_{i.r.\ calc}$ (V=500 cal./mole)
336.07	20.21±.1	19.14	1.07±.1	1.16
369.46	21.43±.1	20.47	.96±.1	1.14

CIS-BUTENE-2 (C_4H_8)

The sample of *cis*-butene-2 was part of the original material prepared by Kistiakowsky and co-workers[18] for the determination of the heats of hydrogenation. The sample was vacuum distilled several times before being introduced into the expansion vessel but after the experiments were carried out it was found that a small trace of water vapor remained in the sample. Because of this the heat capacity values given in Table VII may be 0.1 to 0.2 percent too low. The experimental results are shown in Table VII.

TRANS-BUTENE-2 (C_4H_8)

The sample used was also part of the material prepared by Kistiakowsky and co-workers.[18] It was subjected to the usual vacuum distillations and was definitely freed of water vapor. The experimental results are shown in Table VIII.

No vibrational analysis of the two isomeric butenes has been suggested as yet, although Gershinowitz and Wilson[19] have studied the infra-red and Raman spectra of these molecules. The important conclusion which can be drawn from their work is that the spectra of the two molecules have very different appearance and the present measurements, which show a difference in vibrational plus internal rotational heat capacities of as much as 12 percent, bring convincing evidence that the fundamental frequencies of the two isomers are significantly

[15] B. L. Crawford, Jr., J. Chem. Phys. **7**, 555 (1939).
[16] B. L. Crawford, Jr. and W. W. Rice, J. Chem. Phys. **7**, 437 (1939).
[17] Gorin, Walter and Eyring, J. Am. Chem. Soc. **61**, 1876 (1939).
[18] Kistiakowsky, Ruhoff, Smith and Vaughan, J. Am. Chem. Soc. **57**, 876 (1935).
[19] Gershinowitz and Wilson, J. Chem. Phys. **6**, 247 (1938).

TABLE VII. *Heat capacity of cis-butene-2.* (C_4H_8).

No. of Runs	T_{Av} °K	Range of ΔP mm	P_{final} Average mm	$\frac{dR}{dT}$ Ohm / Degree	Rad. Corr. Percent	C_p'	C_p	C_p^0 cal./mole deg.
5	298.58	38.424–26.831	759.20	1.1114	0.135	18.47±.05	20.06	19.39
5	332.85	38.088–32.972	769.00	1.1009	.164	20.37±.03	21.54	21.09
5	371.24	38.554–32.275	769.40	1.0868	.157	22.46±.05	23.30	23.01

TABLE VIII. *Heat capacity of trans-butene-2.* (C_4H_8).

No. of Runs	T_{Av} °K	Range of ΔP mm	P_{final} Average mm	$\frac{dR}{dT}$ Ohm / Degree	Rad. Corr. Percent	C_p'	C_p	C_p^0 cal./mole deg.
6	298.60	38.472–35.244	766.50	1.1114	0.13	20.04±.03	21.55	20.98
5	332.90	38.350–33.436	767.75	1.1009	.14	21.96±.03	23.06	22.69
5	371.50	38.322–36.302	765.95	1.0866	.17	23.97±.04	24.78	24.53

different. The neglect to allow for such differences in the schematized frequency assignments occasionally proposed[20] leads evidently to significant errors in the comparative values of the calculated thermodynamic functions.

A different approach to this problem of the thermodynamic functions of the more complex organic molecules is through a frankly empirical set of recursion type formulas derived from experimental measurements on the gaseous heat capacities. The data collected in the first three articles of this series show indeed the possibility of setting up such equations but we prefer to await the accumulation of a little more experimental material on heavier hydrocarbons, the work now in progress in this laboratory, before claiming their general validity.

Professor E. B. Wilson, Jr. has advised us on several phases of the present work, for which we wish to express to him our appreciation.

[20] K. S. Pitzer, J. Chem. Phys. **5**, 473 (1937); M. Huggins, *ibid.* **8**, 181 (1940).

Statistical Mechanics of Cooperative Phenomena

JOHN G. KIRKWOOD
Baker Laboratory, Cornell University, Ithaca, New York

(Received June 6, 1940)

A direct method of successive approximation to the configurational partition function, based on the use of local free energies, is described. The method serves to clarify the assumptions underlying the Bethe method of local configurations and the quasi-chemical method of Guggenheim and Fowler.

THE theoretical treatment of cooperative phenomena initiated by Bragg and Williams[1] has received extension by statistical mechanical methods at the hands of several investigators. Three methods of approximation to the configurational partition function have been proposed, the method of local configurations by Bethe,[2] the method of moments by the writer,[3] and the quasi-chemical method by Guggenheim and Fowler.[4,5] The method of local configurations and the quasi-chemical method led to closed expressions for the partition function, but both are based upon approximations, the nature of which is not entirely clear. The method of moments leads to an exact expansion of the logarithm of the partition function in powers of the reciprocal temperature, at the sacrifice of closed expressions for the thermodynamic functions of the system. Bethe and the writer[6] have recently shown that the method of local configurations is valid to the third moment of the configurational energy. Moreover, Fowler and Guggenheim[5] have demonstrated the equivalence of the method of local configurations and the quasi-chemical method.

In the present article a method of successive approximation to the partition function based on the use of local free energies is described. In the light of this method, the nature of the assumptions underlying both the Bethe method of local configurations and the quasi-chemical method is clarified. In addition, closed expressions for the configurational entropy and free energy of solid solutions are developed. These expressions were first presented by Bethe and the writer[6] without proof and were later proposed by Fowler and Guggenheim[5] on the basis of the quasi-chemical method.

Although the general features of the method to be described are applicable to the calculation of the partition functions associated with other types of cooperative phenomena, we shall restrict ourselves here to the problem of order and disorder in solid solutions. We therefore consider a binary solid solution of arbitrary composition built up of two interpenetrating lattices A and B of N sites each. An arbitrary site of either lattice is assumed to have as neighbors z sites of the opposite lattice. The lattice sites are supposed to be occupied by atoms of two types, denoting by N_1^A, N_1^B, N_2^A, N_2^B the numbers of atoms of the respective types on the two lattices. We denote the corresponding atom fractions by x_1^A, x_1^B, x_2^A, and x_2^B. To facilitate the calculation of the partition function we introduce the long range order parameter of Bragg and Williams,

$$\begin{gathered} s=x_1^A-x_1^B; \quad x_1^A=N_1^A/N=x_1+s/2 \\ x_1^B=x_1-s/2; \quad x_2^A=x_2-s/2 \\ x_2^B=x_2+s/2, \end{gathered} \tag{1}$$

where x_1 and x_2 are the atom fractions $(N_1^A+N_1^B)/2N$ and $(N_2^A+N_2^B)/2N$ of the crystal as a whole. If $f(s)$ is the partition function of the crystal in a specified state of long range order s, the configurational partition function is

$$f=\sum_{s=-1}^{+1} f(s), \tag{2}$$

where the sum extends over all accessible values of s between zero and unity. Since $f(s)$ possesses a sharp maximum, $\log f$ may be set equal to the logarithm of the maximum term in the sum (2)

[1] Bragg and Williams, Proc. Roy. Soc. **A145**, 699 (1934); **A151**, 540 (1935); **A152**, 231 (1935).
[2] Bethe, Proc. Roy. Soc. **A150**, 552 (1935).
[3] Kirkwood, J. Chem. Phys. **6**, 70 (1939).
[4] Guggenheim, Proc. Roy. Soc. **A169**, 304 (1938).
[5] Fowler and Guggenheim, Proc. Roy. Soc. **A174**, 189 (1940).
[6] Bethe and Kirkwood, J. Chem. Phys. **7**, 578 (1939).

with an error of negligible order of magnitude $0(N^{-1})$. In order to calculate the partition function $f(s)$ corresponding to a fixed value of s, a unique specification of the set of configurations corresponding to this value of s is required. Such a specification is provided by a set of variables $\xi_1 \cdots \xi_N$, $\eta_1, \cdots, \eta_N$, each limited to a domain of two values, zero and unity. The variable ξ_a states the number of atoms of type 1 in site a of lattice A and the variable η_b the number of atoms of type 1 in site b on lattice B. As a consequence of their definition, the configuration variables satisfy the following relations,

$$\sum_{a=1}^{N} \xi_a = N_1{}^A, \quad \sum_{b=1}^{N} \eta_b = N_1{}^B. \tag{3}$$

If interactions between atoms which are not nearest neighbors are neglected, the configurational energy of the crystal may be expressed in the form

$$\begin{aligned} E &= E_0 - \alpha kT\sigma(\xi_1, \cdots \eta_N), \\ E_0 &= N_1 z V_{11}/2 + N_2 z V_{22}/2, \\ \alpha &= [(V_{11}+V_{22})/2 - V_{12}]/kT, \\ \sigma &= \sum_{a,b=1}^{N} \lambda_{ab}[\xi_a(1-\eta_b)+(1-\xi_a)\eta_b], \end{aligned} \tag{4}$$

where λ_{ab} is unity if sites a and b are nearest neighbors and zero otherwise.

$$\sum_{a=1}^{N} \lambda_{ab} = \sum_{b=1}^{N} \lambda_{ab} = z, \tag{5}$$

We may therefore write the configurational partition function in the following form,

$$f(s, \alpha) = \sum_{\substack{\xi_1 \cdots \xi_N \\ \Sigma \xi_a = N_1{}^A}}^{1} \sum_{\substack{\eta_1 \cdots \eta_N \\ \Sigma \eta_b = N_1{}^B}}^{1} e^{\alpha\sigma(\xi_1 \cdots \eta_N)}. \tag{6}$$

From Eq. (6), we obtain by differentiation

$$\begin{aligned} \partial \log f/\partial\alpha &= (\sigma)_{Av}, \\ (\sigma)_{Av} &= \Big(\sum_{\xi_1 \cdots \eta_N} \sigma e^{\alpha\sigma}\Big)/\Big(\sum_{\xi_1 \cdots \eta_N} e^{\alpha\sigma}\Big), \end{aligned} \tag{7}$$

where the summation variables in Eq. (7) as in Eq. (6) are subject to the restraints, Eq. (3). When α is zero, the partition function reduces to the total number of configurations consistent with the specified value of s. Using Sterling's formula for factorials, we may write

$$\log f(s, 0) = -N \sum_{n=1}^{2} [x_n{}^A \log x_n{}^A + x_n{}^B \log x_n{}^B]. \tag{8}$$

Integration of Eq. (7) with the use of Eq. (8), leads to the following expression for the free energy, $A(s,\alpha)$.

$$A/NkT = \sum_{n=1}^{2} [x_n{}^A \log x_n{}^A + x_n{}^B \log x_n{}^B] - (1/N)\int_0^{\alpha} (\sigma)_{Av} d\alpha. \tag{9}$$

Equation (9) provides an exact expression for the configurational free energy, insofar as coupling between configuration and lattice vibrations can be neglected. Since all pairs of nearest neighbor sites are equivalent, Eqs. (4) and (7) yield

$$(\sigma)_{Av} = Nz\{[\xi(1-\eta]_{Av} + [(1-\xi)\eta]_{Av}\}, \tag{10}$$

where $[\xi(1-\eta)]_{Av}$ and $[\eta(1-\xi)]_{Av}$ are mean values of the specified functions of ξ and η for an arbitrary pair of neighbor sites. The mean value of any function, $y(\xi, \eta)$, of two of the configuration variables only may be written as follows,

$$\begin{aligned} (y)_{Av} &= \sum_{\xi,\eta=0}^{1} y(\xi, \eta) e^{-W(\xi,\eta)/kT}, \\ W(\xi, \eta) &= A(\xi, \eta) - A, \\ e^{-A(\xi,\eta)/kT} &= \sum_{\substack{\xi_1 \cdots \xi_{N-1} \\ 0}}^{1} \sum_{\substack{\eta_1 \cdots \eta_{N-1} \\ 0}}^{1} e^{\alpha\sigma(\xi_1, \cdots \eta_N)}, \\ &\qquad \sum_{a=1}^{N-1} \xi_a = N_1{}^A - \xi \quad \sum_{b=1}^{N-1} \eta_b = N_1{}^B - \eta \end{aligned} \tag{11}$$

where $W(\xi, \eta)$ is the local free energy of a single pair of neighbor sites of specified configuration $[\xi, \eta]$, equal to the work of formation of the specified local configuration from the average crystal. The derivative of $W(\xi, \eta)$ with respect to α is easily calculated from Eqs. (7) and (11).

$$-\frac{1}{kT}\frac{\partial W(\xi, \eta, \alpha)}{\partial \alpha} = [\sigma(\xi, \eta)]_{Av} - [\sigma]_{Av}. \tag{12}$$

When α is equal to zero, $-W(\xi, \eta, \alpha)/kT$ reduces to the logarithm of the ratio of the number of configurations, consistent with the specified

values of ξ and η, to the total number of configurations of the crystal,

$$-W(\xi,\eta,0)/kT=\xi\log x_1{}^A+\eta\log x_1{}^B+(1-\xi)\log x_2{}^A+(1-\eta)\log x_2{}^B. \quad (13)$$

Integration of Eq. (12) with the use of (13) gives

$$e^{-W(\xi,\eta)/kT}=(x_1{}^A)^{\xi}(x_2{}^A)^{1-\xi}(x_1{}^B)^{\eta}\times(x_2{}^B)^{1-\eta}e^{-w(\xi,\eta)/kT}, \quad (14)$$

$$-w(\xi,\eta)/kT=\int_0^{\alpha}\{[\sigma(\xi,\eta)]_{Av}-[\sigma]_{Av}\}d\alpha.$$

Eqs. (10), (11), and (12) lead to the following expression for $[\sigma]_{Av}$

$$[\sigma]_{Av}=Nz\{x_1{}^Ax_2{}^Be^{-w(1,0)/kT}+x_2{}^Ax_1{}^Be^{-w(0,1)/kT}\}. \quad (15)$$

Since ξ, η each have a domain of two values only, zero and unity, we may express $w(\xi,\eta)$ as a function of these variables in the following form

$$w(\xi,\eta)=\epsilon_{00}-\epsilon_{10}\xi-\epsilon_{01}\eta+\epsilon_{11}\xi\eta. \quad (16)$$

The four values of the function $w(\xi,\eta)$ are not independent, but satisfy three equations which may be obtained by substitution from Eq. (14) in the following generally valid relations

$$\sum_{\xi,\eta=0}^{1}e^{-W(\xi,\eta)/kT}=1,$$

$$[\xi]_{Av}=\sum_{\xi,\eta=0}^{1}\xi e^{-W(\xi,\eta)/kT}=x_1{}^A, \quad (17)$$

$$[\eta]_{Av}=\sum_{\xi,\eta=0}^{1}\eta e^{-W(\xi,\eta)/kT}=x_1{}^B.$$

The first of Eqs. (13) follows directly from the definition of $W(\xi,\eta)$, Eq. (11). The second and third of Eqs. (13) follow from Eqs. (3) and the fact that all sites of lattice A or lattice B are equivalent in the average crystal. Thus $[\xi_a]_{Av}$ and $[\eta_b]_{Av}$ are independent of the site indices a and b and equal to $x_1{}^A$ and $x_1{}^B$, respectively, for any value of α. By means of Eqs. (14) and (17), the coefficients ϵ_{10}, ϵ_{01}, and ϵ_{00} in the expansion of $w(\xi,\eta)$, Eq. (16), may be expressed in terms of ϵ_{11} the coefficient of $\xi\eta$. By elimination of ϵ_{10}, ϵ_{01}, and ϵ_{00} in this manner and substitution of the resulting expressions for $w(\xi,\eta)$ in Eq. (15), we obtain after some tedious algebraic transformations,

$$\frac{[\sigma]_{Av}}{Nz}=\frac{2s^2+(1-s^2-q^2)e^{\epsilon/kT}+(1+s^2-q^2)\varphi}{(1+s^2-q^2)+(1-s^2+q^2)e^{\epsilon/kT}+2\varphi},$$

$$\varphi=\{s^2+(1-s^2-q^2)e^{\epsilon/kT}+q^2e^{2\epsilon/kT}\}^{\frac{1}{2}}, \quad (18)$$

$$q=x_1-x_2,\quad s=x_1{}^A-x_1{}^B,$$

$$\epsilon=w(1,1)+w(0,0)-w(1,0)-w(0,1),$$

where, for simplicity in notation, the symbol ϵ_{11} has been replaced by ϵ. Equation (1) has been employed to express $x_1{}^A$, $x_1{}^B$, $x_2{}^A$, $x_2{}^B$ in terms of s and q, the latter denoting the difference in atom fraction of the two components in the crystal as a whole. By Eqs. (14) and (15), we may write

$$-\frac{\epsilon}{kT}=\int_0^{\alpha}\frac{\partial^2[\sigma(\xi,\eta)]_{Av}}{\partial\xi\partial\eta}d\alpha. \quad (19)$$

In order to calculate ϵ as a function of α, it is necessary to determine $[\sigma(\xi,\eta)]_{Av}$. This could be done by a continuation of the method employed in the calculation of $[\sigma]_{Av}$ with local free energies of sets of four sites in specified configurations. An alternative procedure consists in the expansion of ϵ in powers of α by the method of moments. Such an expansion leads to the following expression for $w(\xi,\eta)$.

$$\frac{w(\xi,\eta)}{kT}=\left[2\xi\eta-(1+q-s)\xi-(1+q+s)\eta+\frac{(1+q)^2-s^2}{2}\right]\alpha+O(\alpha^2). \quad (20)$$

The corresponding expansion of ϵ is evidently

$$\epsilon/kT=2\alpha+O(\alpha^2). \quad (21)$$

When the expansion (21) is substituted in Eq. (18), the following approximation to $[\sigma]_{Av}$ is obtained,

$$[\sigma]_{Av}/Nz=\frac{2s^2+(1-s^2-q^2)e^{2\alpha}+(1+s^2-q^2)\varphi}{(1+s^2-q^2)+(1-s^2+q^2)e^{2\alpha}+2\varphi},$$

$$\varphi(\alpha)=\{s^2+(1-s^2-q^2)e^{2\alpha}+q^2e^{4\alpha}\}^{\frac{1}{2}}. \quad (22)$$

As we shall presently show, the approximation (22) leads directly to the Bethe theory of super-

lattices. The Bragg-Williams theory is obtained when the total free energy of the crystal is expanded in powers of α by the method of moments with retention of the first moment only. The Bethe theory, on the other hand, is obtained by introducing the same type of approximation for the local free energy ϵ. Thus we may say that the Bethe theory is based upon the application of the Bragg and Williams approximation to the local free energy ϵ, rather than to the total free energy of the crystal. One may ask why the first moment approximation to $w(\xi, \eta)$, Eq. (20), rather than the corresponding approximation to ϵ, Eq. (21), should not be used for the calculation of $[\sigma]_{Av}$ in Eq. (15). If this is done, an approximation agreeing with the exact expansion of the total free energy of the crystal to the second moment in energy is obtained. It may be verified that the Bethe approximation is valid to the third moment in energy, and therefore somewhat better. The reason for this is not difficult to understand. The $w(\xi, \eta)$ of Eq. (20) do not yield $W(\xi, \eta)$ satisfying Eqs. (17), whereas these relations are satisfied automatically if Eqs. (18) and the first moment approximation to ϵ is employed in the calculation of $[\sigma]_{Av}$.

Although it is possible to express the integral, $\int_0^\alpha [\sigma]_{Av} d\alpha$, in terms of elementary functions with the integrand Eq. (22), the result is very cumbersome. We shall therefore give expressions for the free energy only for the special cases $q=0$ and $s=0$. When $q=0$ the atom fraction of the two components are equal. Equations (9) and (22) lead to the result;

$$\frac{A}{2NkT}=\left(\frac{1+s}{2}\right)\log\left(\frac{1+s}{2}\right)+\left(\frac{1-s}{2}\right)\log\left(\frac{1-s}{2}\right)+\frac{\alpha z}{2}-zG(\alpha, s^2),$$

$$G(\alpha, s^2)=-\left(\frac{1+s}{4}\right)\log\left[\frac{2(s+\varphi)}{(1+\varphi)(1+s)}\right]-\left(\frac{1-s}{4}\right)\log\left[\frac{2(\varphi-s)}{(\varphi+1)(1-s)}\right], \quad (23)$$

$$\varphi(\alpha, s)=[s^2+(1-s^2)e^{2\alpha}]^{\frac{1}{2}}.$$

The equilibrium value of s is to be determined by the condition $\partial A/\partial s=0$. A discussion of the order-disorder transformation and the accompanying heat capacity anomaly, based upon Eq. (23), has been given by Bethe and the writer. The results are identical with those of the indirect method originally formulated by Bethe. When $G(\alpha, s^2)$ is expanded in powers of α and the result is compared with the exact expansion of $A/2NkT$ by the method of moments, it is found that Eq. (23) is valid to terms in α^3, that is to the third moment in the energy.

When α is negative, the long range order s is constrained to the value zero. In this case, Eqs. (9) and (22) yield

$$\frac{A}{2NkT}=\left(\frac{1+q}{2}\right)\log\left(\frac{1+q}{2}\right)+\left(\frac{1-q}{2}\right)\log\left(\frac{1-q}{2}\right)-zG(-\alpha, q^2), \quad (24)$$

$$G(-\alpha, q^2)=-\left(\frac{1+q}{4}\right)\log\left[\frac{2(\varphi+q)}{(\varphi+1)(1+q)}\right]-\left(\frac{1-q}{4}\right)\log\left[\frac{2(\varphi-q)}{(\varphi+1)(1-q)}\right],$$

$$\varphi(-\alpha, q^2)=[q^2+(1-q^2)e^{-2\alpha}]^{\frac{1}{2}}.$$

When α is negative, there is instead of a phase change of the second kind, one of the first kind with a critical solution temperature below which the solid solution separates into two phases. The critical solution phenomenon has been investigated by the writer[7] using the method of moments, and by Rushbrooke,[8] using the method of local configurations. We shall therefore not discuss in detail application of the closed expression, Eq. (24), to the problem of critical solution phenomena, but remark that, as in the superlattice case, the results agree with the method of moments to the third moment in the energy, that is to terms in α^3 in the free energy.

The foregoing analysis serves to illuminate the nature of the approximations underlying the method of local configurations and the quasi-chemical method and demonstrates that they are both valid to the third moment of the configurational energy. All three methods, the method of moments, the method of local configurations, and

[7] Kirkwood, J. Phys. Chem. **43**, 97 (1939).
[8] Rushbrooke, Proc. Roy. Soc. **A166**, 296 (1938).

the quasi-chemical method reduce in first approximation to the Bragg-Williams form and the higher approximations do not give rise to very large deviations from the Bragg-Williams theory. It is the writer's opinion that improved agreement with experiment is not to be sought in refinements in the statistical calculation of the partition function, but rather in improvements of the physical model upon which this calculation is based. For example, the dependence of the interaction energies V_{11}, V_{22} and V_{12} on the lattice parameter of the crystal is of considerable importance.[6]

In conclusion, the writer wishes to express his thanks to Professor Bethe for his comments on the method proposed in the present article.

AUGUST, 1940 JOURNAL OF CHEMICAL PHYSICS VOLUME 8

The Joule-Thomson Effect in Mixtures of Helium and Argon*

J. R. ROEBUCK AND H. OSTERBERG
Department of Physics, University of Wisconsin, Madison, Wisconsin

(Received April 20, 1940)

The Joule-Thomson effect has been measured in four mixtures of helium and argon. The apparatus and methods are those used repeatedly in previous work. The measurements of the isenthalpic curves cover the range −100° to 250°C and up to 200 atmos. From these measurements μ has been computed and plotted, and the trends with temperature, pressure, and composition are shown. μ is read from these curves and tabulated. In part of the region $\mu=0$ and these inversion curves are plotted as functions of pressure, temperature, and composition. Mixtures of helium and nitrogen have been similarly measured.

THE measurements on the Joule-Thomson effect in air,[1,2] in helium,[3,4] in argon[5] in nitrogen,[6] and in four mixtures of helium and nitrogen[7] are here extended to four mixtures of helium and argon. Reference is made to the above articles for details of apparatus and methods. Our usual pressure range of 1 to 200 atmos. is maintained here, but our temperature is reduced to −100° to 250°C. The experimental work was done between May and November of 1935. It has seemed advisable to proceed with the collection of other data even though this led to considerable delay in publication. Complete data on carbon dioxide has now been collected.

The work on the Joule-Thomson effect in carbon dioxide has yielded as well data on the vapor pressure of the liquid. This data was just enough different from that in the literature to arouse suspicion of trouble. Hence the vapor pressure was measured statically using the piston gauge and the resulting data compared with the readings made on the open tube mercury manometer[8] at the ice point, and with the measurements of Meyer and Van Dusen.[9] The observed disagreement led to a careful search of the records on the piston gauge. In 1912 the piston gauge was checked against an open-tube mercury manometer very successfully, but in the computation of a factor to translate gauge-load

* The senior author's attention has been called lately to the reprinting by E. Justi in "Spezifische Wärme, Enthalpie, Entropie, etc." of Table XIV from my second article, reference 2, on the Joule-Thomson effect in air. As indicated in that article the source of this data was a large chart from H. Hausen. Unfortunately in reading off the values from the chart serious errors were made in the 100-atmos. group. The data for μ at 100 atmos. should have been as follows:

	−150°C	−140	−120	−100	−75	−50	−25	0	+25°C
Roebuck	+0.019	0.044	0.165	0.285	0.287	0.247	0.215	0.178	0.152
Hausen	−0.006	0.016	0.164	0.283	0.308	0.268	0.227	0.186	0.158

The agreement is markedly improved.

[1] Roebuck, Proc. Am. Acad. **60**, 537 (1925).
[2] Roebuck, Proc. Am. Acad. **64**, 287 (1930).
[3] Roebuck and Osterberg, Phys. Rev. **43**, 60 (1933).
[4] Roebuck and Osterberg, Phys. Rev. **45**, 332 (1934).
[5] Roebuck and Osterberg, Phys. Rev. **46**, 785 (1934).
[6] Roebuck and Osterberg, Phys. Rev. **48**, 450 (1935).
[7] Roebuck and Osterberg, J. Am. Chem. Soc. **60**, 341 (1938).
[8] Roebuck and Cram, Rev. Sci. Inst. **8**, 215 (1937).
[9] Meyer and Van Dusen, Bur. Stand. J. Research, **10**, 381 (1933).

TABLE I. *Helium and argon mixtures.*

No.	HELIUM %	ARGON %
0[3]	100	0
1	75.8	24.2
2	50.6	49.4
3	33.5	66.5
4	16.6	83.4
5[3]	0	100.

readings into atmospheres a numerical error was made. The factor 1.457 should have been 1.404. The factor computed from the work on the vapor pressure of carbon dioxide at the ice point by the open tube mercury manometer and by the piston gauge, is 1.410. This value (1.410) was used to calculate the vapor pressure in atmospheres read at a set of temperatures between 0°C and 30°C. All these values checked to less than 0.1 percent with readings of Meyer and Van Dusen. The factor has thus shifted from 1.404 to 1.410 or 0.4 percent in the 27-year interval.

In this interval a series[1–7] of papers have been published on work employing this piston gauge in which the factor 1.457 was always used. The numbers representing the pressure in all these papers have to be multiplied by 0.9677 to correct this error. Suitable corrections must also be made in the derived quantities like μ. As opportunity offers this data will be reworked to make these corrections. They have been applied to the data of this article.

LIQUEFACTION

The presence of liquefaction anywhere in the system led to the same difficulties with erratic data, as described in the preceding article on He-N_2 mixtures.[7] For similar reasons no attempt was made to take data with liquefying conditions present anywhere in the system. The bath temperature was in consequence never set below about -100°C and of the curves measured at this temperature only the helium-rich mixture (No. 1) curve was carried to the lowest pressures. Until data has been gathered in the simpler parts of this field, the more difficult may well be avoided.

GAS SUPPLIES

The helium was part of that supplied by the Bureau of Mines for the previous work on pure helium.[3] It was purified before use by passage over activated cocoanut charcoal cooled by liquid air as in the earlier work.[3]

The argon was a gift from the Air Reduction Sales Company through Mr. F. P. Gross, Jr. It had been prepared for use in incandescent lamps and was stated to contain 99.5 percent argon, 0.5 percent nitrogen, with negligible quantities of oxygen and water vapor.

The mixtures were made up by admitting the desired measured quantities of the constituent gases to the flow system and mixing thoroughly. The mixtures were carefully analyzed by absorbing the argon in liquid-air-cooled charcoal.[3] The two methods of knowing the composition agree. The analytical data are given in Table I.

Since both the He+air and the He+N_2 mixture work had shown that the Joule-Thomson effect varied less with composition for the helium-rich mixtures, these He+A mixtures were crowded somewhat toward the pure argon side. Sufficient of each mixture for the projected work was made up at once so that the compositions should be very constant. To avoid excess loss of argon the lubricating water was discharged only near atmospheric pressure where the dissolved helium and argon are both small in quantity.

EXPERIMENTAL RESULTS

The data for mixtures 1–4 are given in Tables II–V. The individual runs are referred to by their approximate bath temperatures. The last temperature and pressure readings in a run are, respectively, the bath temperature and the inlet high pressure. The temperatures are in degrees centigrade and the pressures in atmospheres absolute.

For reasons similar to those given in the He+N_2 mixture article,[7] it was not considered necessary to duplicate the individual runs. The high precision with which the points fall on a curve and the consistency of the family of curves and of the family of their derivatives are sufficient assurance of the reliability of the data.

ISENTHALPIC CURVES

The data of Tables II–V are plotted, respectively, in Figs. 1–4, with temperature as ordinate

and pressure as abscissa. The coincidence of the points with the curves in the accurate plots from which these figures were traced, leaves very little to be desired.

The corresponding curves for pure helium[3] and for pure argon[5] should be considered together with these four groups of curves for the four mixtures. A comparison of the curves of these six figures with the corresponding six figures for the $He+N_2$ mixtures[7] shows them to be remarkably similar. In the six figures, a

TABLE II. *Mixture No. 1.*

No.	p_2	l_2	No.	p_2	l_2	No.	p_2	$-l_2$
	250° Curve			*100° Curve*			*−50° Curve*	
1	2.5	262.78	1	3.8	109.61	1	1.9	48.38
2	19.6	261.81	2	19.4	108.91	2	19.6	48.43
3	41.1	260.46	3	41.2	107.82	3	42.4	48.64
4	63.3	259.12	4	63.4	106.71	4	64.0	48.88
5	84.1	257.77	5	85.3	105.56	5	84.0	49.19
6	105.7	256.38	6	107.1	104.42	6	107.8	49.60
7	130.8	254.77	7	130.3	103.18	7	130.8	50.06
8	154.2	253.20	8	153.4	101.89	8	153.5	50.55
9	194.8	250.93	9	194.8	99.73	9	194.8	51.61
	200° Curve			*50° Curve*			*−100° Curve*	
1	2.9	211.56	1	3.2	57.81	1	1.9	101.00
2	19.6	210.83	2	19.4	57.33	2	19.5	100.39
3	42.1	209.51	3	42.1	56.44	3	42.0	99.79
4	64.1	208.25	4	63.7	55.55	4	64.0	99.34
5	85.4	206.94	5	83.8	54.63	5	84.1	99.06
6	107.1	205.62	6	107.8	53.62	6	108.1	98.86
7	130.3	204.24	7	130.6	52.63	7	131.3	98.78
8	152.2	202.84	8	153.4	51.60	8	159.1	98.84
9	194.8	200.59	9	194.8	49.64	9	194.8	99.00
	150° Curve			*0° Curve*				
1	2.5	161.37	1	4.8	+6.23			
2	19.6	160.50	2	19.5	5.85			
3	40.6	159.37	3	41.1	5.23			
4	64.0	158.06	4	63.1	4.53			
5	85.1	156.85	5	84.0	3.89			
6	107.7	155.58	6	107.5	3.08			
7	130.6	154.20	7	130.8	2.29			
8	151.9	152.87	8	152.2	1.51			
9	194.8	150.55	9	176.0	+0.60			
			10	194.8	−0.18			

TABLE III. *Mixture No. 2.*

No.	p_2	l_2	No.	p_2	l_2	No.	p_2	$-l_2$
	250° Curve			*100° Curve*			*−50° Curve*	
1	3.8	258.39	1	4.6	100.71	1	2.5	69.63
2	19.5	258.11	2	19.5	100.97	2	19.7	66.86
3	43.3	257.28	3	43.4	101.11	3	41.9	63.69
4	66.9	256.40	4	66.9	101.13	4	67.0	60.65
5	90.2	255.45	5	87.9	101.09	5	87.4	58.54
6	110.0	254.62	6	110.8	100.96	6	110.5	56.47
7	132.7	253.74	7	132.7	100.76	7	132.0	54.84
8	154.5	252.76	8	154.3	100.51	8	154.2	53.39
9	170.0	252.06	9	194.7	100.14	9	194.7	51.48
10	194.7	251.05						
	200° Curve			*50° Curve*			*−100° Curve*	
1	4.1	206.37	1	1.9	46.22	1	67.0	116.89
2	19.5	206.09	2	19.5	47.09	2	88.0	112.99
3	43.5	205.48	3	42.6	47.84	3	110.5	109.49
4	67.1	204.78	4	66.7	48.46	4	132.4	106.65
5	88.3	204.15	5	87.6	48.89	5	155.6	104.34
6	111.0	203.39	6	110.2	49.25	6	194.7	101.25
7	133.0	202.64	7	134.6	49.51			
8	154.9	201.85	8	154.3	49.67			
9	170.3	201.35	9	194.7	49.64			
10	194.7	200.46						
	150° Curve			*0° Curve*				
1	5.8	153.74	1	1.9	−9.26			
2	19.5	153.75	2	19.3	−7.74			
3	43.3	153.51	3	42.2	−6.17			
4	66.9	153.17	4	66.9	−4.57			
5	87.7	152.81	5	87.9	−3.52			
6	110.5	152.37	6	110.2	−2.52			
7	132.8	151.85	7	133.9	−1.70			
8	154.3	151.33	8	154.3	−1.07			
9	194.7	150.33	9	194.7	−0.54			

TABLE IV. *Mixture No. 3.*

No.	p_2	l_2	No.	p_2	l_2	No.	p_2	$-l_2$
	250° Curve			*100° Curve*			*−50° Curve*	
1	4.4	252.62	1	5.1	90.22	1	2.5	92.98
2	19.5	252.69	2	19.8	91.39	2	19.3	86.35
3	42.4	252.87	3	42.7	93.03	3	41.8	78.57
4	64.4	252.73	4	65.6	94.49	4	64.7	72.21
5	87.4	252.57	5	87.4	95.68	5	87.6	66.69
6	108.5	252.35	6	109.6	96.77	6	109.9	62.07
7	132.6	252.03	7	132.6	97.73	7	133.3	58.23
8	155.6	251.66	8	154.1	98.48	8	154.5	55.18
9	194.8	251.01	9	170.8	98.99	9	194.7	51.25
			10	194.8	99.71			
	200° Curve			*50° Curve*				
1	4.7	199.36	1	3.6	32.97			
2	19.6	199.83	2	19.5	35.15			
3	42.3	200.31	3	42.5	37.92			
4	64.3	200.54	4	64.3	40.24			
5	87.2	200.75	5	87.5	42.44			
6	108.4	200.86	6	108.4	44.22			
7	132.6	200.85	7	132.8	45.98			
8	155.4	200.82	8	155.6	47.46			
9	194.8	200.66	9	194.8	49.64			
	150° Curve			*0° Curve*				
1	4.5	145.74	1	4.1	−26.42			
2	19.6	146.61	2	19.3	−23.13			
3	42.4	147.54	3	42.1	−18.67			
4	65.3	148.36	4	64.1	−14.97			
5	87.1	148.92	5	87.1	−11.48			
6	108.5	149.43	6	108.7	−8.59			
7	132.6	149.90	7	132.8	−5.82			
8	154.1	150.22	8	155.2	−3.59			
9	170.5	150.35	9	170.7	−2.19			
10	194.8	150.67	10	194.8	−0.28			

TABLE V. *Mixture No. 4.*

No.	p_2	l_2	No.	p_2	l_2	No.	p_2	$-l_2$
	250° Curve			*100° Curve*			*−50° Curve*	
1	4.6	245.57	1	5.6	75.41	1	4.4	125.13
2	19.4	246.44	2	20.5	78.01	2	19.6	112.76
3	42.4	247.55	3	42.3	81.51	3	41.5	98.24
4	65.2	248.42	4	65.2	84.72	4	64.5	86.70
5	86.8	249.13	5	87.2	87.71	5	87.2	77.40
6	109.0	249.74	6	109.7	90.26	6	107.9	70.55
7	131.3	250.30	7	131.9	92.63	7	130.5	64.28
8	154.9	250.76	8	153.5	94.61	8	153.4	59.17
9	194.8	250.77	9	175.9	96.50	9	175.7	54.90
			10	194.8	98.32	10	194.8	51.39
	200° Curve			*50° Curve*			*−100° Curve*	
1	4.8	191.11	1	4.1	16.51	1	109.7	114.29
2	22.1	192.33	2	19.8	20.74	2	130.8	110.00
3	42.0	193.94	3	42.3	25.96	3	153.1	106.26
4	66.2	195.47	4	64.1	30.61	4	175.7	103.35
5	87.4	196.67	5	86.2	34.78	5	194.8	101.47
6	109.5	197.80	6	106.8	38.31			
7	131.5	198.76	7	130.8	41.90			
8	154.2	199.59	8	153.4	44.93			
9	177.5	200.41	9	194.8	49.64			
10	194.8	200.62						
	150° Curve			*0° Curve*				
1	5.4	134.58	1	2.5	−49.26			
2	19.9	136.34	2	19.3	−42.09			
3	42.0	138.86	3	41.7	−33.88			
4	66.2	141.22	4	64.6	−26.56			
5	87.4	143.07	5	86.5	−20.49			
6	109.7	144.85	6	107.8	−15.45			
7	131.3	146.29	7	131.6	−10.38			
8	154.4	147.74	8	153.5	−6.37			
9	177.5	148.99	9	176.2	−2.85			
10	194.8	150.04	10	194.8	−0.18			

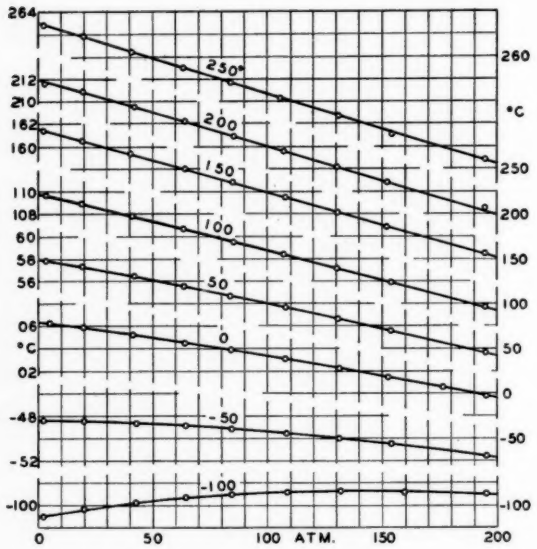

FIG. 1. Mix No. 1. Temperature *versus* pressure at constant enthalpy.

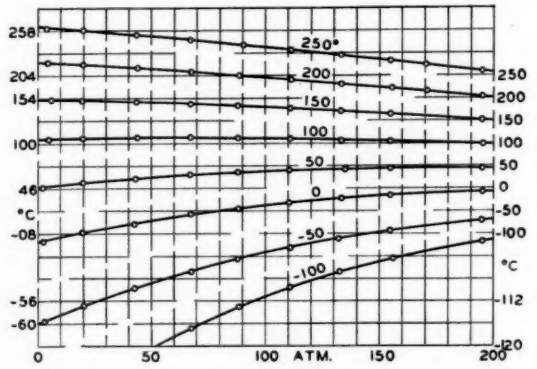

FIG. 2. Mix No. 2. Temperature *versus* pressure at constant enthalpy.

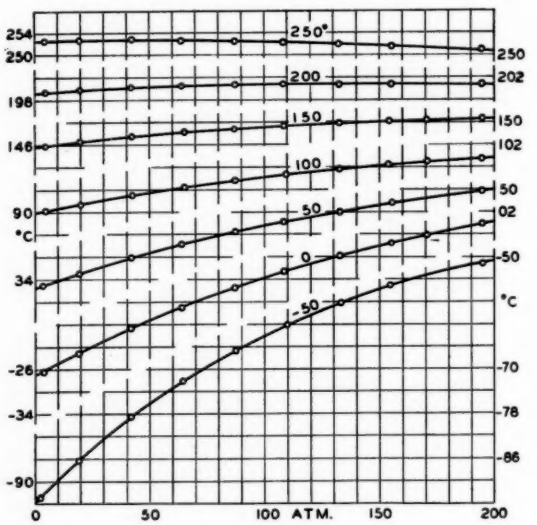

FIG. 3. Mix No. 3. Temperature *versus* pressure at constant enthalpy.

comparison of the isenthalpic curves for any one bath temperature shows how the straight lines of negative slope for pure helium shift regularly to the concave-downward curves of large positive slope for argon. The situation is the same as first observed in our mixture work with air in helium.[3]

One observes again the marked similarity between the family of isenthalpic curves for one pure gas (e.g. for argon) at a series of bath temperatures, and the family of curves corresponding to a series of compositions all at the same temperature.

To observe the effect of the composition and temperature on the total drop, the Δt for a pressure drop from 200 to 15 atmos. was read off from these isenthalpic curves of Figs. 1–4. In Fig. 5 these values of Δt are plotted against composition giving a set of curves, one for each of four bath temperatures. The four curves have the same general character as Fig. 5 in the helium[3] article, and Fig. 5 in $He+N_2$ mixture[7] article. Here, in Fig. 5, the rise at the left-hand end of the curves is not present, the 250° curve starting practically horizontally. This is probably due to the higher critical temperature of the argon over both air and nitrogen. It is probable that at bath temperatures higher than 250°C the rise would appear in this case also.

The slope of all these curves increases toward the pure argon side of the figure, and also increases with falling temperature. The data was not carried to low enough temperatures to enter the region where with pure argon this increase reverses.

JOULE-THOMSON COEFFICIENT, $\mu=(dt/dp)_h$

As in previous work, the numerical values of μ are obtained by taking the ratio of the successive and corresponding differences of temperature and of pressure for each experimental run. These values of μ were plotted against the corresponding average pressure to give a set of isenthalpic curves for each mixture. In the large scale plot

(25×40 cm) the experimental points drop on smooth curves at least as well as with previous data, leaving only small irregularities to be smoothed out. It has not seemed necessary to reproduce these curves.

From these unpublished curves values of μ for a series of selected pressures were read off and the corresponding temperatures read off from the isenthalpic curves of Figs. 1–4. These values of μ and t were then plotted as isopiestics. The points obtained from successive differences show necessarily considerably more variation than the original isenthalpic curves. This cross plot was used to help adjust the μ *vs.* p curves through the experimental points to obtain as consistent families as possible, without in any case leaving the experimental points farther than the spread of these points justifies.

The four families of curves, one family for each mixture, are reproduced in Figs. 6–9.

The abscissa scale is the same in all four figures, but to offset the increase in the average value of μ, the ordinate scale is shifted by a factor of 2 between each Fig. 6, 7, 8, and 9. These families resemble each other less than the four similar families of the He+N_2 mixtures, due here to a closer approach to the critical temperature of the higher critical-temperature component. Some of the curves here enter the region where μ decreases with decreasing temperature. Again, however, each family looks like an appropriate section from the family for pure air, argon, or nitrogen. The theorem of corresponding states is again suggested.

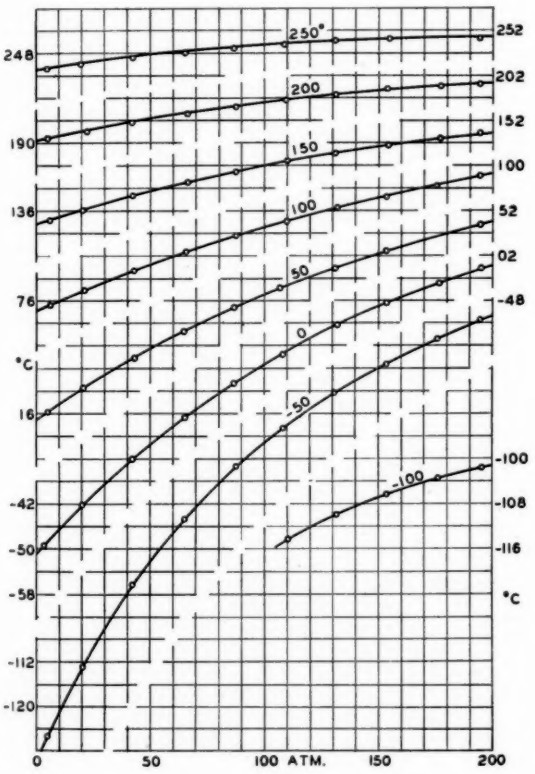

FIG. 4. Mix No. 4. Temperature *versus* pressure at constant enthalpy.

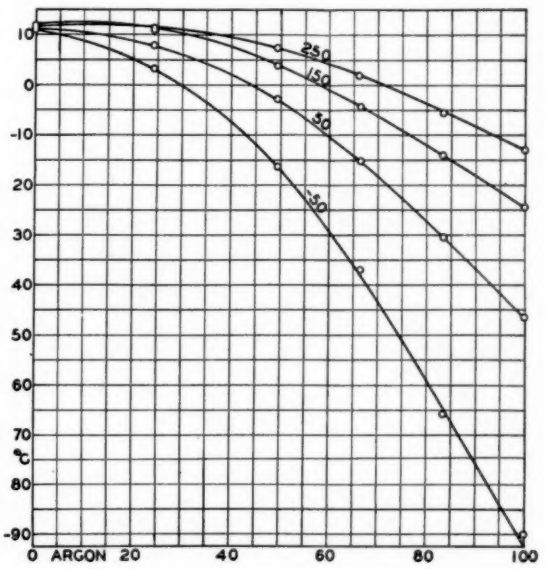

FIG. 5. Temperature change for a pressure drop of 200 to 15 atmos. as a function of composition at several initial temperatures.

The previous observation for the isenthalpic curves of Figs. 1–4, that the effect of a change in composition resembles greatly the effect of a change in temperature, holds again in these families, Figs. 6–9.

The numerical data for μ have been picked off the large scale plots from which Figs. 6–9 were traced and are collected in Tables VI–IX. With mixture No. 1 the negative values of μ at the highest temperature and lowest pressure are the same as for pure helium; but these values fall numerically with rising pressure, while with pure helium they remain constant except at our lowest attainable temperature. With all these mixtures μ decreases with rising temperature and falling pressure except for 3 values in Table

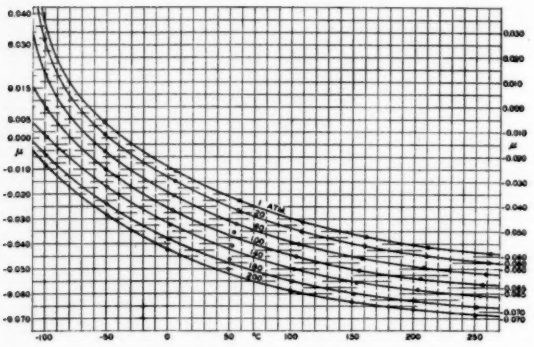

FIG. 6. Mix No. 1. μ *versus* temperature at constant pressure.

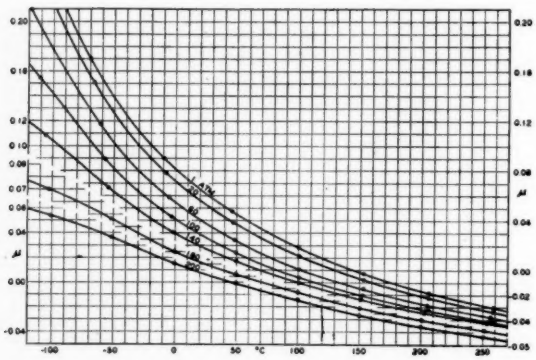

FIG. 7. Mix No. 2. μ *versus* temperature at constant pressure.

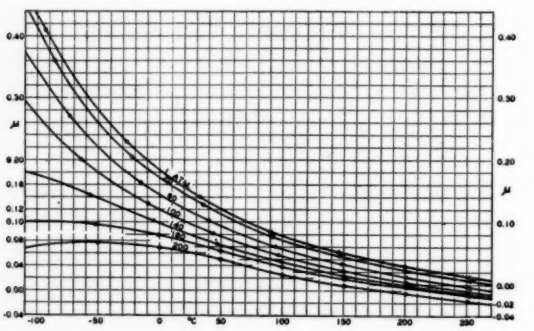

FIG. 8. Mix No. 3. μ *versus* temperature at constant pressure.

IX (Mix. 4) where the influence of the critical conditions appears. The maximum value of μ is below that for pure argon at the same temperature and pressure.

The effect of the composition on μ is shown graphically in Figs. 10, 11 and 12, where μ is plotted against composition at a series of constant temperatures and at the three constant

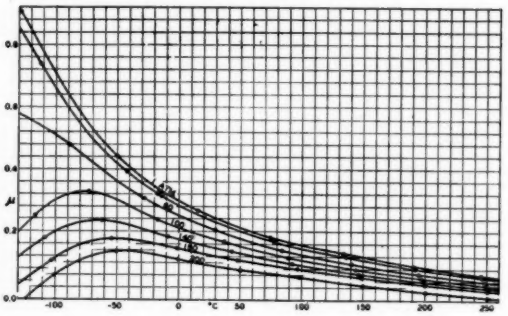

FIG. 9. Mix No. 4. μ *versus* temperature at constant pressure.

TABLE VI. $\mu \times 10^2$; *Mix No. 1;* He *75.8 percent,* A *24.2 percent.*

$t°c$ \ p	1	20	60	100	140	180	200
250	−5.83	−5.95	−6.15	−6.37	−6.56	−6.77	−6.85
200	5.55	5.66	5.90	6.13	6.34	6.55	6.63
150	5.11	5.24	5.52	5.77	5.99	6.21	6.34
100	4.47	4.61	4.91	5.18	5.45	5.72	5.88
50	3.61	3.76	4.08	4.40	4.68	5.01	5.19
0	2.40	2.57	2.92	3.30	3.65	4.03	4.22
−50	−0.69	−0.92	−1.32	−1.75	2.21	2.66	2.82
−100	+3.37	+2.82	+1.87	+0.79	−0.14	−0.65	−0.78

TABLE VII. $\mu \times 10^2$; *Mix No. 2;* He *50.6 percent,* A *49.4 percent.*

$t°c$ \ p	1	20	60	100	140	180	200
250	−2.84	−3.19	−3.65	−4.04	−4.21	−4.33	−4.34
200	1.67	2.07	2.71	3.15	3.40	3.55	3.57
150	−0.13	−0.67	−1.50	2.01	2.32	2.56	2.62
100	+1.84	+1.15	+0.11	−0.59	−1.01	−1.32	1.48
50	4.50	3.66	2.37	+1.39	+0.70	+0.14	−0.07
0	8.19	7.20	5.51	4.12	2.96	1.99	+1.57
−50	13.84	12.61	10.27	8.14	6.28	4.53	3.63
−100	—	—	+17.79	+14.17	+10.36	+6.90	+5.40

TABLE VIII. $\mu \times 10^2$; *Mix No. 3;* He *33.5 percent* A *66.5 percent.*

$t°c$ \ p	1	20	60	100	140	180	200
250	+1.34	+0.72	−0.38	−1.03	−1.48	−1.68	−1.68
200	2.94	2.32	+1.25	+0.45	−0.13	−0.38	−0.38
150	5.05	4.41	3.23	2.22	+1.41	+0.92	+0.83
100	7.80	7.10	5.69	4.55	3.63	2.86	2.54
50	12.12	11.28	9.40	7.73	6.32	5.41	5.01
0	18.40	17.18	14.43	12.05	9.88	7.93	6.88
−50	27.90	25.82	21.93	17.96	13.83	9.63	7.73
−100	43.30	41.15	34.30	27.20	17.55	10.07	7.10

TABLE IX. $\mu \times 10^2$; *Mix No. 4;* He *16.6 percent,* A *83.4 percent.*

$t°c$ \ p	1	20	60	100	140	180	200
250	5.75	5.15	3.85	2.70	1.90	1.20	0.95
200	8.45	7.63	6.05	4.75	3.85	3.00	2.60
150	11.70	10.80	8.95	7.45	6.10	5.20	4.60
100	15.50	14.50	12.60	10.80	9.05	7.70	7.05
50	21.05	20.10	17.75	15.35	13.00	10.65	9.55
0	29.85	28.40	25.00	21.15	17.35	14.50	13.05
−50	44.15	41.80	36.15	30.10	22.90	17.55	15.60
−100	70.80	66.10	51.00	29.95	19.75	11.35	8.00

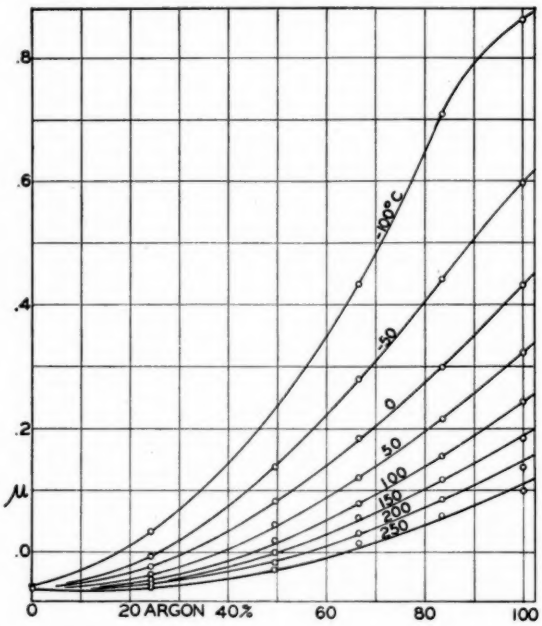

FIG. 10. μ *versus* composition at a series of constant temperatures but all at one atmos. pressure.

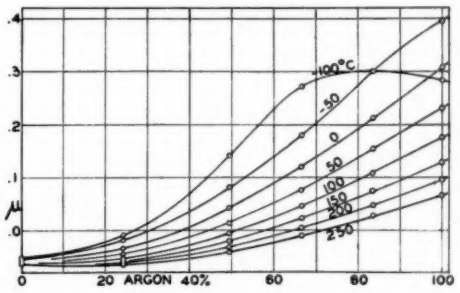

FIG. 11. μ *versus* composition at a series of constant temperatures but all at 100 atmos. pressure.

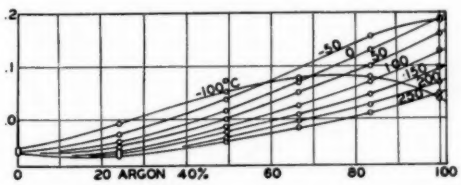

FIG. 12. μ *versus* composition at a series of constant temperatures but all at 200 atmos. pressure.

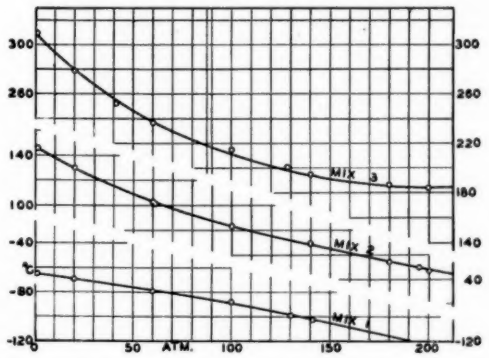

FIG. 13. Pressure as a function of temperature for $\mu=0$ for three mixtures.

pressures of 1, 100, and 200 atmospheres in the three figures, respectively. These include also the necessary data for pure helium and pure argon. The points fall systematically on smooth curves as in the corresponding situation for the $He+N_2$ mixtures. With the He+A mixtures however the curves exhibit less pronounced minima, but from the trend of the curves in the three figures it is apparent that they will become more pronounced at higher temperatures. The critical temperature of argon being higher than that of nitrogen is apparently a reason for this higher temperature.

Several of the low temperature curves enter the temperature field in which μ for argon shows the rapid decrease characteristic of the approach to the critical temperature from above. Here evidently the properties of the mixture are largely controlled by those of the argon constituent.

INVERSION CURVES, $\mu=0$

In three of the four families of curves Figs. 1–4, the isenthalpic curves show maxima ($\mu=0$). In the mixture richest in helium, No. 1, the maxima show in the two lowest temperature curves; in No. 2 they lie about the middle of the group; in No. 3 they lie near the upper part of the temperature range; and in No. 4 the highest temperature (250°C) is not high enough for them to appear.

The pressures and temperatures at which $\mu=0$ may be taken off the isenthalpic curves of Figs. 1, 2 and 3. They may also be read from the curves of Figs. 6, 7 and 8. These data are plotted in Fig. 13. Only the upper branch of each curve appears. The curves are much less regular than the corresponding group[7] for $He+N_2$, particularly the curve for mixture No. 3. Within this uncertainty they confirm the earlier conclusion that the curves approach zero pressure without any material change of their small curvature.

The curves of Fig. 14 exhibit the effect of

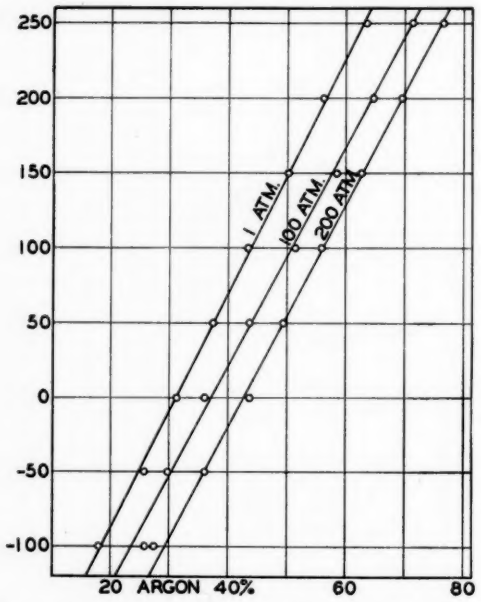

FIG. 14. Temperature as a function of composition for $\mu=0$ and three constant pressures.

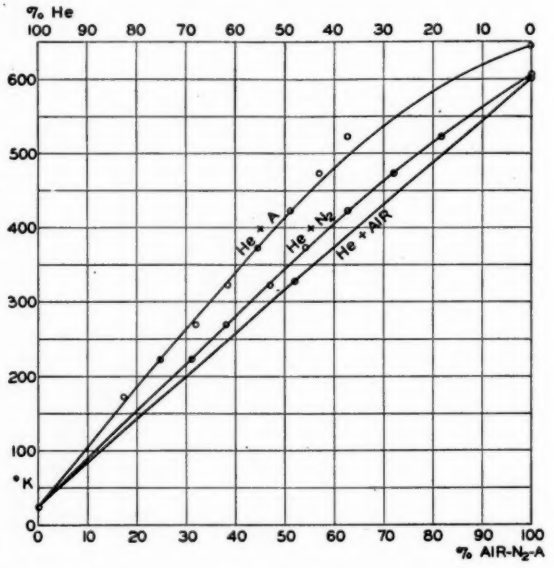

FIG. 15. Temperature as a function of composition for $\mu=0$ and $p=1$ atmos. for several mixtures.

composition on the temperature at which $\mu=0$ for three pressures, 1, 100, and 200 atmos. The curves are not quite so regular as in the He+N_2 case, but are very similar to them. The situation where $\mu=0$, shifts to lower temperature with increase in pressure or in He proportion. This applies of course only to these upper branches of the inversion curves. The lower branches fall in the general region where condensation occurs and were not measured.

As in the case[7] of He+N_2 a mixture of He and A may be made, the reciprocal of whose average coefficient of expansion between 0°C and 100°C (α_0^{100}) is itself the temperature of the ice point on the Kelvin scale. It contains about 35 percent by volume of argon, whereas it required about 46 percent N_2. This smaller proportion can be attributed to the effect of the higher critical temperature of the argon.

We have estimated[4] the temperature as 23.6°K at which pure helium has $\mu=0$ at 1 atmos. For pure argon[5] this temperature is above the temperature range of our experiments. It can be estimated however from the nitrogen[6] data using the theorem of corresponding states. In the nitrogen[6] article this temperature for N_2 is given as 334°C (607°K). This gives 373°C (645°K) for argon. This data (t against composition for $p=1$, $\mu=0$) for the range of composition of one pure material to the other, and for the mixtures He+Air, He+N_2, and He+A is plotted in Fig. 15.

The single point for the air mixture coming from the preliminary work on He[3], falls almost exactly on a straight line between the points for pure air and pure He. The He+N_2 points fall well on a smooth curve which is straight for the first half from pure He, but is concave downward for the rest. The temperature is not far from a linear function of the composition.

The He+A points do not fall well on a smooth curve and the whole curve is concave downward. Like the He+N_2 curve the greatest curvature is at the higher temperature. While the experimental data for individual runs is fully as consistent as in any of the previous work, there appear to be somewhat greater inconsistencies in the comparisons of data from the various parts of the field than is to be observed in the He+N_2 case.

In the work with helium[3] tests for air impurity and repurification were relatively simple matters. With nitrogen the addition of air disturbs the purity more slowly, air being $\frac{4}{5}$ nitrogen, and also the nitrogen being cheap could be discarded. But with the argon, air impurity has a relatively large effect on its properties, we had no adequate

TABLE X. *Temperature of inversion for $p=0$ in reduced units.*

	Mix No.	t_i°C	T_i°K	T_c°K	T_i/T_c	
He+A	1	−54.1	209	404	5.17	
He+A	2	135	420	77.2	5.44	5.44
He+A	3	290	583	102	5.71	

tests for the presence of air, repurification was beyond our available experimental means, and the argon was too expensive to discard. All of the data in this article were taken on a single cylinder of argon by mixing it with helium, measuring the argon-rich mixtures first. But also the measurements were carried out rapidly and with a minimum of difficulty with an apparatus in which leaks were small. It is, nevertheless, to be expected that the data contain a larger element of uncertainty on account of air impurity, than in any of the previous work.

The hypothetical critical temperature of these mixtures was calculated as described in the $He+N_2$ article.[7] Using these T_c values the observed inversion temperatures of the mixture were shifted to a reduced temperature scale. The data are given in Table X. Table X of the article[7] on $He+N_2$ mixtures gives the corresponding data for other mixtures and some pure gases. The average value of 5.44 is larger than in this previous work where, for example, $He+N_2$ mixtures[7] give 5.18.

By chance, reference to the above use of a linear variation of T_c with composition, was found in a copy of Nernst's *Theoretical Chemistry* where he cites two references.[10,11]

Our thanks are due to the Wisconsin Alumni Research Foundation whose generous assistance enabled full time to be devoted to the experimental part of this work.

The helium used here and in other work was supplied by the Bureau of Mines of the United States Government. We thank them for their help which made this extensive work with helium possible.

We also wish to thank the Air Reduction Sales Company and Mr. F. P. Gross, Jr., for their gift of the argon which made this work possible.

In this as in some other problems, grants from the Rumford Fund of the American Academy of Arts and Sciences have been very helpful.

Much of the reduction of the experimental data and the preparation of the curves were carried out by Mr. H. R. Kelly, whose assistance is gratefully acknowledged. Our thanks are also due to Mr. T. A. Murrell who carried out the major part of the recalculation and redrafting necessary for the correction of the pressure scale.

[10] Pawlewski, Berichte (Berlin) **16**, 33 (1883).
[11] G. C. Schmidt, Lieb. Ann. **266**, 266 (1891).

AUGUST, 1940 JOURNAL OF CHEMICAL PHYSICS VOLUME 8

Thermodynamic Properties of Methyl Cyanide and Methyl Isocyanide

RAYMOND H. EWELL AND JAMES F. BOURLAND
Department of Chemistry, Purdue University, Lafayette, Indiana

(Received April 9, 1940)

THE structures of methyl cyanide (CH_3CN) and methyl isocyanide (CH_3NC) have been determined by Brockway[1] by means of electron diffraction, and their vibration frequencies have been determined by Badger and Bauer[2] from a study of the infra-red and Raman spectra. These studies provide all the necessary data for computing the thermodynamic properties of these substances in the ideal gaseous state on the basis

[1] L. O. Brockway, J. Am. Chem. Soc. **58**, 2516 (1936).
[2] R. M. Badger and S. H. Bauer, J. Am. Chem. Soc. **59**, 303 (1937).

TABLE I. *Molecular constants of methyl cyanide and methyl isocyanide.*

	Methyl Cyanide	Methyl Isocyanide
C−H distance	1.09A	1.09A
C−C or C−N distance	1.54A	1.48A
C≡N or N≡C distance	1.16A	1.17A
∠HCH	109½°	109½°
∠HCC or ∠HCN	109½°	109½°
I_1	5.3×10^{-40}	5.3×10^{-40}
$I_2=I_3$	97.3×10^{-40}	86.8×10^{-40}
$I_1I_2I_3$	$50{,}000\times10^{-120}$	$39{,}900\times10^{-120}$
Molecular weight	41.05	41.05
Symmetry number	3	3

TABLE II. *Vibration frequencies of methyl cyanide and methyl isocyanide in cm⁻¹.*

	METHYL CYANIDE	METHYL ISOCYANIDE
C−H stretching[3]	3000[3]	3000[3]
C−C or C−N stretching[1]	917[1]	928[1]
C≡N or N≡C stretching[1]	2250[1]	2161[1]
HCH bending[3]	1370[1]	1414[1]
	1417[2]	1456[2]
HCC or HCN bending[2]	1040[2]	1041[2]
CCN or CNC bending[2]	376[2]	290[2]

of the rigid rotator-harmonic oscillator approximation. Tables I and II give the assembled molecular data.

The calculations were made using the well-known relations

$$-\frac{F^0-E_0{}^0}{T}=3/2R\ln M+4R\ln T+1/2R\ln I_1I_2I_3 -R\ln\sigma+257.40-R\sum_1^{12}\ln(1-e^{-x}),$$

$$\frac{H^0-E_0{}^0}{T}=4R+R\sum_1^{12}\frac{e^x}{e^x-1},$$

$$S^0=\frac{H^0-E_0{}^0}{T}-\frac{F^0-E_0{}^0}{T},$$

$$C_p=4R+R\sum_1^{12}\frac{x^2e^x}{(e^x-1)^2},$$

where

$$x=hc\bar{\nu}/kT=1.432\bar{\nu}/T$$
$$R=1.9869.$$

Inserting the data from Table I, gives

CH_3CN:

$$-\frac{F^0-E_0{}^0}{T}=2.53+4R\ln T-\left(\frac{F^0-E_0{}^0}{T}\right)_{\text{vib}},$$

CH_3NC:

$$-\frac{F^0-E_0{}^0}{T}=2.30+4R\ln T-\left(\frac{F^0-E_0{}^0}{T}\right)_{\text{vib}}.$$

The Einstein vibrational functions were evaluated by using a table calculated by Sherman and Ewell.[3] The calculated values of the thermodynamic functions are given in Tables III and IV. The heat capacity data were fitted to three constant equations as follows:

CH_3CN: $C_p=4.77+29.1\times10^{-3}T+10.45\times10^{-6}T^2$ (0.5 percent, 273–773°K),

CH_3NC: $C_p=6.14+24.2\times10^{-3}T+6.16\times10^{-6}T^2$ (0.5 percent, 273–773°K).

[3] J. Sherman and R. B. Ewell, unpublished.

TABLE III. *Calculated thermodynamic properties of methyl cyanide in the ideal gaseous state.*

t°C	$-(F^0-E_0{}^0)/T$	$(H^0-E_0{}^0)/T$	S^0	$C_p{}^0$
0	47.72	9.42	57.14	11.93
25	48.57	9.65	58.22	12.48
50	49.36	9.89	59.25	13.12
100	50.82	10.38	61.20	14.12
150	52.14	10.90	63.04	15.29
200	53.39	11.40	64.79	16.19
300	55.69	12.39	68.08	17.93
400	57.90	13.34	71.24	19.62
500	59.69	14.28	73.97	21.04

TABLE IV. *Calculated thermodynamic properties of methyl isocyanide in the ideal gaseous state.*

t°C	$-(F^0-E_0{}^0)/T$	$(H^0-E_0{}^0)/T$	S^0	$C_p{}^0$
0	47.87	9.83	57.70	12.28
25	48.75	10.05	58.80	12.76
50	49.68	10.28	59.96	13.25
100	51.10	10.74	61.84	14.26
150	52.47	11.22	63.69	15.26
200	53.76	11.70	65.46	16.20
300	56.09	12.66	68.75	18.05
400	58.21	13.56	71.77	19.63
500	60.21	14.47	74.68	21.04

It is unfortunate that the heat of combustion data for methyl cyanide and methyl isocyanide are so uncertain,[4] otherwise the equilibrium constants for some interesting and possibly technically useful reactions could be calculated. Some calculations have been made with the combustion data tabulated by Bichowsky and Rossini.[4] While the results are too unreliable to warrant giving them in detail, the general conclusions are briefly as follows: (1) Methyl cyanide could be obtained in good yields by dehydrogenation of ethylamine above 350°C; (2) Ethylene and ammonia could combine to give methyl cyanide and hydrogen in good yields above 500°C.

[4] F. R. Bichowsky and F. D. Rossini, *Thermochemistry of Chemical Substances* (Reinhold Publishing Corporation, New York, 1936).

On the Stable Relative Orientation of Groups Connected by a Carbon-Carbon Single Bond

VERNER SCHOMAKER AND D. P. STEVENSON
Gates and Crellin Laboratories of Chemistry, California Institute of Technology, Pasadena, California
(Received June 17, 1940)

LANGSETH and his co-workers[1] have recently applied the results of essentially incomplete spectroscopic studies of liquid cyclohexane, symmetrical tetrachloroethane, and ethylene deuterobromide to a discussion of the intramolecular forces restricting internal rotation about the C−C bond. We believe that none of their structural conclusions is correct. Their discussion is based on their conclusion that in these molecules the opposed or eclipsed configurations are the stable ones. Insofar as liquid cyclohexane and symmetrical tetrachloroethane are concerned this conclusion is most probably incorrect since it directly contradicts the results of a great number of essentially more straightforward studies of these and similar molecules in the gaseous and solid phases, and since it is probable that molecules in the liquid generally have structures closely related to those in the gas and the solid, at least when these are not too different. But whatever may be the structures of these molecules in the liquid, it is certainly true that the structures of the free molecules are more pertinent to a discussion of intramolecular forces. These structures indicate that there is a general tendency for the staggered configurations to be the stable ones, and Langseth's general discussion[1c] must accordingly be without significance. Some of the existing evidence on cyclohexane, symmetrical tetrachloroethane, and related molecules is briefly given below together with a preliminary report on an electron diffraction investigation of the structure of gaseous symmetrical tetrachloroethane. We know of no direct evidence regarding the stable configuration of the ethyl bromide molecule. We believe, however, that in ethyl bromide and in ethane it is the staggered configuration which is the more stable, as it is in the hydrocarbons and substituted hydrocarbons for which unambiguous structural information exists. It seems likely therefore that Langseth's assignments of the two isomeric components[1d,2] of the C−Br stretching frequency of ethylene deuterobromide should be reversed.

X-ray studies of crystalline cyclohexane,[3a] β-benzene hexabromide and hexachloride,[3b] and 1,4-di-iodocyclohexane[3c] uniformly eliminate the possibility of the planar cyclohexane ring, proposed by Langseth and Bak, as does the electron diffraction investigation of gaseous cyclohexane by Pauling and Brockway.[4] Beach and his co-workers[5] have found staggered configurations for ethylene chloride, chlorobromide, and bromide, and 1,1,2-trichloroethane as we have for the 2,3-dibromobutanes and propylene bromide. Klug reported crystalline ethylene iodide[7] to have a *trans* and thus staggered configuration.

Our electron diffraction photographs[8] of gaseous symmetrical tetrachloroethane were obtained

TABLE I.

MAX.	MIN.	C_n	s_0	MAX.	MIN.	C_n	s_0
	1	−3	1.61	6		12	11.85
1		5	2.63		7	−10	12.74
	2	−7	3.68	7		9	13.64
2		10	4.74		8	−4	14.38
	3	−5	5.54	8		6	15.54
3		3	6.14		9	−8	16.72
	4	−11	6.77	9		7	17.97
4		12	7.68		10	−2	18.70
	5	−5	8.47	10		3	19.54
5		5	9.43		11	−6	20.55
	6	−13	10.54	11		5	21.85

[1] a. A. Langseth and B. Bak, J. Chem. Phys. **8**, 403 (1940). b. A. Langseth and H. J. Bernstein, *ibid.* **8**, 410 (1940). c. A. Langseth, H. J. Bernstein and B. Bak, *ibid.* **8**, 415 (1940). d. A. Langseth, H. J. Bernstein and B. Bak, *ibid.* **8**, 430 (1940).

[2] M. de Hemptinne and C. Velghe, Physica **5**, 958 (1938).

[3] a. O. Hassel and H. Kringstad, Tidskr. Kemi. Bergvesen, **10**, 128 (1930). b. R. G. Dickinson and C. Bilicke, J. Am. Chem. Soc. **50**, 764 (1928). c. E. Holmöy and O. Hassel, Zeits. f. physik. Chemie **B16**, 234 (1932).

[4] L. Pauling and L. O. Brockway, J. Am. Chem. Soc. **59**, 1223 (1937).

[5] a. J. Y. Beach and K. J. Palmer, J. Chem. Phys. **6**, 639 (1938). b. J. Y. Beach and A. Turkevich, J. Am. Chem. Soc. **61**, 303 (1939). c. A. Turkevich and J. Y. Beach, *ibid.* **61**, 3127 (1939).

[6] a. D. P. Stevenson and V. Schomaker, J. Am. Chem. Soc. **61**, 3173 (1939). b. V. Schomaker and D. P. Stevenson, unpublished observations.

[7] H. P. Klug, Zeits. f. Krist. **90**, 495 (1935).

[8] L. O. Brockway, Rev. Mod. Phys. **8**, 231 (1936).

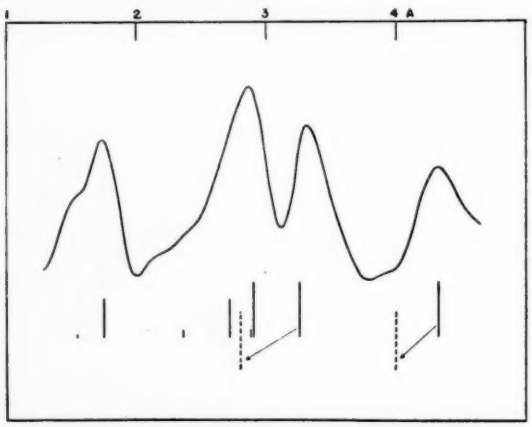

FIG. 1. The radial distribution function for symmetrical tetrachloroethane. The solid vertical lines give the interatomic distances to be expected for a molecule with bond distances and angles as in ethyl chloride and methylene chloride. The lengths of the lines indicate the relative importance of the distances in the scattering formula for the more symmetrical (C_{2h}) model. For the less symmetrical staggered model (C_2) the 3.25A line would become three times as long as the 4.31A line. The dotted lines correspond to the orientation-dependent distances in the symmetric (C_{2v}) eclipsed model; for the C_2 eclipsed model the longer of these distances becomes three times as important as the shorter one. The arrows relate the corresponding orientation-dependent distances of the two types of models.

from a sample (b.p. 142.8±0.1°) which was part of the middle fraction obtained on distilling a large quantity of Eastman symmetrical tetrachloroethane through a 25-cm helix packed column with controllable reflux ratio. The photographs were taken with the high temperature nozzle.[9] The temperature of the boiler was varied from 70° to 120°. The wave-length of the electrons was 0.0615A (a_0 for gold, 4.070A) and the camera distance was 10.85 cm.

The photographs showed eleven rings whose measured s values ($s=(4\pi/\lambda)\sin(\vartheta/2)$) are given in Table I along with the coefficients C_n of the radial distribution function.[10] Characteristic features of the diffraction pattern are the relatively weak third and fifth maxima, the broad appearance of the eighth and the shelf-like nature of the tenth maximum.

The radial distribution function shown in Fig. 1 has maxima at 1.74, 2.86, 3.31 and 4.32A. The first of these (1.74A) corresponds to the carbon-chlorine bond distance (1.76A), and the second (2.86A) to an unresolved average of the nonbonded carbon-chlorine distance (2.74A in ethyl chloride[11a]) and the distance between chlorine atoms bound to the same carbon atom (2.92A in methylene chloride[11b]). The positions of the other two maxima at 3.31A and 4.32A correspond to the chlorine-chlorine distances (3.25A and 4.32A) which would be expected if the bond distances and bond angles are the same as the corresponding distances and angles in ethyl chloride and methylene chloride and if the molecule has one (or both) of the "staggered" relative orientation of the two $-CHCL_2$ groups about the C−C bond. Moreover, it may be seen from Fig. 1 that these peaks are in complete disagreement with the distances to be anticipated for the "opposed" configuration proposed by Langseth and Bernstein.[1b] The peaks of the radial distribution function which depend on the relative orientation of the two ends of the molecule are quite narrow. It therefore seems likely that the molecules are fairly rigid. In particular, the sharpness of the 3.31A peak indicates that the amplitude of libration is less than that (15–20°) which has been estimated for ethylene chloride, etc.[5,6] The approximate 3 : 2 ratio of the heights of the 3.31A and 4.32A peaks of the radial distribution function suggest that the gas at the temperatures of our experiments consist of a roughly equimolal mixture of the two staggered isomers. We believe that the complete treatment of our data by the correlation method will provide a more precise estimate of the relative abundance of the two isomers as well as the answer to the rather large discrepancy between the position of the 3.31A peak of the radial distribution function and the value calculated from our model. Our tentative conclusions regarding the relative abundance and rigidity of the isomers are in good agreement with those of Smyth and McAlpine[12] from dipole moment measurements on the gas.

We are indebted to Professor Linus Pauling for helpful counsel about the matters discussed in this paper.

[9] L. O. Brockway and K. J. Palmer, J. Am. Chem. Soc. **59**, 2181 (1937).

[10] a. L. Pauling and L. O. Brockway, J. Am. Chem. Soc. **57**, 2684 (1935). b. Verner Schomaker, American Chemical Society Meeting, Baltimore, Maryland, April, 1939.

[11] a. J. Y. Beach and D. P. Stevenson, J. Am. Chem. Soc. **61**, 2643 (1939). b. L. E. Sutton and L. O. Brockway, *ibid.* **57**, 479 (1935).

[12] C. P. Smyth and K. B. McAlpine, J. Am. Chem. Soc. **57**, 979 (1935).

Thermal Diffusion Separation of Radioactive and Ordinary Hydrogen Isotopes

G. T. SEABORG, A. C. WAHL AND J. W. KENNEDY
Department of Chemistry, University of California, Berkeley, California

(Received June 11, 1940)

IT seems reasonable that in the separation of gaseous isotopes by the thermal diffusion method of Clusius and Dickel[1,2] the separation factor* should be independent of the relative concentrations of the two components. The simplified equation of Enskog[3] indicates that the separation factor for the elementary thermal diffusion process is independent of concentration. However, it is not impossible that a variation in S.F. with mole fraction could arise from the process producing multiplication of the unit separation by convective action; also, the results on the separation of the chlorine isotopes reported by Clusius and Dickel[2] indicate a variation in S.F. amounting to a factor of about two or three between the values at high mole fractions (70 percent to 40 percent Cl^{35}) and at low mole fractions (12 percent to 0.6 percent Cl^{35}).†

To test the behavior of a Clusius and Dickel column at extremely small mole fractions we have employed a radioactive isotopic species, namely the long-lived radioactive H^3 of Alvarez and Cornog.[4] A column was constructed 7.5 meters in length and with an inside diameter of 1.0 cm. A water-cooling jacket served to keep this tube at room temperature; provision was made for electrically heating an axial, molybdenum wire (0.40 mm diameter). A 5-liter gas reservoir was connected to the top of the column, and samples were withdrawn from the bottom.

In a set of preliminary experiments we studied the separation of deuterium-hydrogen mixtures. With the wire at 250°C and the gas at 1 atmosphere pressure, equilibrium was reached after 3 days and thermal conductivity analyses of samples removed showed 18 percent deuterium in the reservoir and 87 percent deuterium at the bottom of the column. These figures give S.F. $=30$. (With the wire at higher temperatures S.F. could not be accurately measured because the deuterium content of the samples withdrawn from the bottom was too large.)

A mixture of deuterium and radioactive H^3 (mole fraction $\sim 10^{-11}$) was introduced into the same column under identical conditions of temperature and pressure as above. The samples withdrawn were analyzed for H^3 content by introduction into a Geiger-Müller counter. At equilibrium we found S.F. $=5.0$. When account is taken of the mass dependence of S.F. according to the equations[3] of Enskog or Chapman it is seen that the effectiveness of the column for separating hydrogen isotopes is substantially the same at moderate or extremely small mole fractions.

We have performed exploratory experiments concerning the dependence of S.F. on the temperature of the hot wire, using deuterium-radioactive H^3 mixtures for convenience in analysis. S.F. increased with increasing temperature, reaching the value 9 at the highest temperature available, 800°C. (To prevent vibration of the wire at this temperature spacers in the column were required even though direct current was used for heating.) It should be possible to increase further this separation by finding the optimum values of temperature, pressure and tube radius. Another way to increase S.F. is to use several such columns in series.[2] It is easily seen that if the S.F. is independent of the mole fraction, as is demonstrated approximately by the present experiments, then the S.F. for several columns in series will be given by the product of the individual S.F.'s. We have actually connected in series with the column described above a second column, which we have previously used

[1] K. Clusius and G. Dickel, Naturwiss. **26**, 546 (1938); **27**, 148 and 487 (1939).
[2] K. Clusius and G. Dickel, Zeits. f. physik. Chemie **B44**, 397 and 451 (1939).
* For this discussion we use the separation factor $(S.F.)=(N_1/N_2)_{bottom}/(N_1/N_2)_{top}$, where N_1 and N_2 are the mole fractions of the isotopes.
[3] See reference 2, page 427.
† An algebraic error in the derivation of an equation in their paper (reference 2, Eq. (26), p. 430) may have led them to exaggerate the magnitude of this variation (Fig. 8, p. 471). In addition the experimental values were necessarily determined in a region where the effect of errors in measurement are magnified.
[4] L. W. Alvarez and R. Cornog, Phys. Rev. **56**, 613 (1939).

in separating[5] the chlorine isotopes, and obtained the expected S.F. although a longer time was required to reach equilibrium (with our coupling arrangement about 10 times as long as for a single column).

It would be interesting to know how well the Clusius and Dickel column would separate deuterium-hydrogen mixtures at the higher temperature (800°C). If the temperature dependence of this S.F. is the same as that of the deuterium-radioactive H^3 mixture, at 800° we would expect S.F. = 54. However, calculations based on the Enskog equation suggest a much higher value. (The same calculations give the temperature dependence of the deuterium-radioactive H^3 separation within a factor of two for the region investigated.) A value of 54 for S.F., which we for these reasons consider a lower limit, would imply that, starting from a large reservoir of the natural isotopic mixture, one column of the type described would produce 1.1 percent deuterium, two such columns would give 37 percent deuterium, and three columns could be used to deliver 97 percent deuterium.

We are indebted to Professor E. O. Lawrence and other members of the Radiation Laboratory, in particular Dr. R. Cornog, for the sample of radioactive hydrogen. Also it is a pleasure to thank Dr. Melvin Calvin, who made available to us his thermal conductivity apparatus.

[5] J. W. Kennedy and G. T. Seaborg, Phys. Rev. **57**, 843 (1940).

LETTERS TO THE EDITOR

This section will accept reports of new work, provided these are terse and contain few figures, and especially few halftone cuts. The Editorial Board will not hold itself responsible for opinions expressed by the correspondents. Contributions to this section should not exceed 600 words in length and must reach the office of the Managing Editor not later than the 15th of the month preceding that of the issue in which the letter is to appear. No proof will be sent to the authors. The usual publication charge ($3.00 per page) will not be made and no reprints will be furnished free.

Silicate Glasses

Volumes, refractions and dispersions of well-annealed silicate glasses are simple additive functions of the compositions, when these properties are calculated for the quantity of glass which contains one gram atom of oxygen and the compositions are expressed as numbers of atoms (N_M) of the "metallic" elements per atom of oxygen. Specifically,

$$V_0 = k + b_{Si} + c_{Si}N_{Si} + \Sigma' c_M N_M,$$
$$(n_\lambda - 1)V_0 = R_{0,\lambda} = \Sigma a_{M,\lambda} N_M,$$

and $$(n_{\lambda_1} - n_{\lambda_2})V_0 = D_{0,\lambda_1\lambda_2} = \Sigma(a_{M,\lambda_1} - a_{M,\lambda_2})N_M.$$

k is a small constant, depending apparently on the annealing technique. The constants b_{Si} and c_{Si} have different values for different ranges of N_{Si}, as shown by the changes of slope of the line in the accompanying figure for Na_2O-SiO_2 glasses. *The same* constants are applicable *over the same ranges* of N_{Si} values, regardless of the kinds and amounts of other metallic elements present, insofar as can be determined from the data at present available. The different slopes indicate a difference in the closeness of the packing of the atoms in the silicon-oxygen framework within different N_{Si} ranges.

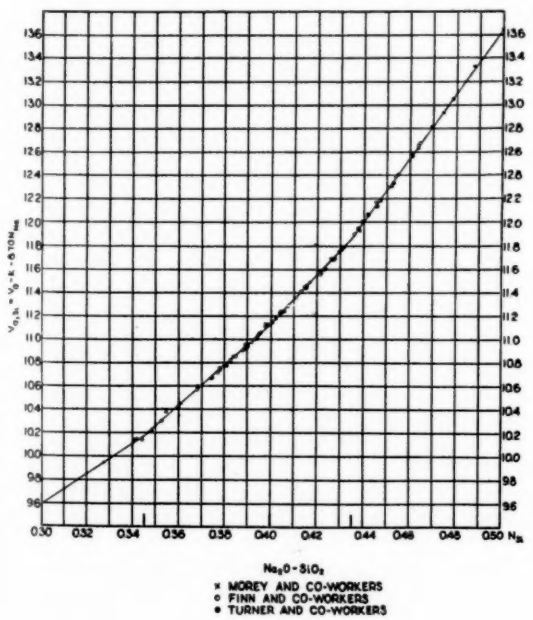

FIG. 1.

The break at $N_{Si}=0.435$ may indicate the limit, below which all the oxygen atoms are approximately in a close-packed arrangement and above which some of them are more loosely packed. $N_{Si}=0.40$, where another break occurs, is the composition required for $(Si_2O_5^{--})_x$ sheets or other structures in which 3 of the 4 oxygens around each Si are bonded also to another Si. The break at about 0.345 is not very well defined by present data. Actually there may be a gradual curvature in this region or there may be two or more breaks, e.g. at 0.333, corresponding to $(SiO_3^{--})_x$ chains or rings (in which 2 of the 4 oxygens surrounding each Si form bridges to other silicons), and at 0.364, corresponding to $(Si_4O_{11}^{-6})_x$ double chains.

Satisfactory data for glasses having N_{Si} less than about 0.27 are lacking. One may predict a definite break at 0.25, however, since below that concentration some of the oxygens must be bonded to no silicons.

Details of this work will be published in the *Journal of the Optical Society of America*.

MAURICE L. HUGGINS

Kodak Research Laboratories,
Rochester, New York,
July 1, 1940.

Elasticity of Crystals

Recent theoretical discussions[1] of the elasticity of crystals, particularly of the rigidity, in the neighborhood of the melting point have brought out the scantiness of relevant experimental material. Some preliminary measurements of the rigidity of polycrystalline aluminum, to 650°C, may consequently be of interest. A dynamical method[2] gave the resonant frequency of torsional vibrations of a right circular cylinder, approximately 20 cm long. The frequencies (of the lowest mode) varied from about 8000 cycles per second at room temperature, to about 5100 at 650°. The melting point of this aluminum (commercial 2S grade) as determined with the same Chromel-Alumel thermocouple which was used for the other temperature measurements, was 663°, using the calibration tables given by the manufacturer. In Table I are given the ratios of frequencies at even temperatures to the frequency at 0°C and the corresponding ratios of rigidity, computed from the relations, $V=2FL$ and $G=V^2\rho$, where V is the velocity of propagation of torsional waves, F the

TABLE I. *Relative rigidity of aluminum.*

t°C	F/F_0	G/G_0
0	1.000	1.000
100	0.973	0.945
200	.942	.883
300	.907	.816
400	.865	.740
500	.816	.657
600	.756	.562
610	.750	.553
620	.743	.542
630	.731	.524
640	.712	.498
650	.648	.412
663	melting point	

fundamental frequency of vibration of a cylindrical rod of length L, ρ the density, and G the rigidity. Corrections for thermal expansion have been applied, according to the data of Hidnert.

These measurements show a considerably smaller falling off of rigidity than do those of Koch and Dannecker,[3] also carried out on polycrystalline aluminum, to 580°; the method of the torsional pendulum used by these writers probably involved strains beyond the elastic limit at the higher temperatures.

It is evidently not possible to say from these results whether the rigidity vanishes at the melting point or retains a finite small value. The interpretation is somewhat complicated by the fact that the measurements deal with an aggregate of crystals; it seems unlikely, however, that an aggregate would remain stable for shearing strains after the crystals of which it was composed had become unstable for shear about any single crystal direction.

The shape of the curve giving the variation of rigidity with temperature is perceptibly different from the shape of the sample curves calculated by Born: The observed variation is smaller at low temperatures, and the decrease in the neighborhood of the melting point more precipitate. Born's curves were calculated, however, for the case of central forces between atoms.

FRANCIS BIRCH
DENNISON BANCROFT

Harvard University,
Cambridge, Massachusetts,
June 24, 1940.

[1] Max Born, J. Chem. Phys. **7**, 591 (1939); L. Brillouin, Phys. Rev. **54**, 916 (1938).
[2] Francis Birch, J. App. Phys. **8**, 129 (1937).
[3] Koch and Dannecker, Ann. d. Physik **47**, 197 (1915).

Lattice Summations for Hexagonal Close-Packed Crystals*

The potential energy of interaction between the atoms or ions of a crystal may be expressed by a set of terms which have the exponential or inverse power form of attraction or repulsion. The work required to remove a single particle from the crystal is determined by summing up the interaction between that particle and all the other particles of the crystal. This summation for the inverse power terms has been made by Lennard-Jones for the cubic crystal.[1] The summations necessary for the determination of the elastic constants of a cubic crystal have been made by Herzfeld and Goeppert-Mayer[2] and by May.[3]

For the hexagonal crystal, the method used by Lennard-Jones could not easily be adopted, so we have used a more tedious and less elegant method. The summations were made directly to ten times the distance between nearest neighbors omitting half the contribution of the outside shell. Then an integration was made from this outside shell to infinity. The crystal considered was the hexagonal close-packed crystal with ideal axial ratio (1.633). Summations were made over $x-y$ planes for the inverse sixth, eighth, tenth, and twelfth power of the distance between particles. The threefold axis of the crystal was chosen as the z axis. From symmetry considerations and the fact that $r^2=x^2+y^2+z^2$, the following relations between the sums entering the elastic constants can be established:

(1) $\Sigma x^2r^{-n-2}=\Sigma y^2r^{-n-2}=\frac{1}{2}(\Sigma r^{-n}-\Sigma z^2r^{-n-2})$,

(2) $\Sigma x^4r^{-n-4}=\Sigma y^2r^{-n-4}=3\Sigma x^2y^2r^{-n-4}$,

(3) $\Sigma x^2y^2r^{-n-4}=\frac{1}{8}(\Sigma r^{-n}-2\Sigma z^2r^{-n-2}+\Sigma z^4r^{-n-4})$,

(4) $\Sigma x^2z^2r^{-n-4}=\Sigma y^2z^2r^{-n-4}=\frac{1}{2}(\Sigma z^2r^{-n-2}-\Sigma z^4r^{-n-4})$.

(5) All sums containing odd powers of any one coordinate are zero. Consequently, only the lattice sums Σr^{-n}, Σz^2r^{-n-2}, and Σz^4r^{-n-4} have to be evaluated in order to obtain the contributions of the interaction potential r^{-n} to all the elastic constants.

The summations were made for $n=6$, and $n=8$.

TABLE I. *Lattice sums for hexagonal close-packed crystals.*

	$n=6$	$n=8$
Σr^{-n}	14.4549	12.8028
Σz^2r^{-n-2}	4.821	4.270
Σx^2r^{-n-2}	4.817	4.266
Σz^4r^{-n-4}	3.114	2.804
Σx^4r^{-n-4}	2.973	2.650
$\Sigma x^2y^2r^{-n-4}$	0.991	0.883
$\Sigma x^2z^2r^{-n-}$	0.854	0.733
Σr^{-n-4}	12.3124	12.1323

Since the lattice sums obtained have almost the same value as for the face-centered cubic crystal, a direct comparison of the two lattice types was made as a numerical check. If one of the threefold axes of the cubic crystal is chosen as the z axis then the first and second $x-y$ planes of the two types of crystal can be made to coincide. The next three planes differ in the two types and the following three differ only by a rotation about the z axis, which does not affect the summation. A summation was made of the inverse sixth and eighth powers over the first three planes on which they differed. The difference beyond these planes is inappreciable. The difference between the two types was found to be exactly the same as the difference taken over the entire crystal as found by us and by Lennard-Jones ($\Delta\Sigma r^{-6}=0.0010$ and $\Delta\Sigma r^{-8}=0.0009$).

BROTHER GABRIEL KANE
Manhattan College,

MARIA GOEPPERT-MAYER
Columbia University,
New York, New York,
July 11, 1940.

* Publication assisted by the Ernest Kempton Adams Fund for Physical Research of Columbia University.
[1] E. Lennard-Jones and A. E. Ingham, Proc. Roy. Soc. **A107**, 636 (1925).
[2] K. F. Herzfeld and M. Goeppert-Mayer, Phys. Rev. **46**, 995 (1934).
[3] A. May, Phys. Rev. **52**, 339 (1937).

An X-Ray Investigation of the Phase Transitions of Sodium Palmitate

In the course of some phase transition studies carried out with the collaboration of Lever Brothers Company, a temperature-controlled x-ray powder camera[1] was employed as a means of detecting the transitions of sodium palmitate. As a result of this investigation evidence is provided for the existence of seven phases, with their corresponding six transitions, between room temperature and the condition of isotropic liquid.

The sodium palmitate used in this experiment was prepared by neutralizing an alcoholic solution of Eastman Kodak Company palmitic acid with alcoholic sodium hydroxide. Alcohol and residual water were removed by evacuation at an elevated temperature. A hot alcohol solution of the sodium palmitate was exactly neutral to phenolphthalein. The anhydrous sodium palmitate was in the form of small fibrous chunks ranging in size from extremely fine powder to pieces approximately 1–2 mm on the long dimension. The material was not unlike satin-spar in appearance.

A small amount of the crystalline solid was loaded and sealed into a fine glass capillary tube. All of the x-ray photographs were taken under identical conditions of exposure and development. The exposure time was two hours, in each case being preceded by 15 minutes of heating under the temperature conditions at which the exposure was to be made. These photographs indicated transitions at 67°, 117°, 138°, 205°, 257°, and 290°C.

The transitions in sodium palmitate have already been investigated by R. D. Vold and M. J. Vold,[2] who employed a dilatometric method. They reported five successive phase changes. The 67° transition found here by x-ray methods was not reported by the Volds. The revised list of successive phases and their corresponding transitions, using the Vold nomenclature, is shown in Table I.

TABLE I.

Phase	Transition Temperature*	
	X-Ray Method (Chesley)	Dilatometer (Vold)
Curd fiber I		
	67°C	
Curd fiber II		
	117°	117°C
Subwaxy		
	138°	135°
Waxy		
	205°	208°
Subneat		
	257°	253°
Neat		
	290°	292°
Isotropic liquid		

* Since x-ray photographs were taken at 5-degree intervals, the above temperatures are correct to ±2.5°C.

It may be recalled that no single method provides an infallible criterion of a transition. The dilatometric method fails if the volume change at a particular transition is extremely small. The data listed by the Volds proves that the volume change from the phase Curd fiber I to the phase Curd fiber II is indeed very small. Nevertheless, the data[2] plotted in their Fig. 1 do show a small volume discontinuity in the region near 70°C. This they either overlooked or failed to recognize as being characteristic of a transition. The x-ray method proves quite sensitive in detecting the 67° transition.

FRANK G. CHESLEY

Mineralogical Laboratory,
Massachusetts Institute of Technology,
Cambridge, Massachusetts,
June 26, 1940.

[1] A full discussion of this instrument will appear elsewhere.
[2] R. D. Vold and M. J. Vold, J. Am. Chem. Soc. **64**, 808 (1939).

Raman Spectrum of Aluminum Bromide

The Raman spectrum of a very pure sample of aluminum bromide, kindly supplied by Dr. H. Pines of the Universal Oil Products Company, has been photographed. The material was kept in the liquid state at 100° by the heat from the mercury arc light sources. The results are as follows: 67.0(5*b*)(*e*, ±*k*), 79.3(5)(*e*, ±*k*), 112.8(5)(±*e*, ±*k*), 140.3(5)(±*e*, ±*k*), 185(0)(*e*), 208.2(10)(±*e*, *i*, ±*k*), 223(1)(±*e*), 407?(0*vd*)(*e*), 488(1*vd*)(*e*). It seems likely that 407 and 488 are not fundamentals. 185 may be the combination of 113 and 67, and 223 may be the combination of 140 and 79.

Two plausible structures for Al_2Br_6 are the halogen bridge model with symmetry D_{2h} adopted by Palmer and Elliott[1] and the ethane-like model with symmetry D_3, D_{3h}, or D_{3d}. The maximum number of frequencies active in the Raman effect permitted by the selection rules is 9 for the former model, while this number is 10, 9, or 6 for D_3, D_{3h}, or D_{3d}, respectively. According to Stitt[2] the number of distinct Raman-active fundamentals for D_3 with free rotation is 6. Since the symmetry D_{3h} (plane of reflection perpendicular to the threefold axis) is not very probable for Al_2Br_6, 6 Raman-active fundamentals might be expected for the ethane-like structure and 9 for the halogen bridge structure. While a clean-cut distinction between these alternatives cannot yet be made, it is probably significant that (1) we have observed 5 strong Raman lines both with Al_2Br_6 and with $Al_2(CH_3)_6$ for which a bridge structure is presumably impossible; (2) the Raman spectrum of C_2Cl_6 consists of 5 lines;[3] and (3) six fundamentals of Si_2Cl_6 are observed in its Raman spectrum[3].

The study of this point will be continued by observation of the Raman and infra-red absorption spectra of some halogen-methyl compounds of aluminum.

E. J. ROSENBAUM

Department of Chemistry,
University of Chicago,
Chicago, Illinois,
June 20, 1940.

[1] Palmer and Elliott, J. Am. Chem. Soc. **60**, 1852 (1938).
[2] Stitt, J. Chem. Phys. **5**, 90 (1937).
[3] Heidenreich, Zeits. f. Physik **97**, 277 (1935).

The Determination of the Proton-Attracting Properties of Liquids*

In a recent article[1] Gordy and Stanford have shown that a plot of the shift in wave-length of the OD vibrational band of the CH_3OD molecule due to hydrogen bonding with a variety of amines of known basicity is a linear function of the logarithm of the ionization constant K_i of the base. By a bold extrapolation they have then estimated the base strengths of a number of weakly basic oxygen compounds, but have apparently overlooked the fact that a value for the basicity of one of these, acetophenone, has previously been obtained by an entirely different method.[2] This depends upon the determination of the range of sulfuric acid-water compositions required for the change in ultraviolet absorption which accompanies the conversion of the base to its conjugate acid. Gordy and Stanford's value of K_i for acetophenone is 1×10^{-20}, that obtained from the data of Flexser, Hammett and Dingwall is 0.9×10^{-20}. Further, somewhat less direct evidence of agreement of the two methods is also available. The Gordy and Stanford value for methyl and benzyl benzoates is 5×10^{-22}; the Flexser, Hammett and Dingwall value for benzoic acid is 6×10^{-22}. The Gordy and Stanford value for nitrobenzene is 4×10^{-25}; one may estimate from the incomplete ionization of the substance in nearly anhydrous sulfuric acid[3] that the value of K_i is in the range from 10^{-24} to 10^{-25}.

The agreement between these two entirely different approaches to the determination of the strengths of very weak bases strikingly confirms the validity of both.

LOUIS P. HAMMETT

Department of Chemistry,
Columbia University,
New York, New York,
July 13, 1940.

* Publication assisted by the Ernest Kempton Adams Fund for Physical Research of Columbia University.

[1] Gordy and Stanford, J. Chem. Phys. **8**, 170 (1940).

[2] Flexser, Hammett and Dingwall, J. Am. Chem. Soc. **57**, 2103 (1935).

[3] Treffers and Hammett, J. Am. Chem. Soc. **59**, 1708 (1937).